UNIVERSITÉ DU QUÉBEC À CHICOUTIMI

MÉMOIRE PRÉSENTÉ À L'UNIVERSITÉ DU
QUÉBEC À CHICOUTIMI COMME EXIGENCE
PARTIELLE DE LA MAÎTRISE EN INGÉNIERIE

par
WEIXIA CHEN

DÉTERMINATION DES PROPRIÉTÉS THERMOPHYSIQUES DE MATÉRIAUX GRANULAIRES

Mars 1998

Mise en garde/Advice

Acknowledgments

Sommaire

Dans ce mémoire nous avons étudié la conductivité thermique, la diffusivité thermique, la capacité thermique et la granulométrie de produits du carbone comme le coke et l'anthracite. Ces propriétés thermophysiques ont été analysées dans la gamme de températures de 20 – 1 000°C.

À faible température, une méthode en régime stationnaire (guarded hot plate technique) a été utilisée. Pour mesurer la diffusivité thermique jusqu'à 1 000°C, un dispositif basé sur un principe de chauffage monotonique, a été développé. La méthode flash a aussi été utilisée pour les mesures de certaines particules de grandes dimensions. De plus, la porosité et la granulométrie ont été déterminées.

Pour l'interprétation des données expérimentales, des modèles faisant appel à des conductivités équivalentes ont été appliqués. La dépendance de la température sur les résultats fait l'objet d'une discussion.

Abstract

This thesis studies the thermal conductivity, thermal diffusivity, heat capacity and granulometry of granular carbon products such as coke and anthracite. These thermophysical properties have been analyzed in the temperature range of 20 — 1 000°C.

At the lower end of the temperature range, the steady-state method (guarded hot plate technique) was used. For measuring the thermal diffusivity up to 1 000°C, a device based on the principle of the monotonic heating regime was developed. The flash method was also used for the measurement of some big particles. Besides, the porosity and granulometry were determined.

For the interpretation of the measurement results, several equivalent conductivity models were applied and evaluated. The characteristics of the temperature dependence of different samples are discussed.

Contents

List of Figures

List of Tables

List of Symbols

a	part of the serial sub-cell, % or dimensionless
a	absorption cross section per unit volume of packing, m^{-1}
A	area of the receiving surface of the sample, m^2
$\mathbf{A}$	matrix of Equation 5.4
b	heating rate, °C/s
B	deformation factor, dimensionless
$\mathbf{B}$	matrix of Equation 5.4
C	heat capacity, J/°C
C_f	form factor in the model of Zehner and Bauer, dimensionless
c_p	specific heat at constant pressure, kJ/kg°C
$\mathbf{C}$	matrix of Equation 5.21
d	mean particle diameter, m, mm, μm
d_i	particle diameter of component i in mixture, m
d_1	the first dwell time, s
d_2	the second dwell time, s
f	dimensionless correction factor
F	function of the particle emissivity and possibly of the particle shape and porosity
h	heat-transfer coefficient, W/m^{2}°C
I	electric current, A
k	thermal conductivity, W/m°C
k_{core}	conductivity of the core of the unit cell, W/m°C
k_e	effective thermal conductivity, W/m°C
k_e'	effective thermal conductivity of the serial sub-cell, W/m°C
k_e''	effective thermal conductivity of the parallel sub-cell, W/m°C

k_g	thermal conductivity of the gas phase, W/m°C
k_r	conductivity by thermal radiation, W/m°C
k_r^g	radiation conductivity of the gas phase, W/m°C
k_s	thermal conductivity of solid, W/m°C
L_1	the first dwell level, °C
L_2	the second dwell level, °C
LC	loop counter
M	mass, kg
M_l	mass of displaced liquid, kg
M_a	weight of the particles in air, kg
M_s	mass of sample, kg
M_w	weight of particle in water, kg
M_1	mass of the pycnometer filled with sample and xylene, kg
M_2	mass of the pycnometer filled with xylene alone, kg
$\mathbf{N}$	matrix of Equation 5.26
P	porosity, % or dimensionless
P_s	porosity of the serial sub-cell, % or dimensionless
P_p	porosity of the parallel sub-cell, % or dimensionless
q	heat flux, Wm^{-2}
Q_i	relative volumetric fraction of component i in the mixture, dimensionless
Q_0	energy absorbed by the sample, J
$\mathbf{Q}$	matrix of Equation 5.24
r	radius, m or mm
R	radius, m or mm
R	thermal resistance, °C/W
s	scattering cross section per unit volume, m^{-1}
T	temperature, K or °C
$\mathbf{T}$	matrix of Equation 5.12

U	voltage, V
V	volume, cm^3
x_i	particle size, m, mm, μm
$\bar{x}$	mean particle size, m, mm, μm
$\mathbf{x}$	matrix of Equation 5.4
$\dot{\mathbf{x}}$	matrix of Equation 5.4
z	axial coordinate, m
α	thermal diffusivity, m^2/s
δ	thickness of sample, m
ϵ	emissivity, dimensionless
ζ	distribution coefficient for polydispersed packings, dimensionless
ϑ	$\frac{\Delta T}{\Delta T_{MAX}}$ normalized temperature, dimensionless
ρ	density, kg/m^3
ρ_b	bulk density, kg/m^3
ρ_p	particle density, kg/m^3
ρ_w	density of water, kg/m^3
ρ_x	density of xylene, kg/m^3
ρ_l	density of displaced liquid, kg/m^3
μ_n	roots of the Bessel function $J_0(r) = 0$
σ_0	Stefan-Boltzmann constant, 5.67×10^{-8} W/m^{2}K^4
σ	standard deviation, dimensionless
φ	flattening coefficient, dimensionless
τ	time, s
ϕ_i	relative weight fraction of component i in the mixture
χ_c	$= k_{core}/k_g$, reduced conductivity of core of unit cell in Zehner and Bauer model

χ_p $= k_s/k_g$ ratio of conductivities of solid particles and gas, dimensionless

χ_r $= k_r/k_g$ reduced conductivity by radiation

Dimensionless Groups

$\text{Bi} = \frac{h\delta}{k}$ Biot number

$\text{Fo} = \frac{\alpha\tau}{\delta^2}$ Fourier number

Chapter 1 INTRODUCTION

Granular materials such as packing anthracite and packing coke that are used in carbon electrode and cathode baking furnaces for aluminium production do not have homogenous structure. It is very important to get reliable data about the thermal conductivity of packing coke and anthracite as a function of granulometry and temperature in a wide temperature range and under conditions very close to those in the industrial process in order that the results of the study can be immediately applicable to the plants, helping to choose an appropriate granulometry of packing materials [1].

However, there are difficulties even with the correct interpretation of the "thermal conductivity" of granular materials as they do not have homogenous structure and consist of solid particles with voids between them. The concept of pure heat conduction within the bulk cannot be strictly applied, as convection and radiation play an important role in the gas filled cavities. Thermal energy is transported through granular materials by a multi-mode mechanism including conduction, convection and radiation.

There are many different methods and devices in the literature but there is not a single "universal" method for measuring the thermophysical properties of materials with various structure and at wide temperature ranges. There is no commercially available device for the present study to test granular carbon

products in a wide temperature range with the possibility of simultaneous chemical reaction.

The objectives of the study are:

- Characterization of the structure of the samples, determination of the bulk density, solid density, porosity, granulometry.

- Development of measurement methods and equipment.

- Determination of thermal conductivity as a function of temperature and granulometry.

- Development of a theoretical model.

The most important achievements of the project are listed below:

1. An experimental method and apparatus, based on the monotonic heating principle was developed (see Figure 1.1), tested and used for the measurements in the high temperature domain [2] of granular carbon products.

    The application of this method provides equivalent thermal conductivity values as a function of temperature.
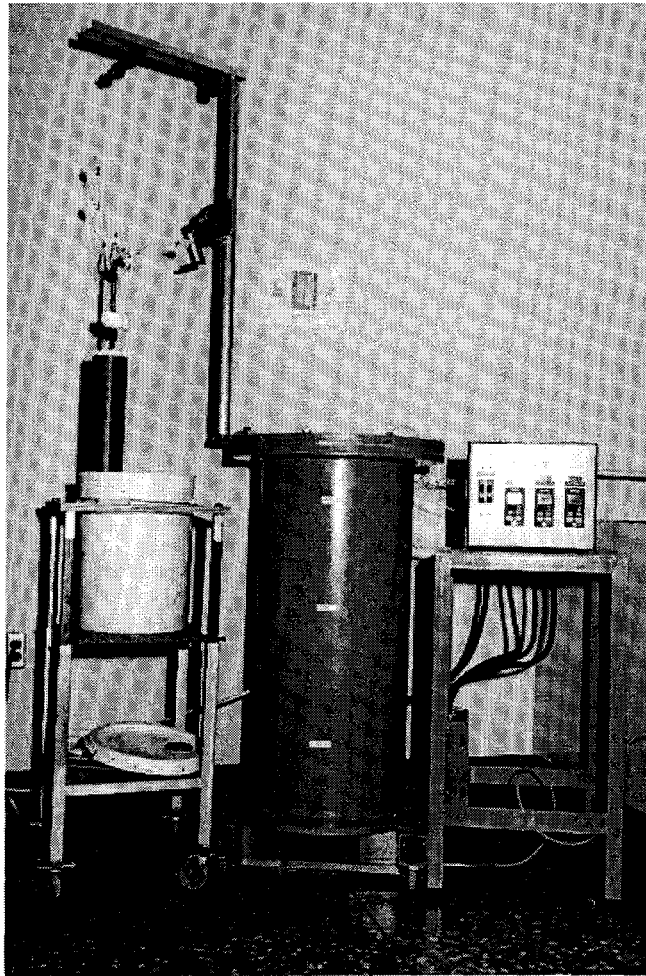
Figure 1.1 General view of the measurement apparatus using the monotonic heating method [2].

2. For better understanding of the role of the solid grains and the intergranular gas as well as the influence of the porosity and granulometry on the value and variation of the equivalent thermal conductivity, several additional measurements were performed. Porosity of the samples was determined from measured solid density. Granulometry of the materials was determined by

sieving tests.

3. An important part of the work was the determination of an equivalent conductivity model, which creates a mathematical correlation between material properties and the structure of the packing coke and the "apparent" conductivity as function of temperature. These models help the interpretation and generalization of the measured results.

4. The equivalent thermal conductivities of all the fourteen samples slightly above room temperature were measured by the guarded-hot plate apparatus. The results obtained from the guarded-hot plate apparatus have high precision, therefore they were used to verify the proper operation of the new transient apparatus with the monotonic heating.

5. The thermal conductivity and diffusivity of the solid grains of the packing coke of samples 6RHUSAGE and 8RHNEUF cut from the biggest grains were measured by flash method. These conductivities are lower than the expected values for a solid carbon (completely graphitized) material without pores.

6. Four coke samples and one anthracite sample were tested in the newly developed monotonic heating apparatus, in the temperature range of 150 – 1 000°C.

   As a general tendency, it was found that at room temperature, the coke samples tested have generally a higher conductivity than other cokes reported

in the literature [3], [4], [5]. Although the character of the temperature dependence is similar to the results reported in reference [5], the increase of the conductivity with temperature was smaller in our measurements than in reference [5]. The two findings do not contradict each other, since in the case of a higher conductivity at room temperature, radiation — which is one of the most important factors on the increase of the equivalent conductivity at elevated temperatures — contributes less to the total heat transfer.

Chapter 2 PHYSICAL BACKGROUND

2.1 The Mechanisms for Heat Transmission Inside Granular Materials

Generally, the mechanisms for heat transmission in a granular material can be represented by Figure 2.1. Thermal energy is transported through the granular material by conduction, convection and radiation.

Radiation

Contact points

Convection
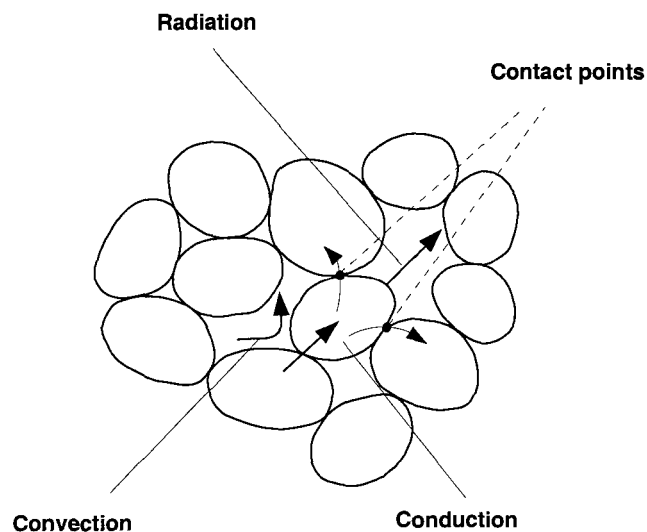
Conduction

Figure 2.1 Mechanism of heat transfer in granular materials

2.1.1 Equivalent conductivity

Because of the complex nature of heat transfer processes inside the granular material, its inhomogeneous structure is treated as if it were only a single, homogeneous conducting medium. The terms "equivalent" or "apparent" thermal conductivity are often used.

Equivalent or apparent conductivity of a granular material is influenced by the following factors:

1. Material property, i.e. the thermal conductivity of each phase (solid, gas).

2. Particle shape, bulk compaction and granulometry: porous, fibre, powder.

3. Temperature.

4. Atmosphere.

2.1.2 Conduction mechanism

The heat conduction in a granular material includes the following aspects:

1. Conduction through the solid particles.

2. Conduction across the gas in the voids and cavities.

3. Conduction across the stagnant gas surrounding the points of contact between particles.

4. Conduction through the points of contact between particles.

For homogeneous solid bodies, the true conduction, i.e. heat transfer by molecular, atomic, and electronic motion, is the predominant mechanism. For heterogeneous materials, the thermal conductivities of the pure components are generally known as functions of the temperature. If the pore dimensions are of the same order of magnitude as the mean free path of the molecules, the conductivity of a gas also becomes a critical function of pressure and pore size. This phenomenon may occur in powders [6].

The conduction in packing materials depends not only upon the thermal conductivity of the particle material and the surrounding gas, but also on the interfacial contact areas through which heat flows and the contact resistance occurring at these interfaces. When the solid phase is not interconnected, the number of contact points between neighboring particles and the quality of the contact —thermal contact resistance— plays an important role.

The contact heat conductance is influenced by many factors, such as the surface roughness, surface waviness, mean slope of individual asperities, mean temperature at the interface, interfacial contact pressure, and mechanical and thermophysical properties of heterogeneous materials [7].

The experimental data [8] reveal the significance of the gas environment on the equivalent thermal conductivity. Although the thermal conductivity of the gas is much lower than that of the solid particles, the gaseous contribution has a dramatic effect on the equivalent thermal conductivity of the packed bed, increasing the equivalent thermal conductivity by a factor of two in most cases. This is because the gaseous area through which heat is conducted is much greater than the spherical contacts of particles.

Because gases are involved, the thermal conduction of each phase is temperature-dependent and for the gases, also pressure-dependent. The effective thermal conductivity depends not only on the porosity but also on the cellular

structures, such as size and shape, orientation and emissivity of the pores, etc. So a generalization based on the porosity alone is not possible. Solid matrices with the same porosity but with various cellular structures have different effective thermal conductivities. Also some high conductivity consolidated solid matrices have conductivities that are nearly independent of porosity (at low porosities).

2.1.3 Convection mechanism

Convection contributes to heat transfer through the system in two ways:

1. In materials with closed pores, natural convection between the solid surfaces enclosing the cavities.

2. Heat exchange between distant cavities and particles by the trans-filtration.

The first effect is present solely in materials with closed pores, while the gas filtration can take place in materials with interconnected pores.

The necessary conditions for the convective motion through porous media are temperature gradient and pressure differences. Inter-cavity gas movement inside the granular material can be the result of pressure differences of different origin. Differential pressure between the external bounding surfaces of the pile or small pressure differences produced by the internal temperature gradients induce gas migration similar to thermodiffusion. As the temperature gradient and the pore size increase, convection may become more important.

It is difficult to investigate the convection in granular media directly. In vacuum there is no convection phenomenon [9] but only heat conduction and radiation. So it is important to develop a thermal conductivity measurement apparatus that can measure in vacuum and different atmospheres.

2.1.4 Radiation mechanism

Heat transfer by radiation in granular materials has received considerable attention, particularly at high temperatures.

Heat is transferred by radiation in three ways:

1. Radiation between adjacent particle surfaces.

2. Radiation between particle surfaces seen through more than one void space.

3. Radiation absorption by the gas.

Radiant transfer far from the boundaries can be expressed in terms of a radiant conductivity k_r which can be added to the true conductivity of the solid.

Reference [10] shows that the many models which have been proposed to describe simultaneous radiation and conduction may be classified in three groups.

The first type of correlations is based on those idealized geometrical arrangements of the phases which permit direct algebraic formulation of the transfer processes. The solid and gas phases are treated as alternating layers perpendicular to the direction of transfer. If the distance between the layers of the solid is assumed to be 1 particle diameter, the following expression is obtained for the

radiant conductivity of the gas phase:

$$k_r^g = 4\sigma_0 D \epsilon T^3 / (2 - \epsilon) \qquad (2.1)$$

where k_r^g is the radiant conductivity of the gas phase, W/mK, σ_0 is the Stefan-Boltzmann constant $= 5.67 \times 10^{-8}$ W/m^{2}K^4, ϵ is the emissivity, T is the temperature, K, D is the particle diameter, m.

The radiant conductivity is defined as the radiant heat flux divided by the temperature gradient.

The second group of models is based on a random walk process. The radiant transfer is interpreted in terms of the diffusion of photons and the following expression is obtained for the radiant conductivity:

$$k_r = 4\sigma_0 l T^3 / 3 \qquad (2.2)$$

where l is mean free path for radiation, m.

In the third type of model the packed bed is considered to be a pseudo-homogeneous material, permitting description of the heat transfer processes by differential equations and boundary conditions. The following expression for the radiant conductivity far away from the boundaries of the packing was obtained:

$$k_r = 16\sigma_0 n^2 T^3 / 3(a + s) \qquad (2.3)$$

where n is the refractive index of the solid relative to the fluid, a is absorption cross section per unit volume of packing, m^{-1}, s is scattering cross section per unit volume, m^{-1}.

Another model is:

$$k_r = 4Fd\sigma_0 T^3 \qquad (2.4)$$

where the exchange factor F is a function of the particle emissivity and possibly the particle shape and porosity, d is particle diameter, m.

In general the radiant conductivity increases with temperature, particle size and emissivity. Radiation becomes important relative to conduction above 870°C, for all the materials tested. The ratio of heat transfer by radiation of opaque particles is about 33% at the temperature of 1 093°C.

2.1.5 Combined transfer mechanism

Heat transfer in a granular material is a combination of conduction, radiation and convection. The conduction contribution, which is usually the most significant, is dependent not only upon the thermal conductivity of the particle material and the surrounding gas, but also on the interfacial contact areas through which heat flows and the contact resistance at these interfaces. According to Reference [10], in beds of glass or aluminum oxide particles of cylindrical or irregular grain, the radiation effects are important only for temperatures above 1 140 K. The convective contribution is principally dependent on the local fluid pressure and the packing density of the bed [11]. This contribution generally increases as the fluid pressure of the void fraction increases.

In Reference [12], an experimental investigation of combined conduction and radiation in a randomly packed bed is reported. In Reference [11], the effective thermal conductivity of packed beds with stagnant gas was theoretically computed. It was found that it can be expressed as:

$$k_e = (k_e)_{\text{COND}} + (k_e)_{\text{RAD}} + (k_e)_{\text{CONTACT}} \qquad (2.5)$$

where $(k_e)_{\text{COND}}$ is gas-solid conductivity, $(k_e)_{\text{RAD}}$ is radiation conductivity, $(k_e)_{\text{CONTACT}}$ is contact conductivity. $(k_e)_{\text{COND}}$ is highly pressure dependent; $(k_e)_{\text{RAD}}$ is slightly pressure dependent and $(k_e)_{\text{CONTACT}}$ is independent of pressure.

2.2 The Role of Combustion Inside the Bulk of the Packing Material

Combustion takes place inside the packing coke as air permeates the granular layer. Especially at high temperatures carbon is burned when in contact with air. This internal combustion has a significant effect on the temperature distribution inside the packing material.

The equivalent thermal conductivity concept cannot include this effect in a similar manner as it can incorporate radiation or gas filtration, simply because the combustion raises local temperature by releasing the heat within the bulk.

The secondary effect of the internal combustion on the equivalent conductivity, namely, the permeability of the granular bed is modified by the gas volumetric flow rate changes due to temperature and composition gradients.

There are certain physical and chemical effects that can cause aging or hysteresis, which may affect the value of the equivalent conductivity. For example, chemical reactions cause irreversible composition changes, a compacted granular material gets looser during the heating-up period and does not return to the original state after cooling back, the micro-convection inside and between the cavities has different patterns during heating and cooling, etc. This means that equivalent conductivity data are generally different during heating and cooling and they also can change during repeated measurements. Obviously, this happens also in real applications during thermal cycling.

Chapter 3 METHODOLOGY FOR THE DETERMINATION OF THE THERMOPHYSICAL PROPERTIES OF GRANULAR MATERIALS [13]

There are numerous methods for the measurement of thermal conductivity and/or thermal diffusivity of materials. There is no single method and arrangement which could cover the whole conductivity range and temperature domain and various structures of materials. In general, the methods can be divided into two approaches according to the principles : *Steady state methods* and *transient methods*.

3.1 Steady-state Methods

Steady-state techniques include the following methods: guarded hot-plate, axial flow, radial flow, panel test, etc.

The measurement of thermal conductivity with steady-state methods presents some difficulties compared to the measurement of other important fundamental properties such as thermodynamic quantities, because the determination of heat flux is involved.

3.1.1 Principle of the technique

The principle of these methods is based on Fourier's law:

$$q = -k\,gradT \qquad (3.1)$$

where: q is heat flux (W/m^2), $gradT$ is temperature gradient ($^\circ$C/m) and k is thermal conductivity (W/m$^\circ$C) which can be calculated easily from the measured heat flux and temperature gradient.

Table 3.1 [14] presents some of the methods. Guarded hot-plate and radial heat flow methods are more convenient for the measurement of the thermal conductivity of poor conductors [1] [14].

Table 3.1 Thermal conductivity measurement techniques

Measurement technique	Key features		Specimen materials	Conductivity range (W/m$^\circ$C)	Uncertainty (%)
	Advantages	Disadvantages			
Axial heat flow	Simultaneous electrical resistivity measurements Temperature coverage (below and above room temperature) High accuracy	Control of radial heat losses above 500 K	Metals and alloys in cylindrical form	10 - 500	0.5 - 2.0
Radial heat flow	Accuracy Flexibility at high temperatures	Large specimen size Long measurement time	Solids and powders in cylindrical form	0.01 - 200	3 - 15

Table 3.1 (Continued)   Thermal conductivity measurement techniques

Direct electrical heating	Very high temperature measurements Multiple property determination including electrical properties Rapid measurements	Sophisticated, often costly equipment Specimen must be an electrical conductor	Wires, rods, tubes of electrical conductors	10 - 200	2 - 5
Guarded hot plate	Adaptable to wide range of commercial materials High accuracy	Stable optical properties Low conductivity materials Long test time (3-12 h)	Thermal insulators	<1.0	2 - 5
Panel test	Simple apparatus	High-temperature gradient in specimen Long test times	Refractory materials in block form	0.05 - 15	15

3.1.2 Guarded hot-plate method

3.1.2.1 Introduction Guarded hot-plate method is the representative measurement method of thermal conductivity for the poorly conductive materials (k < 1 W/mK). There are two basic measurement configurations: (1) the conventional symmetrically arranged guarded hot plate where the heater assembly is sandwiched between two specimens (Figure 3.1), and (2) the biguarded arrangement where the heat flow is through one specimen and the back of the main heat/guard plane is rendered adiabatic by using another planar guard heater (Figure 3.2). The apparatus are used in preference for porous materials at around ambient temperature. This method is convenient for testing granular materials with different grain structures, as well as the sample preparation and the calculation of conductivity. The precision/accuracy at ambient temperature lies within ± 2% and ± 5% [14].
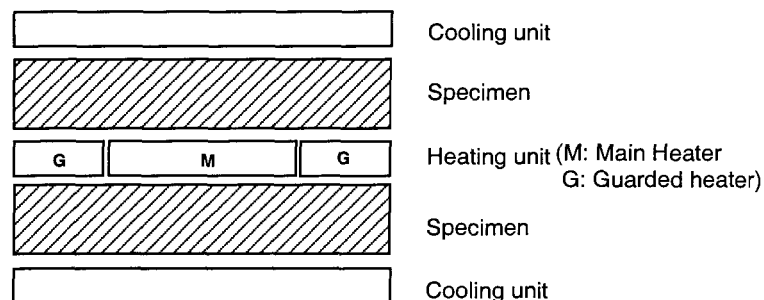
Figure 3.1 Guarded hot plate apparatus with two specimens

[Cooling unit diagram]	Cooling unit
[Specimen diagram - hatched]	Specimen
G | M | G	Heating unit (M: Main Heater G: Guarded heater)
[Flux meter diagram]	Flux meter
[Guard plate diagram]	Guard plate
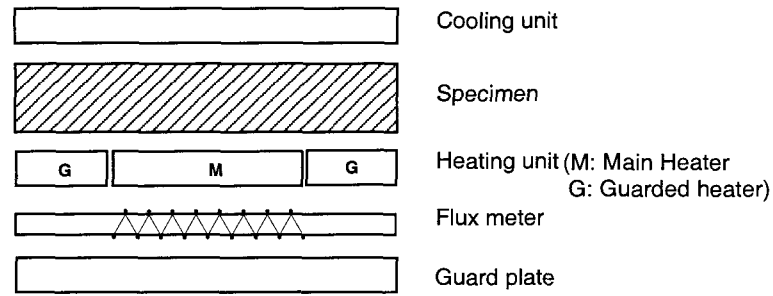
Figure 3.2 Biguarded hot plate apparatus

3.1.2.2 Principle of the Guarded Hot-plate Method

This measurement method is based on Fourier's law, considering the case of a medium limited by one (or two) parallel infinite plane(s) [14], assuming that ΔT is small and $k(T)$ is constant, we can get:

$$q = -k\frac{(T_2 - T_1)}{\delta} \qquad (3.2)$$

where: q is heat flux (Wm^{-2}), T_2 is the temperature (°C) of the "hot surface" of the specimen, T_1 is the temperature (°C) of the "cold surface" of the specimen, δ is the specimen thickness (m), and k is the thermal conductivity, (W/m°C).

The main problem for determining the thermal conductivity is that heat may escape from the edges of the slab, or if the edges are covered with insulation, a two-dimensional temperature profile may result, which can cause an error in the measurement. In order to reduce the error, guarded heaters are installed around the central hot plate. Electrical current generates heat in the guard independently of the central plate; this guard is maintained at a temperature as close as possible to

the temperature of the central plate. The guard is essential for correct functioning of the method: its function consists in maintaining the heat flow lines parallel in the central measurement zone. So the purpose of the guard is to reduce the lateral losses as much as possible.

3.1.2.3 Advantages

1. Convenient sample preparation, testing and calculating.

2. High accuracy.

3.1.2.4 Disadvantages

1. As the limitation of the insulation material and the heat flux sensor the apparatus works only slightly above room temperature $(20 - 80°C)$.

2. The test can not be done in different gas atmospheres.

3. The measurement requires a very long time, because the time to reach steady state in the sample and the measuring device is on the order of hour(s).

3.2 Transient Techniques

Transient techniques include the following methods: pulse method, temperature wave method, electron bombardment heat input method, monotonic heating regime method, etc.

Transient methods consist of the measurement of temperature and of accurate recording of the time dependence of temperature at the specimen boundary.

This is more convenient than the measurement of heat fluxes in steady-state techniques, that are difficult to control and measure accurately. With these methods, more than one property (thermal diffusivity, thermal conductivity, and specific heat) can be determined or calculated and they can be used from very low to very high temperatures and offer a wide conductivity measurement range. It is easier to measure thermal diffusivity. The thermal conductivity can be calculated relatively simply and accurately from the diffusivity if the two other thermophysical properties involved in the same relationship, density and specific heat, are either known or directly measured.

3.2.1. Principle of the technique

The evaluation is based on the measurement of transient temperature histories

$$T = T(\vec{r}, \tau) \tag{3.3}$$

at fixed points, where, T is temperature, K, r is the radius at any fixed point (m), τ is the time, s.

The differential equation of transient heat conduction for one-dementional heat conduction and constant properties is

$$\rho c_p \left(\frac{\partial T}{\partial \tau} \right) = div(k \, gradT) \tag{3.4}$$

where: ρ is the density of the sample, kg/m^3; c_p is the specific heat, kJ/kg°C; *div* and *grad* are the differential operators, divergence and gradient, respectively; k is the thermal conductivity, W/m°C.

There are many different methods (flash, transient calorimetry, hot-wire, monotonic heating regime, temperature waves, etc.). Some are listed in Table 3.2 [14].

Table 3.2 Transient techniques

Measurement technique	Key features		Specimen materials	Diffusivity range (m^2/s)	Uncertainty (%)
	Advantages	Disadvantages			
Pulse method (flash)	Wide property range Wide temperature coverage Small and simple specimens Simple and rapid measurement Multilayer specimens Multiple specimen facility	Not well suited for coarse matrix materials Not convenient for translucent materials Sophisticated error analysis	All solids and encapsulated liquid metals Specimens: Disks 6 - 16 mm diameter	10^{-7}-10^{-3}	1.5 - 5
Temperature wave method	Wide property range Very wide materials range Suitable for very high pressures Suitable for multiproperty measurement	Quasistationary temperature conditions necessary Complex mathematical treatment Complex error analysis	Solids, liquid metals, liquids, and gases Specimens: rods, cylinders, hollow cylinders, etc.	10^{-7}-10^{-4}	1 - 5 (solids) 1 - 3 (fluids) 5 - 9 (liquid metals)

Table 3.2 (Continued)   Transient techniques

Electron bombardment heat input method	High-temperature coverage Small specimens Applicable to electrical conductors and nonconductors AC techniques applicable Simultaneous specific heat movement possible	Complex experimental apparatus High-vacuum conditions required Arduous mathematics	Metals, nonmetals, liquid metals Specimens: disks 6 - 9 mm, plates 0.25 cm^2 and more, hollow cylinders 6 - 8 mm i.d. 15 - 20 mm o.d.	10^{-7} - 5×10^{-5}	2 - 10
Monotonic heating regime method	Wide materials range Continuous measurement in very wide temperature range Simple apparatus Simple measurement	Not very suitable for good thermal conductors	Ceramics, plastics, composites, thermal insulators Specimens: cylinders, plates, parallelepipeds	10^{-8}-10^{-5}	2 - 12

3.2.2 Monotonic heating method

The monotonic heating regime methods include a large group of methods theoretically based on some particular "regular" solutions of heat conduction equation with the temperature or heat flux boundary conditions. These methods are all referred to as the methods for thermal diffusivity studies with monotonic heating.

Chapter 3

The first, the second, and the third kind of regular regimes are distinguished. In the case of the first kind of regular regime, a sample is heated stepwise at constant ambient temperature. In the second kind of regular regime, heating proceeds at a constant rate (ambient temperature is a linear time function which implies a constant heat flux effect on a sample). The third kind of regular regime is a developed temperature wave. The term "monotonic regime" is used in studies implying heating rate close to linear.

Despite a great variety of methods for calculating thermal diffusivity, they are all based on and primarily approximated by the well-developed solutions of linear heat conduction equations for the simplest heat transfer cases.

The conduction equation (Equation 3.4), when expressed in cylindrical coordinates, becomes

$$\frac{\partial T}{\partial \tau} = \alpha \left(\frac{\partial^2 T}{\partial r^2} + \frac{1}{r} \frac{\partial T}{\partial r} \right) \tag{3.5}$$

For the infinite cylinder the boundary condition at the external surface is:

$$T_{\text{surface}} = b\tau \tag{3.6}$$

where b is the heating rate, K/s.

The temperature is

$$T(r) = b \left(\tau - \frac{R^2 - r^2}{4\alpha} \right) + \frac{2b}{R\alpha} \sum_{n=1}^{\infty} e^{-\alpha \mu_n^2 \tau} \frac{J_0(r\mu_0)}{\mu_n^3 J_1(R\mu_n)} \tag{3.7}$$

where α is the diffusivity, m²/s, R is the radius of the sample, m, μ_n is the roots of the Bessel function $J_0(r) = 0$ [15].

We can calculate the temperature distribution inside a cylindrical sample as shown in Figure 3.3. After an initial period all temperature distributions along the radius are similar, shifted upwards.

Figure 3.4 shows the temperature history on the surface and in the center of the sample. After an initial period at all internal points the temperature increases linearly.
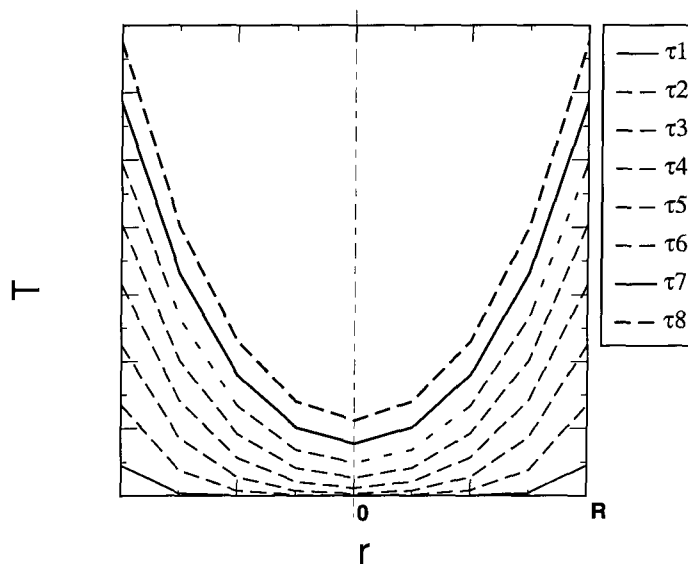
Figure 3.3 Temperature distribution inside a cylindrical sample
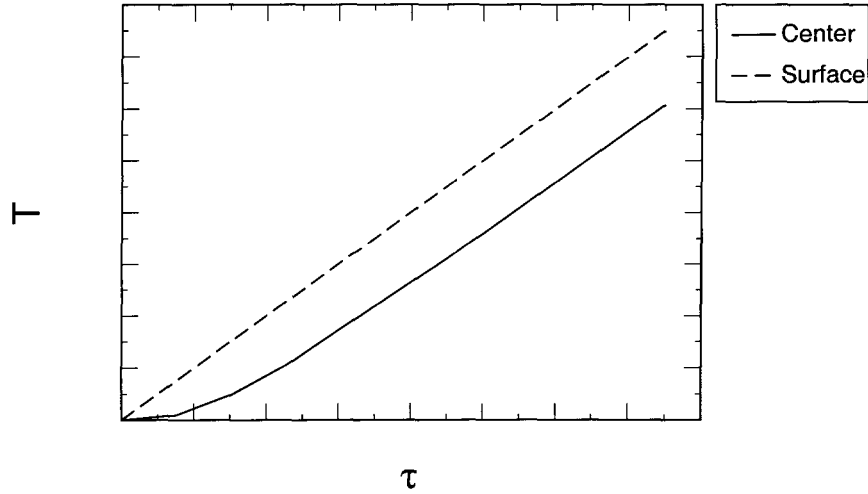
Figure 3.4 Temperature history on the surface and in the center of the sample

$$\Delta T = T_{\text{surface}} - T_{\text{center}} = \frac{bR^2}{4\alpha} - \frac{2b}{R\alpha}\sum_{n=1}^{\infty} e^{-\alpha\mu_n^2\tau}\frac{1}{\mu_n^3 J_1(R\mu_n)} \qquad (3.8)$$

The exponential term tends towards zero after an initial period. Thus the diffusivity is

$$\alpha = \frac{bR^2}{4\Delta T} \qquad (3.9)$$

Using the definition of thermal diffusivity

$$\alpha = \frac{k}{\rho c_p} \qquad (3.10)$$

the thermal conductivity k can be calculated

$$k = \alpha\rho c_p = \frac{bR^2\rho c_p}{4\Delta T} \qquad (3.11)$$

So the thermal conductivity can be determined from Equation 3.11 by measuring the temperature difference between the surface and the centre after an initial period if the density and the heat capacity are known.

Advantages:

1. Measurement in a very wide temperature range (from 25°C to 1 000–1 300°C) and various gas atmospheres.

2. Determination of temperature dependence.

3. These methods offer the potential to determine more than one property.

3.2.3 Flash method [16]

3.2.3.1 Introduction

The flash method is one of the best-known transient techniques for testing thermal diffusivity of solids. This method was first developed by Parker [17]. The measurement requires a small disc shaped sample, which is instantaneously heated by a light pulse from a laser or a xenon flash lamp on one side. On the other side, at the rear surface, the transient temperature rise is recorded and diffusivity values are computed from temperature rise versus time data (Figure 3.5).
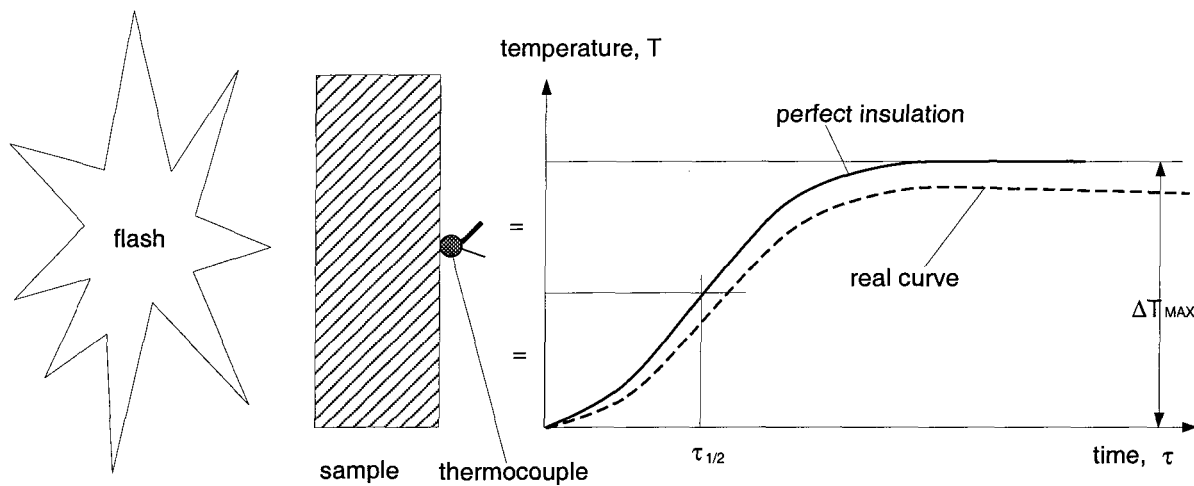
Figure 3.5 Principle of the flash method

This method does not use temperature or heat flux measurements directly for evaluating diffusivity. The diffusivity is determined by means of length and time measurements.

The flash method can be used for a wide range of solids from best conducting metals to insulators. As the size of sample is small, the method is not convenient for testing materials with grain structure coarser than 1mm.

3.2.3.2 Principle of the method

To calculate the thermal diffusivity in case of perfect insulation [17], the formula is:

$$\alpha = 1.37 \frac{\delta^2}{\pi^2 \cdot \tau_{1/2}} = 0.1388 \frac{\delta^2}{\tau_{1/2}} \qquad (3.12)$$

where: δ is the thickness of the sample (m), $\tau_{1/2}$ is the "half-rise" time (s) which is the length of the period to reach half of the maximum temperature value at the rear surface of the sample.

The volumetric heat capacity ρc_p can be calculated by the formula:

$$\rho c_p = \frac{Q_0}{\delta \cdot A \cdot \Delta T_{\text{MAX}}} \tag{3.13}$$

where: ρ is density, kg/m^3, c_p is specific heat, J/kg$^\circ$C, Q_0 is pulse energy, absorbed by the sample, J, A is the area of the receiving surface of the sample, m^2, ΔT_{MAX} is maximum temperature increase in the sample, $^\circ$C.

Because the pulse of energy cannot be measured easily, the second sample which is a reference material with known heat capacity is simultaneously exposed to the flash and measured. The volumetric heat capacity of the sample is then

$$\rho c_p = (\rho c_p)_{\text{REF}} \frac{\delta_{\text{REF}}}{\delta} \frac{\Delta T_{\text{MAX,REF}}}{\Delta T_{\text{MAX}}} \tag{3.14}$$

Chapter 4 EXPERIMENTAL STUDY OF THE THERMOPHYSICAL PROPERTIES OF GRANULAR MATERIALS NEAR ROOM TEMPERATURE

4.1 Characterization of the Samples

Fourteen sorts of packing coke samples were analyzed in this project. The description of the samples is listed in Table 4.1. Most of them are polydisperse granular materials with variation of the particle sizes from smaller than 80 μm to larger than 28 mm. Some particles have a foamed structure as there are cavities and holes inside.
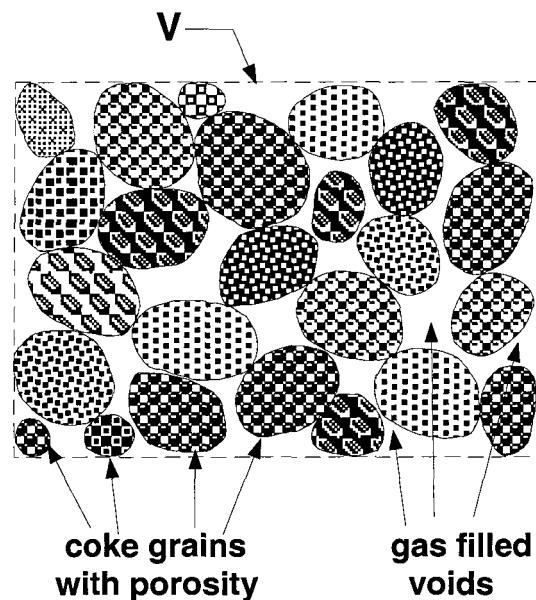
Figure 4.1 Structure of the packing coke

Hence the packing coke can be considered as a hierarchic, two-level hetero-

geneous system (see Figure 4.1). In the bulk, the gas (air) forms a continuous

phase, with a disperse solid (coke grain) inside. On a smaller geometric scale, the

individual particles are also two-phase systems, but there the solid carbon material

forms the continuous phase and the gas phase is dispersed in the pores inside.

Table 4.1 Description of the samples

Sample	Description
1ARGVERT	Green petroleum coke
2FCUNEUF	Mixed used/new fluid coke from Sebree
3FCNEUF	New petroleum fluid coke (Sebree)
4FCUSAGE	Used petroleum fluid coke (Sebree)
5PEUSAGE	Poussier usagé Pechiney
6RHUSAGE	Poussier usagé Riedhammer
7RHUSAGE	Poussier usagé Riedhammer
8RHNEUF	Poussier neuf Riedhammer
9RHUSAGE	Poussier usagé Riedhammer
10PENEUF	Poussier neuf Pechiney
11PEUSAG	Poussier usagé Pechiney
12PEUSAG	Poussier usagé Pechiney
13PEUSAG	Poussier usagé Pechiney
14RHUSAG	Poussier usagé Riedhammer

There are several parameters in use to describe multiphase systems. Mass and volume fractions play a primary role in the characterization of such systems [2]. The following density parameters can be defined [18]:

- *real density* ρ_{solid} is the weight of a unit volume of a substance measured under specified or standard conditions, excluding the pore volume and interparticle voids contained in the specimen.

- *density of the gas phase (air)* ρ_{gas} in the intergranular voids and inside the pores within the grains,

- *bulk density* ρ_{bulk} of the granular material (the total m mass of grains + gas inside the volume, divided by the volume, see Figure 4.1. This density is always smaller than the real solid density and is always greater than the gas density.

- *apparent density of the grains or particle density* $\rho_{particle}$ is the weight per unit volume of a substance, measured under specified or standard conditions, including the pore volume but excluding the interparticle volume. This density is smaller than the real solid density and is bigger than the bulk density.

The geometrical structure of the packing coke can be characterized by parameters like porosity (volume fraction), mean diameter of the particles, size distribution (granulometry), shape of particles. All these parameters have an influence on the equivalent thermal conductivity of the granular material, but the

most important of them are the porosity and mean particle diameter.

Volume fraction of the gas inside the packing coke can be characterized by different porosities in a two-level porosity model:

- *porosity of the grains* $P_{particle}$, which is the ratio of the volume of the gas in the pores, inside the particles to the total volume of the particles. Here we have not made a distinction between open and closed pores, since for the measurement of the equivalent thermal conductivity this aspect is not of primary importance.

- *bulk porosity* P_{bulk}, which is characterizing the volume occupied by the gas in the intergranular voids. This parameter considers the grains as "compact solids".

- *total porosity* P, which provides the total volume fraction of the gas inside the packing material, including both the voids between the grains and the pores inside the grains (particles).

The correlations between these parameters are given below.

The densities and porosities:

$$\rho_{bulk} = P\rho_{gas} + (1 - P)\rho_{solid} \tag{4.1}$$

$$\rho_{bulk} = P_{bulk}\rho_{gas} + (1 - P_{bulk})\rho_{particle} \tag{4.2}$$

$$\rho_{particle} = P_{particle}\rho_{gas} + (1 - P_{particle})\rho_{solid} \tag{4.3}$$

The total porosity and the bulk porosity are correlated by the ratio of the real solid density and particle (grain) density, after neglecting the gas density:

$$P_{bulk} = 1 + \frac{\rho_{solid}}{\rho_{particle}}(P - 1) \qquad (4.4)$$

$$P = P_{bulk} + P_{particle} - P_{bulk}P_{particle}$$

or $\qquad (4.5)$

$$P = P_{bulk} + (1 - P_{bulk})P_{particle}$$

where $(1 - P_{bulk})$ is the volume fraction of the grains (particles).

4.1.1 Density

The densities of the samples were determined at room temperature. We have determined the bulk densities of all the 14 samples, and measured the particle and real solid densities for some of the samples.

4.1.1.1 Real density

Real density is defined as the mass divided by the volume occupied by the material excluding pores and voids. In the measurement, voids must be eliminated and pores in the material must be filled with a liquid. This requirement is met by grinding the coke particles to a size smaller than 75 μm.

The measurement method is according to ASTM standard D5004–89.

In all other aspects the experimental procedure follows the steps described in the xylene displacement method. As we have only a limited amount of material

from each coke samples, we did not grind them. Instead of doing that, we used the fine fractions (< 75 μm diameter) that we obtained during the screening of the samples for the granulometric analysis.

As sample 1ARGVERT is a nearly perfect monodisperse granular material, we did not have fines to perform this measurement.

The real density is:

$$\rho_{solid} = \frac{M \cdot \rho_l}{M_l} \qquad (4.6)$$

where: ρ_{solid} is the real density, M is the mass of the sample, ρ_l is the density of displaced liquid, and M_l is the mass of displaced liquid.

The procedure is as follows:

I Sample preparation

Sieve sample by No. 200 sieve to get 50 g of coke which is finer than 75 μm.

II Pycnometer calibration (Determination of pycnometer volume)

1. Clean and dry the pycnometer and its stopper, then weigh the empty pycnometer together with its stopper to 0.1 mg (mass M_0).

2. Fill the pycnometer with freshly boiled (to remove air) and cooled distilled water, and replace the stopper. Immerse the pycnometer up to the neck in the 25 ± 0.1°C water bath for 1 hour.

3. At the end of the temperature stabilization period, check the capillary to be certain it is completely filled. Remove the pycnometer from the 25°C bath, rinse immediately with acetone, dry, and weigh to 0.1 mg (mass M_3).

4. Calculate the volume, V, of the pycnometer in cubic centimeters using Equation 4.7.

$$V = \frac{M_3 - M_0}{\rho_w} \qquad (4.7)$$

where: M_0 is the mass of the empty pycnometer, g, M_3 is the mass of the water filled pycnometer, g, and ρ_w is the density of water at 25°C (0.9970 g/cm^3).

III Determination of the density of xylene

Follow the procedure in 1 through 3 of II, but use xylene instead of water. Calculate density, ρ_x, of xylene at 25°C in g/cm^3 using Equation 4.8.

$$\rho_x = \frac{M_2 - M_0}{V} \qquad (4.8)$$

where: M_0 is the mass of the empty pycnometer, g, M_2 is the mass of the xylene-filled pycnometer, g, and V is the pycnometer volume, cm^3.

IV Determine the real density of coke

1. Clean and dry the pycnometer and its stopper thoroughly.

2. Weigh the pycnometer with its stopper to 0.1 mg (mass M_0). The temperature of the pycnometer is to be close to ambient room temperature.

3. Introduce approximately 10 g of the dried and cooled analysis sample into the pycnometer.

4. Replace the stopper, remove any coke adhering to outer pycnometer surface and re-weigh. The difference between this mass and M_0 is the sample mass (mass M_s).

5. Fill the pycnometer with enough xylene to wet and cover the sample and swirl gently to aid wetting and to displace air. Add additional xylene until the pycnometer is about two-thirds full and place it. Leave under vacuum until all bubbling stops.

6. Remove the pycnometer from the desiccator, fill it with xylene, and place it in the $25 \pm 0.1°C$ bath with stopper in place. Immerse the pycnometer up to the neck in the water bath for 1 hour.

7. At the end of the temperature stabilization period, check the capillary to be certain it is completely filled. Remove excess xylene on the stopper by dabbing with filter paper. Remove the pycnometer from the 25°C bath, rinse immediately with acetone, dry, and weigh to 0.1 mg (mass M_1).

8. Determine the density of the sample in g/cm^3 from the equation as follows:

$$\rho_{real} = M_s \left(\frac{\rho_x}{M_s - (M_1 - M_2)} \right) \qquad (4.9)$$

Where: M_s is the mass of sample, g, ρ_x is the density of xylene at 25°C, g/cm^3, M_1 is the mass of the pycnometer filled with sample and xylene, g, M_2

is the mass of the pycnometer filled with xylene alone, g, $M_s - (M_1 - M_2)$ is the mass of xylene displaced by coke, g, and $\frac{\rho_x}{M_s - (M_1 - M_2)}$ is the volume of xylene displaced by coke, cm^3.

4.1.1.2 Particle Density

The density of particles between 75 μm to 5 mm The mass of the coke is measured directly and the volume derived by determining the mass of liquid (Xylene) displaced when coke is introduced into a pycnometer. The density of particles larger than 75 μm up to the largest that can be put into the pycnometer can also be determined by the same method of real density. The measuement procedures are same as II—III, pp.35—36.

The density of particles larger than 5 mm There are some samples with very big particles, like for example sample 7RHUSAGE, where we were able to select grains of 10–25 mm diameter. The measurement of the particle density with the particles larger than 5 mm is by using the buoyancy (wet balance) method.

The procedure is as follows:

1. Measure the mass of particle (mass M_a) in air.

2. Put the particle in water for 24 hours.

3. Measure the weight of the particle in the water (M_w)

4. Calculate the particle density as follows:

$$\rho_{particle} = \frac{M_a \rho_w}{(M_a - M_w)} \qquad (4.10)$$

Where: $\rho_{particle}$ is particle density, g/cm^3, M_a is the weight of particle in the air, g, M_w is the weight of particle in water, g, ρ_w is the density of water, g/cm^3.

4.1.1.3 Bulk density

Bulk density is an indicator of packing coke porosity. The bulk density of a granular material is equal to the mass of the particles divided by the volume they occupy, including the space between the particles.

The measurement method is referenced to the standard ASTM D 4292.

Procedures:

1. Weigh 200.0 ± 0.1 g of the coke. Pour the coke slowly through a funnel into the graduate.

2. Vibrate for 5 minutes.

3. Measure the compacted volume.

4. Calculate the bulk density as follows:

$$\rho_{bulk} = \frac{M}{V} \qquad (4.11)$$

where: ρ_{bulk} is the bulk density, g/cm^3, M is the mass of the sample in the graduate, g, V is the volume of the sample in the graduate, cm^3. The temperature of the sample and graduated glass must be kept at 20°C.

The results of the bulk density, the particle density and the real density are given in Table 4.2

Table 4.2 Density of coke

Code	Bulk Density (kg/m^3)	Particle Desity (kg/m^3)	Real Density (kg/m^3)	Real Density (kg/m^3) (From Alcan)
1ARGVERT	584	1331	*	—
2FCUNEUF	1134	1874	2391	2116
3FCNEUF	1106	1829	1822	1936
4FCUSAGE	1127		2186	2248
5PEUSAGE	978			2121
6RHUSAGE	743			2175
7RHUSAGE	644	1427**		2129
8RHNEUF	677			2064
9RHUSAGE	683			2134
10PENEUF	720			2069
11PEUSAG	1076			2124
12PEUSAG	1084			2122

Table 4.2 (Continued)   Density of coke

13PEUSAG	1121			2120
14RHUSAG	713			2383

* First, this is a monodisperse sample without fine fractions. Second, the liquid displacement method is not applicable correctly to green coke.

** In the case of this sample, we measured the particle density of selected big (~20 mm diameter) particles, using the wet balance method.

4.1.2 Specific heat

The thermal capacity of coke 3FCNEUF was measured by using of calorimetry method. With this method an adiabatic calorimeter was used.

Procedures:

1. The sample is heated to 70°C in a thermostat.

2. Inject the cold water whose temperature is 1 – 2°C below the room temperature into the bucket. Lower the bucket into the jacket with the stirrer at the rear.

3. Turn on the motor of stirrer and run for 5 minutes to attain temperature equilibrium.

4. Read and record the temperature of calorimeter and the sample.

5. Put the sample immediately into the water, close the calorimeter quickly and run the motor to stir the water and the sample.

6. Read and record the calorimeter temperature. The temperature will start to rise. This rise will be rapid during the first few minutes, and then become slower until a stable maximum is reached. In order to be sure that a stable maximum has been reached, take calorimeter readings at one minute intervals until the same temperature is observed in three successive readings. Record this as the final maximum temperature.

So the specific heat of coke is

$$c_p = \frac{(c_{pw}m_w + c_{pb}m_b)(T - T_1)}{m(T_2 - T)} \tag{4.12}$$

where c_p is the specific heat of coke, kJ/kg°C, c_{pw} is the specific heat of water, kJ/kg°C, m_w is the weight of the water in the bucket, g, c_{pb} is the specific heat of the stainless steel bucket, kJ/kg°C, m_b is the weight of the bucket, g, T_1 is the temperature of cold water and the bucket, °C, T_2 is the temperature of sample, °C, T is the temperature of the mixture, °C. The result is in Table 4.3. This value compares well with data in Reference [27].

Table 4.3 Specific heat

Sample	Specific heat (kJ/kg°C)
3FCNEUF	0.871

4.1.3 Porosity

The volume fraction occupied by voids, i. e. , the total void volume divided by the total volume occupied by the solid matrix and void volumes, is called porosity.

4.1.3.1 Particle porosity

From [19]

$$P_{particle} = \frac{\rho_{solid} - \rho_{bulk}}{\rho_{solid} - \rho_{gas}} \approx 1 - \frac{\rho_{bulk}}{\rho_{solid}} \tag{4.13}$$

where ρ_{solid} is the real density of a solid body, kg/m^3, ρ_{bulk} is the bulk density, kg/m^3 and $P_{particle}$ is the particle porosity (ρ_{solid} is constant). Increasing porosity P or gas content means decreasing apparent density ρ_{bulk}, and increasing gas content means lower thermal conductivity, so decreasing ρ_{bulk} is generally connected with decreasing thermal conductivity.

4.1.3.2 Bulk porosity

The volume fraction of the intergranular air is bulk porosity. The formula of bulk porosity is

$$P_{bulk} = \frac{\rho_{particle} - \rho_{bulk}}{\rho_{particle} - \rho_{gas}} \approx 1 - \frac{\rho_{bulk}}{\rho_{particle}} \tag{4.14}$$

4.1.4 Granulometry

One of the main influences for the equivalent conductivity of packing materials is granulometry which is characterized by the size distribution of the non-homogeneous materials. Sieve analysis is one of the simplest, most widely used methods of particle size analysis, that covers the approximate size range 20 μm to 28 mm using standard woven wire sieves. A sample is separated into several particle diameter ranges by a series of sieves. Then each range is weighed. Finally, distribution of the particle size can be determined by the tabular calculation method. We determined the granulometry of the four first samples by using the sieving method according to ISO 2325–1986(E).

Apparatus

1. Sieve, the opening size range is 80 μm to 28 mm.

2. Sieve vibrator.

The Procedure of the measurement

1. Choosing the sieves

We choose a series of sieves which usually consists of four or five sieves according to the kind of sample. Sieves are stacked in ascending order of mesh size.

2. Separating the sample

The sample is fed into the top sieve. A closed pan, a receiver, is placed at the bottom of the stack to collect the fines and a lid is covered at the top to prevent loss of powder. The stack is hung on the vibrator, the timer is set to 15 minutes. After vibration the sample is separated into different sizes.

3. Weighing each size of the sample

Each size of the sample separated is weighed.

Sieving is deemed complete when the number of particles passing through the minimum size of sieve is negligible compared with the total number of particles.

The Results of the measurements

The results are listed in Table 4.4.

Table 4.4 Sieving results

Mesh size (mm)		< 0.08	0.08 - 0.16	0.16 - 0.315	0.315 - 0.63	0.63 - 1.25	1.25 - 2.5	2.5 - 5	5 - 10	10 - 14	14 - 20	20 - 28	Sum
Weight (g)	1ARGVERT	-	-	-	3.05	1.01	278.3	1.15	-	-	-	-	283.51
	2FCUNEUF	24.34	118.85	332.85	82.95	36.12	35.44	-	-	-	-	-	630.55
	3FCNEUF	17.99	226.73	542.21	69.10	7.85	17.50	34.25	1.41	25.70	4.04	-	946.78
	4FCUSAGE	1.40	121.20	325.01	96.99	55.79	60.46	52.47	50.24	24.19	6.60	62.78	858.13

Analysis the results

For getting the granulometry curves, the results are transformed into mean diameters of the particles and weight percentage respectively according to [20].

Table 4.5 Relative percentage frequency distribution: tabular calculation of mean size
Sample 1ARGVERT

Particle size range x_1 to x_2 mm	Interval dx_i mm	Average size x_i mm	Percentage in range $d\phi_i$ %	Percentage per mm $d\phi_i/dx_i$	$x_i d\phi_i$ mm
0.315 to 0.63	0.315	0.4725	1.08	3.429	0.5103
0.63 to 1.25	0.625	0.94	0.36	0.5806	0.3385
1.25 to 2.5	1.25	1.875	98.16	78.528	184.05
2.5 to 5	2.5	3.75	0.4	0.16	0.6

The mean particle size is:

$$\bar{x} = \frac{\sum x_i d\phi_i}{\sum d\phi_i} = 1.87 \, \text{mm} \tag{4.15}$$

The standard deviation is defined as:

$$\sigma = \sqrt{\frac{\sum (x_i - \bar{x})^2 \Delta\phi_i}{\sum \Delta\phi_i}} \approx 0 \, \text{mm} \tag{4.16}$$

Table 4.6 Relative percentage frequency distribution: tabular calculation of mean size
Sample 2FCUNEUF

Particle size range x_1 to x_2 mm	Interval dx_i mm	Average size x_i mm	Percentage in range $d\phi_i$ %	Percentage per mm $d\phi_i/dx_i$	$x_i d\phi_i$ mm
0 to 0.08	0.08	0.04	3.86	48.25	0.1544
0.08 to 0.16	0.08	0.12	18.85	235.65	2.262
0.16 to 0.315	0.16	0.2375	52.79	340.58	12.54
0.315 to 0.63	0.315	0.4725	13.16	41.78	6.22
0.63 to 1.25	0.625	0.94	5.73	9.24	5.39
1.25 to 2.5	1.25	1.875	5.6	1.12	10.5

The mean particle size is:

$$\bar{x} = \frac{\sum x_i d\phi_i}{\sum d\phi_i} = 0.37 \, \text{mm} \tag{4.17}$$

The standard deviation is defined as:

$$\sigma = 0.41 \, \text{mm} \tag{4.18}$$

Table 4.7 Relative percentage frequency distribution: tabular calculation of mean size
Sample 3FCNEUF

Particle size range x_1 to x_2 mm	Interval dx_i mm	Average size x_i mm	Percentage in range $d\phi_i$ %	Percentage per mm $d\phi_i/dx_i$	$x_i d\phi_i$ mm
0 to 0.08	0.08	0.04	1.90	23.75	0.076
0.08 to 0.16	0.08	0.12	23.95	299.375	2.874

Table 4.7 (Continued)   Relative percentage
frequency distribution: tabular calculation of mean size
Sample 3FCNEUF

0.16 to 0.315	0.16	0.2375	57.27	349.484	3.230
0.315 to 0.63	0.315	0.4725	7.30	23.175	3.449
0.63 to 1.25	0.625	0.94	0.83	1.339	0.780
1.25 to 2.5	1.25	1.875	1.85	1.48	3.469
2.5 to 5	2.5	3.75	3.62	1.448	13.575
5 to 10	5	7.5	0.15	0.03	1.125
10 to 14	4	12	2.71	0.678	32.52
14 to 20	6	17	0.43	0.0717	7.31

$$\bar{x} = \frac{\sum x_i d\phi_i}{\sum d\phi_i} = 0.68\,\mathrm{mm} \tag{4.19}$$

$$\sigma = 2.29\,\mathrm{mm} \tag{4.20}$$

Table 4.8 Relative percentage frequency distribution: tabular calculation of mean size
Sample 4FCUSAGE

Particle size range x_1 to x_2 mm	Interval dx_i mm	Average size x_i mm	Percentage in range $d\phi_i$ %	Percentage per mm $d\phi_i/dx_i$	$x_i d\phi_i$ mm
0 to 0.08	0.08	0.04	0.16	2	0.0064
0.08 to 0.16	0.08	0.12	14.12	176.5	1.694
0.16 to 0.315	0.16	0.2375	37.89	244.32	8.994
0.315 to 0.63	0.315	0.4725	11.30	35.873	5.339

Table 4.8 (Continued)   Relative percentage
frequency distribution: tabular calculation of mean size
Sample 4FCUSAGE

0.63 to 1.25	0.625	0.94i	6.50	10.484	6.11
1.25 to 2.5	1.25	1.875	7.05	5.64	13.219
2.5 to 5	2.5	3.75	6.11	2.444	22.913
5 to 10	5	7.5	5.85	1.17	43.875
10 to 14	4	12	2.94	0.735	35.28
14 to 20	6	17	0.77	0.128	13.09
20 to 28	8	24	7.32	0.915	175.68

$$\bar{x} = \frac{\sum x_i d\phi_i}{\sum d\phi_i} = 3.26\,\text{mm} \qquad (4.21)$$

$$\sigma = 6.52\,\text{mm} \qquad (4.22)$$

The granulometry curves

Figures 4.2 - 4.8 are the granulometry curves of the samples 1ARGVERT, 2FCUNEUF, 3FCNEUF and 4FCUSAGE. Figure 4.2 shows that 98.16% of the particles mean diameter of sample 1ARGVERT is 1.87 mm. So the sample 1ARGVERT can be thought as a uniform particle material. For the samples 2FCUNEUF, 3FCNEUF, and 4FCUSAGE, the behavior of a polydisperse material must be considered for the equivalent conductivity analysis.
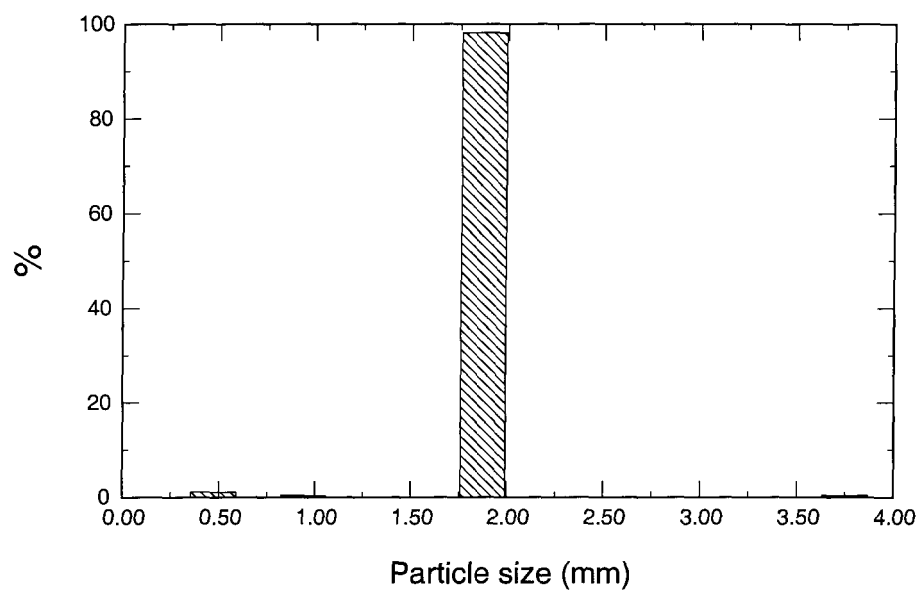
Figure 4.2 Percentage distribution of sample 1ARGVERT
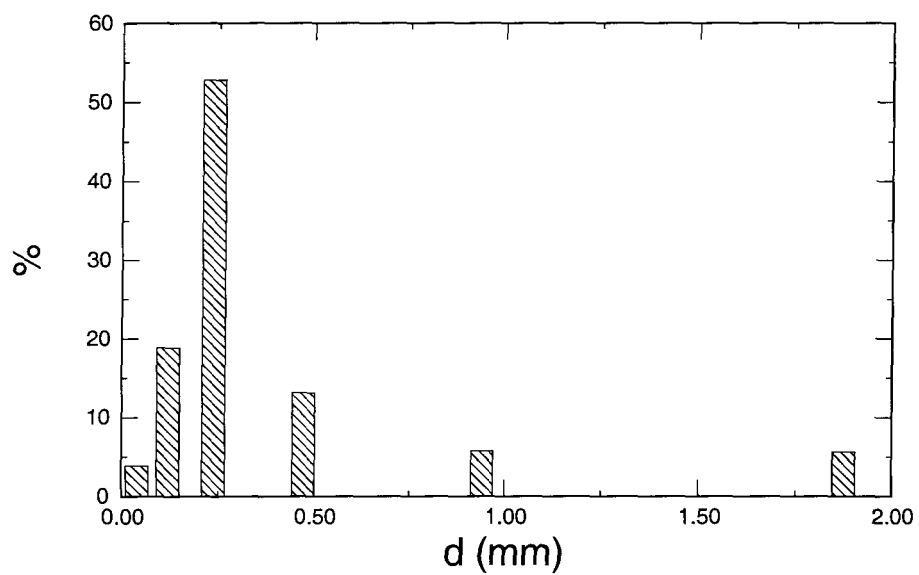
Figure 4.3 Percentage distribution of sample 2FCUNEUF
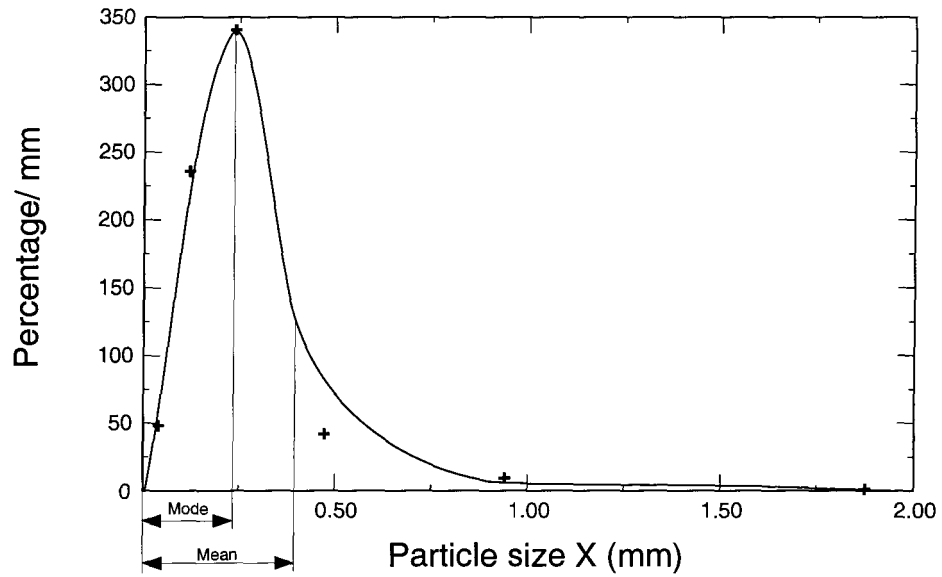
Figure 4.4 Relative percentage frequency curve of sample 2FCUNEUF
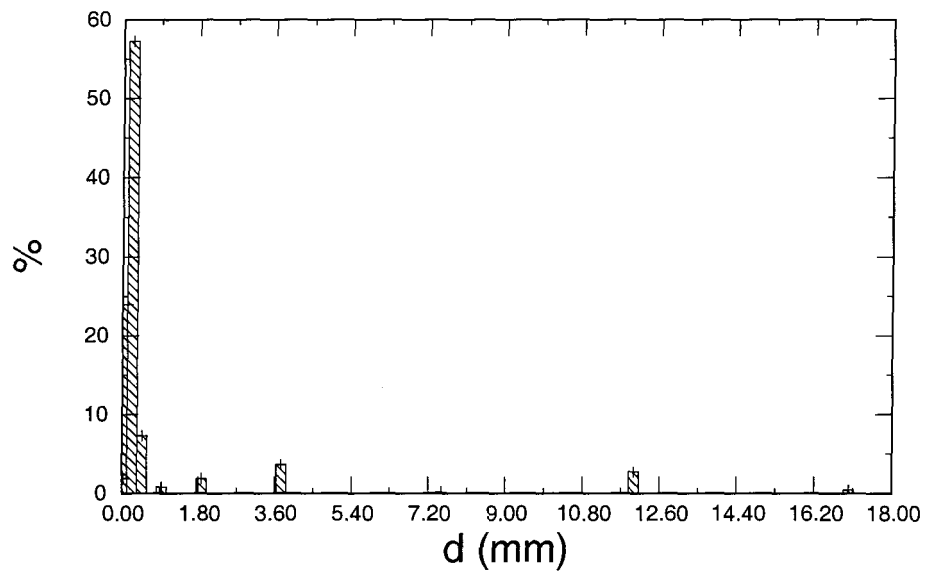
Figure 4.5 Percentage distribution of sample 3FCNEUF
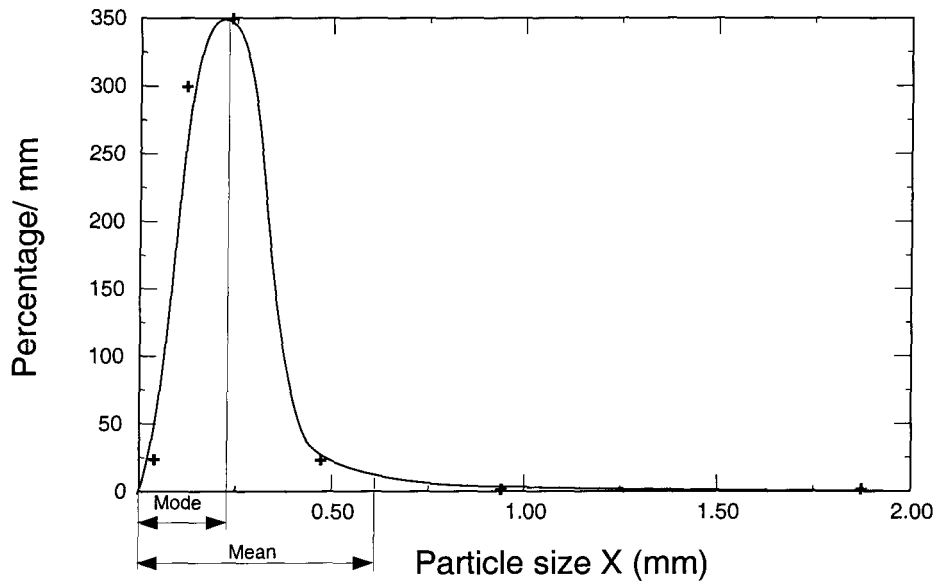
Figure 4.6 Relative percentage frequency curve of sample 3FCNEUF
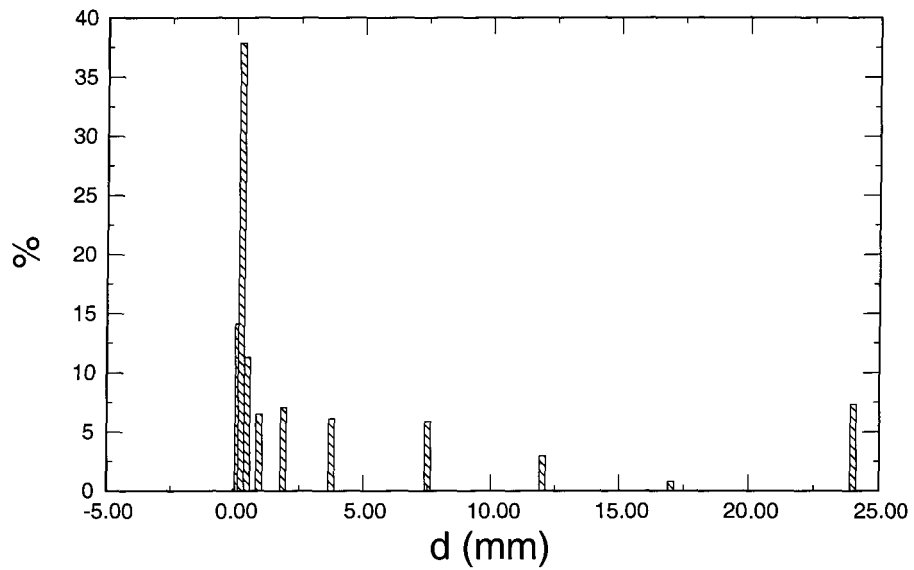
Figure 4.7 Percentage distribution of sample 4FCUSAGE

Chapter 4
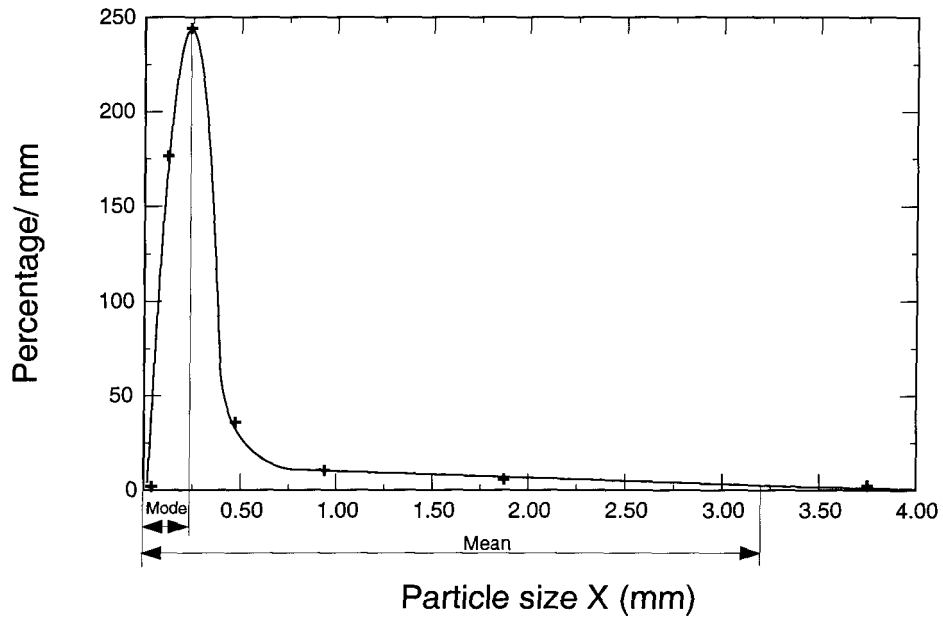
Figure 4.8 Relative percentage frequency curve of sample 4FCUSAGE

4.2 Thermal Conductivity Measurements Using the Guard-Heating Method

4.2.1 Apparatus

GRIPS has developed a device for samples with a conducting cross section of 150 mm × 150 mm (see Figures 4.9, 4.10 and 4.11). In this device, the area is divided into nine uniform, individually controlled and heated sections. The central square, which is equipped with a bottom guard heater (G9) and a "thermal null-indicator" is installed between the lower surface plate of the main heater and the upper surface plate of the bottom guard heater for detecting the heat flow from the main heater to the bottom guard heater. The bottom heater is controlled in a way to reduce the rear heat loss to zero, forcing the total electric energy input of the main heater through the sample. The lateral parasite heat fluxes are eliminated by the eight heated sections surrounding the central one. These lateral guards are maintained at a temperature as close as possible to the temperature of the central one. The purpose of the guard is to reduce the lateral losses as much as possible [1]. When the null-indicator is zero and the temperatures in eight heated plates are the same as the central one, there is no heat loss in axial and lateral direction. Thus a one-dimensional steady-state heat conduction is created.

This arrangement makes it possible to determine the thermal conductivity of granular materials at the temperature range slightly above ambient temperature, between approximately 25 and 80°C.
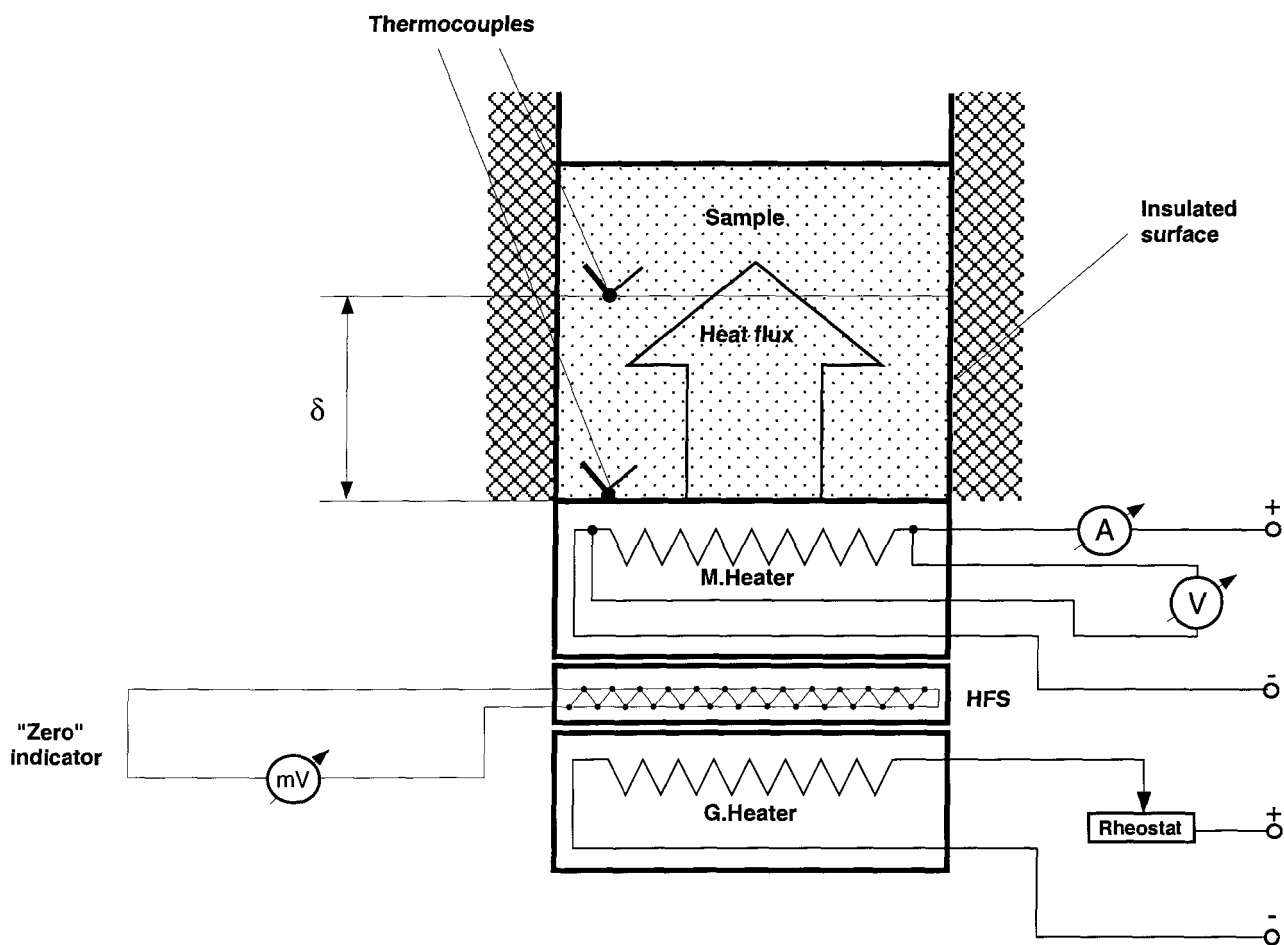
Figure 4.9 Guard heating method apparatus [13]
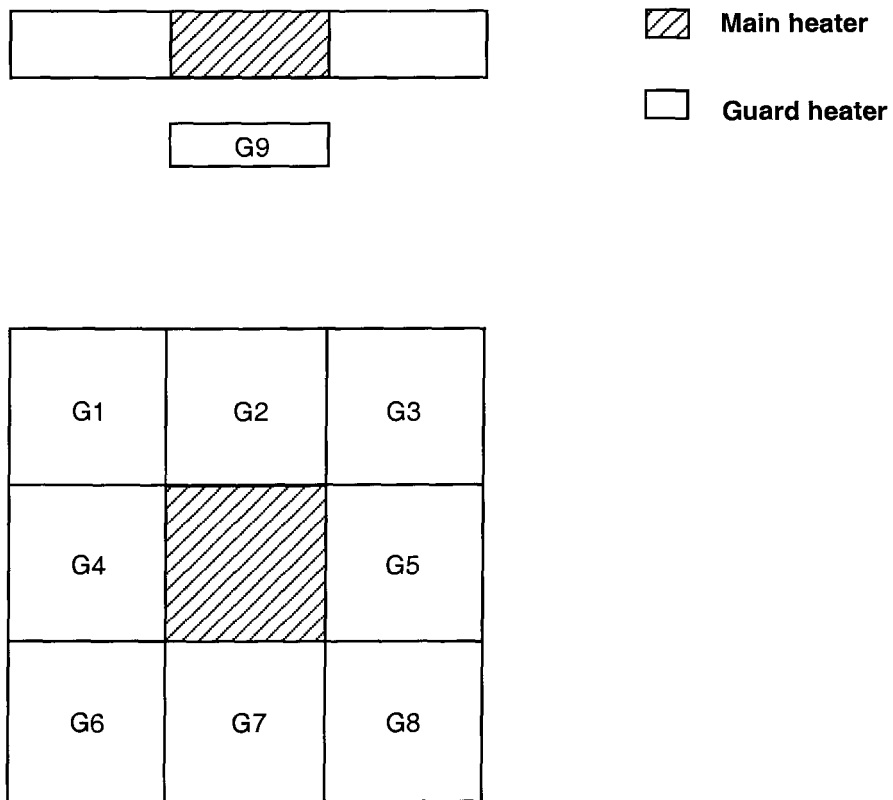
Figure 4.10 Heaters in the guarded heating method
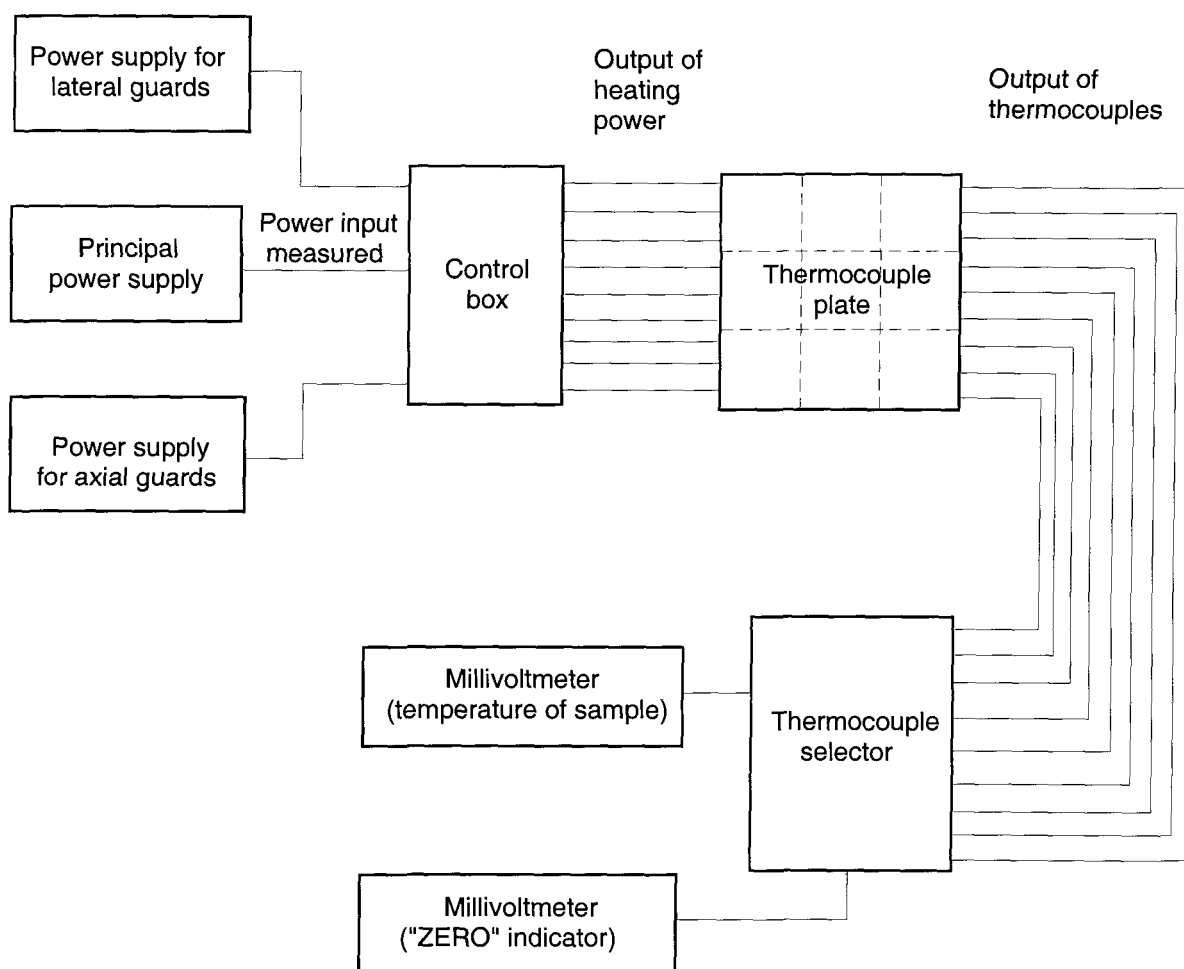
Figure 4.11 Schema of guarded heating method [21]

4.2.2 Sample preparation

This method does not need special sample preparation. However, mechanical treatments have a great influence upon the experimental results. The error occurs for particles varying greatly in size. Vibrations make samples more compact, but they also can result in segregation of the different particle fractions. The feeding

or shaking of samples causes the segregation or size separation. The large particles tend to accumulate at the top and side, small ones in the middle.

To reduce these influencing factors, the samples should be mixed well and randomly picked. The measurements should be done with 3 to 4 different thicknesses.

4.2.3 Evaluation

Under the condition of one-dimensional steady-state heat conduction inside the sample, we can calculate the thermal conductivity according to Fourier law (Equation 3.1). The thermal conductivity is

$$k = \frac{q \cdot \delta}{\Delta T} \tag{4.23}$$

Where δ is the thickness of the sample, m, ΔT is the temperature difference across the thickness of the sample, °C, $q = \frac{I \cdot U}{A}$, I is the electric current, A, U is voltage, V, A is the heating area, m^2.

Although the limited temperature range covers only a small portion of the industrial range, the measurements with this apparatus gave the differences due to the type and structure of the coke samples. Also, as these measurements provide directly the thermal conductivity, they give an important tool to validate the results of the transient measurements, which give the thermal diffusivity.

4.3 Study of the Solid Conductivity by Using the Flash Method [21] [16]

4.3.1 Apparatus

In the laboratory of GRIPS a cheap photographic type flash lamp is used as energy source, and spring loaded, needle-type thermocouple wires are measuring the rear surface temperature history. Instead of increasing pulse energy, we focused our attention on improvement of the measurement of small temperature transients by improving the signal-to-noise ratio at the source of the signal.

With the flashlamp, the typical temperature amplitude is around $1°C$, which means that using chromel-alumel type thermocouple, the whole voltage transient to be measured and recorded lies in the $0 - 50$ microvolt range. Extra efforts were made to minimize the pickup of electromagnetic noise by the wire loop between the thermocouple junction and the preamplifier. The two sharpened tip thermocouple wires are pressed individually against the sample surface, so the electrical circuit is through the sample itself. The wires protrude a few millimeters from a metallic box, which acts as a shield. Three spring loaded, self-adjusting insulator pins keep the sample parallel to the surface of the metallic box, leaving only a small gap for the movement of the thermocouple pins. Two identical holders are integrated into the box for the sample and reference materials. The distance between the sample and the reference is kept at minimum to ensure homogeneous distribution of pulse energy.

The preamplifiers are placed directly under the samples inside the electromagnetically shielded box to minimize the length of input wires. As the knowledge of the temperature level is not important for the evaluation, the reference junctions of the thermocouples are left at ambient temperature. The output of the preamplifiers is in the millivolt range so the signals can be easily recorded by a standard laboratory data acquisition system.

Generally, measurements are taken at 1 millisecond intervals. The reading is started by the manual release of the flash unit, then the data acquisition process is optically triggered by the flashlight itself, using the signal from a fast-response photosensor built into the sample holder.

During the development phase, a special study was made to ensure the uniformity of the flash energy distribution over the twin sample holder. The heating pattern of the flash at various reflector settings, with and without optical beam modifiers, was analyzed by infrared thermography. A series of aperture plates was installed between the flash and sample holder to improve the parallelism of the beam and to prevent unwanted lateral reflections. The measured temperature transients are primarily stored and analyzed by a computer.

4.3.2 Sample preparation

The sample size is 25 mm (diameter) × 2.0 mm (thickness). Packing materials with heterogenous, discontinuous structure require special attention during sample

preparation. Obviously, if the characteristic size of inhomogeneities (grains, particles, bubbles, cavities) are of comparable or bigger size than the sample thickness, the specimen is not characteristic of the bulk of the material.

To test these types of materials, we apply a thin, extremely well conducting thin metallic foil (electrolytic copper) on one or both parallel surfaces of the sample. Hard rolled foils with $10 - 15$ micrometer thickness are easy to handle and their contribution to the heat capacity of the sample is generally only $2 - 6\%$. The critical point in their application is the good and uniform thermal contact between the foil and the sample. Self-adhesive foils have a thin, but non-metallic, poorly conductive glue layer and sometimes they show a tendency to entrap small quantities of air.

A better solution to attach the foils to the surface of the specimens was found by using a conductive resin with high solid silver content. A special roller-applicator is used for spreading the resin uniformly over the surface of the foil, at the same time preventing it from penetrating into the cavities of the sample.

4.3.3 Evaluation

The first step of evaluation [16] is the determination of thermal diffusivity using the classical formula (Equation 3.12). Then the volumetric heat capacity of the sample is calculated from the ratio of thickness, maximum temperatures, and the properties of the reference material (Equation 3.14).

The effect of the losses is corrected as follows:

The heat conduction process during the experiment is described in dimensionless form, assuming that small temperature variations permit the application of the linear theory.

Using the basic definitions of the theory of heat conduction, the transient temperature distribution can be expressed in the following form

$$\vartheta = \vartheta(\text{Fo}, \text{Bi}) \tag{4.24}$$

where $\vartheta = \Delta T / \Delta T_{\text{MAX}}$ is the normalized temperature, $\text{Fo} = \alpha\tau/\delta^2$ is the Fourier number and $\text{Bi} = h\delta/k$ is the Biot number.

Analyzing the character of the transient heat conduction within the sample, one can find that in the cooling period the temperature on the rear surface is a function of a single variable only, namely that of the FoBi product.

Under real conditions during the measurement, the Biot number has a small value, so the cooling history after the point of the second inflexion can be well described by the following simple exponential term

$$\vartheta = \vartheta^* exp(-\text{BiFo}^*) \tag{4.25}$$

Where ϑ^* denotes a dimensionless temperature after the second point of inflexion, and Fo* is calculated from the corresponding time instant.

Chapter 4

The numerical factor of 1.37 in Equation 3.12 is not constant in case of non-zero heat losses, but depends on $Fo_{1/2}Bi$, where $Fo_{1/2}$ is the dimensionless time corresponding to the $\tau_{1/2}$ half-rise time.

$$(Fo_{1/2}\pi^2)$$
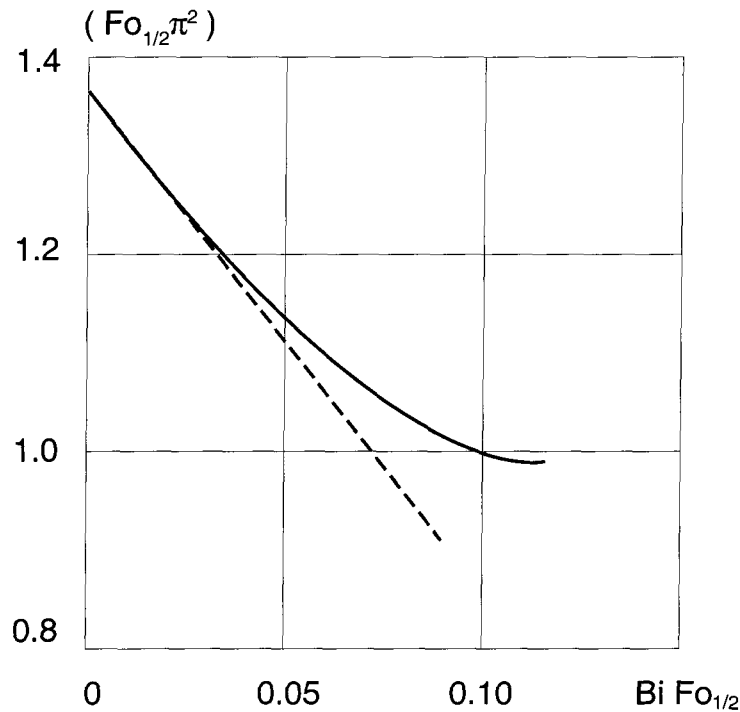
Figure 4.12 Correlation between the dimensionless groups for the non perfectly insulated case

For small deviations from the perfectly insulated case, the curve can be approximated by a linear formula

$$\frac{\alpha_{CORR}}{\alpha} = f = 1 - 3.94BiFo_{1/2} \qquad (4.26)$$

Where f is a dimensionless correction factor, α_{CORR} is the diffusivity value corrected according to heat losses ($Bi > 0$), and α is calculated from Equation 3.12.

During the evaluation, the exponent in Equation 4.25 is determined from an exponential curve fitting. In case of a noise-free smooth curve, the exponent can be found as the logarithm of the ratio of two consecutive temperatures

$$BiFo^*_{2-1} = ln\frac{\vartheta_2}{\vartheta_1} \tag{4.27}$$

Where Fo^*_{2-1} is the dimensionless time interval between points 2 and 1, and ϑ_1, ϑ_2, are the corresponding temperatures.

From Equation 4.27 and from the definitions of the dimensionless variables we obtain

$$BiFo_{1/2} = \frac{\tau_{1/2}}{\tau_2 - \tau_1}BiFo^*_{2-1} \tag{4.28}$$

Using the definition of the f correction factor, we can calculate the corrected value of the diffusivity

$$\alpha_{CORR} = f\alpha \tag{4.29}$$

Finally, the conductivity of the sample

$$k = (\rho c_p)\alpha_{CORR} \tag{4.30}$$

Chapter 5 DETERMINATION OF THE THERMOPHYSICAL PROPERTIES IN A WIDE TEMPERATURE RANGE

5.1 Development of the Experimental Apparatus Using the Monotonic Heating Regime

We have developed a monotonic heating apparatus. The sample is filled into an annular cylindrical vessel, which provides points for temperature measurement on the surface and in the center (see Figure.5.1) [1]. Three controllers were used to control the temperature on the surface of the sample separately according to a linear increase of the temperature. After an initial period of time the temperature in the center increases linearly.

To complete the above tasks, a heating system with the controllable heating rate on the surface of the sample was developed. The schema of the apparatus (in Figure 5.1) shows that the cylindrical sample is heated by a furnace inside a vessel. The temperature on the surface of the sample measured by the thermocouples is transmitted to the controller. The controller output signal is sent to the heater system to adjust the heating energy so that the desirable heating rate on the surface of the sample can be obtained.
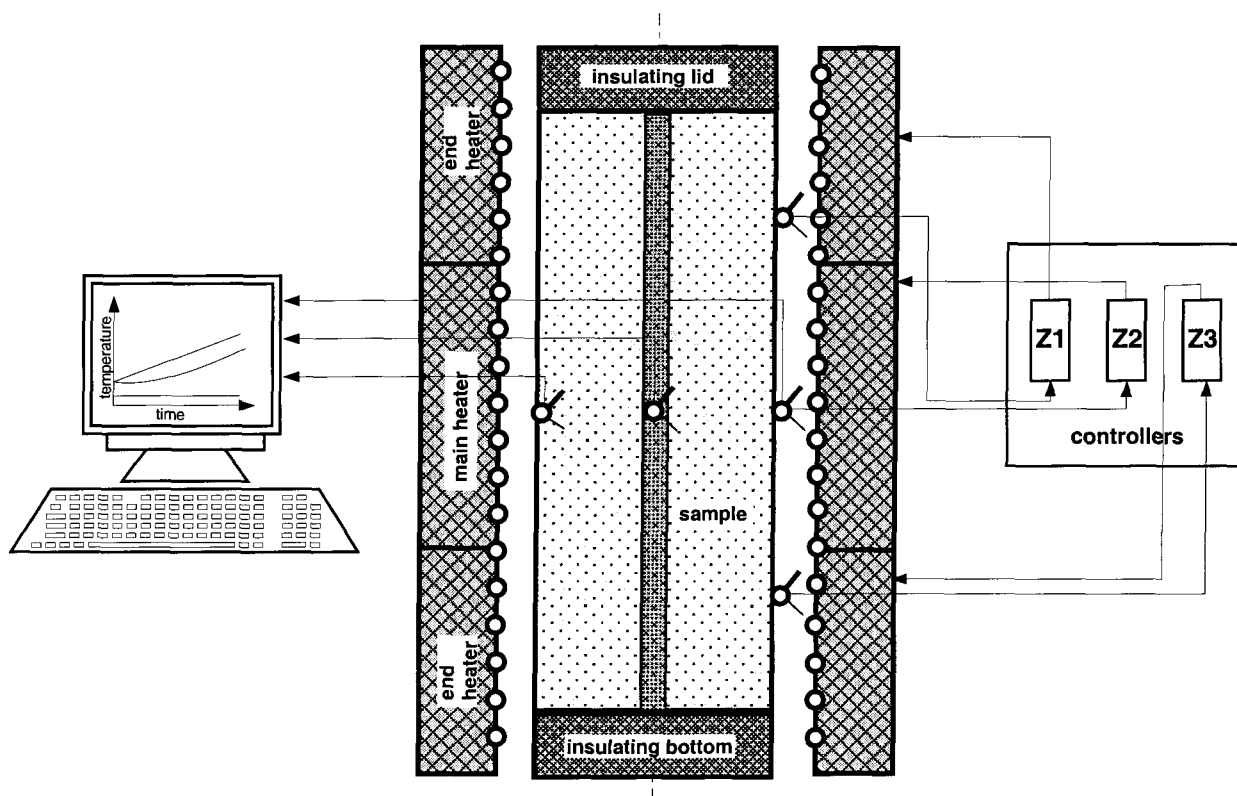
Figure 5.1 Schematic layout of the sample compartment of the monotonic heating apparatus

5.1.1 Dynamic model of the experimental apparatus

Definition of the model

To analyze the dynamic behavior of the experimental setup we have developed a model in Figure 5.2 which includes the following four parts:

m1: the heater — electrical resistance wire embedded in a ceramic material.

m3 and m4: sample compartment — packing coke in a stainless steel container.

m5: external stainless steel shell (vessel).
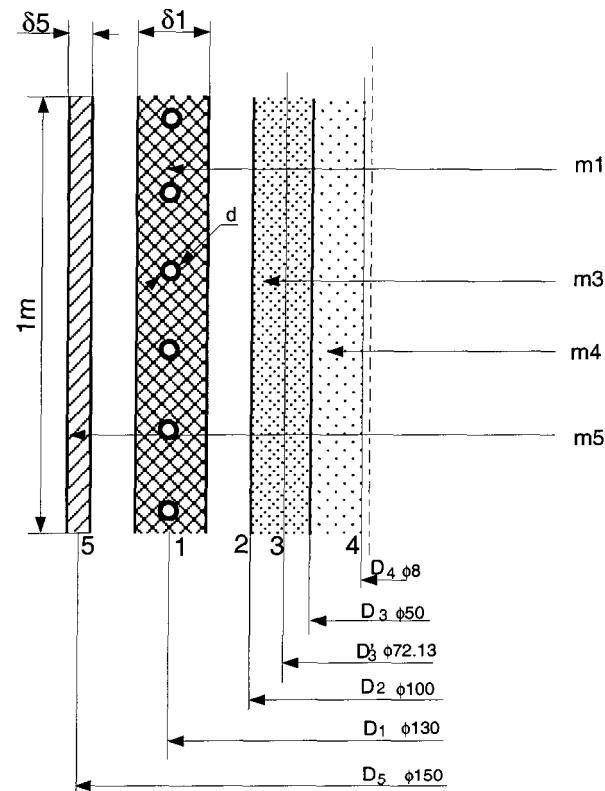
Figure 5.2 The lumped parameter model of the system

During the analysis, the hollow cylindrical furnace, the external shell as well as the sample are treated as infinitely long bodies with cylindrical symmetry. All numerical calculations were made for a 1 meter long section of the long cylinder. The sample was divided into two-lumps, in order to keep the dynamic model as simple as possible. This two–lump model does not describe precisely the details of the heat conduction inside the sample, but reflects well the second-order character of the transients. Because there is no heat flux in the center of the sample the

point 4 is treated as the central axis for calculation of the thermal resistance of the lump model.

Electrical analogy

To obtain the set of equations which describe the dynamic behavior of the system, an electrical analog circuit was set up according to Figure 5.3.
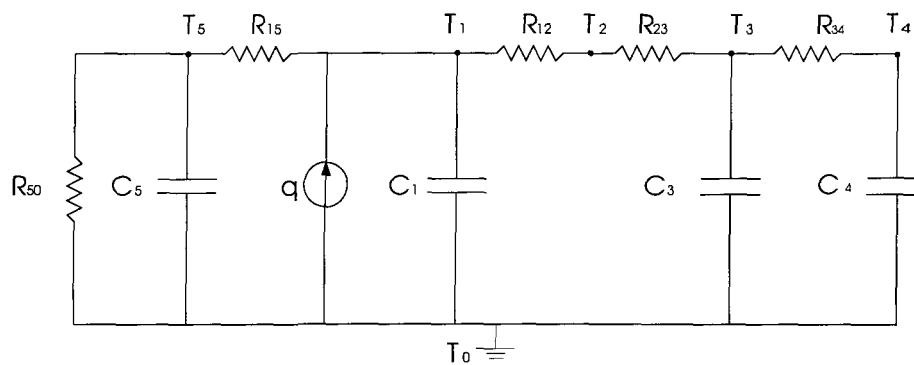
Figure 5.3 Electrical analogy of the heating system

Where:

q: heat source, W.

T_1: temperature of the heater, °C.

C_1: heat capacity of heater, kJ/°C.

T_2: temperature of the sample surface (point 2), °C.

T_3: temperature of the lump of the sample with the mass of m3, °C.

C_3: heat capacity of the lump of the sample with the mass of m3, kJ/°C.

T_4: temperature of the second lump of the sample with the mass of m4, °C.

C_4: heat capacity of the second lump of the sample with the mass of m4, kJ/°C.

T_5: temperature of the vessel, °C.

C_5: heat capacity of the vessel, kJ/°C.

R_{15}: thermal resistance between the heater and the vessel, °C/W.

R_{50}: thermal resistance from the vessel to the environment, °C/W.

R_{12}: thermal resistance from the heater to the surface of the sample, °C/W.

R_{23}: thermal resistance from the surface of the sample to point of T_3 inside the sample, °C/W.

R_{13}: $R_{12}+R_{23}$, °C/W.

R_{34}: thermal resistance from the point of T_3, inside the sample, to point of T_4, the center of the sample, °C/W.

Differential equation

The matrix of the system is:

$$\begin{bmatrix} sC_1 + \frac{1}{R_{13}} + \frac{1}{R_{15}} & -\frac{1}{R_{13}} & 0 & -\frac{1}{R_{15}} \\ -\frac{1}{R_{13}} & \frac{1}{R_{13}} + \frac{1}{R_{34}} + sC_3 & -\frac{1}{R_{34}} & 0 \\ 0 & -\frac{1}{R_{34}} & \frac{1}{R_{34}} + sC_4 & 0 \\ -\frac{1}{R_{15}} & 0 & 0 & \frac{1}{R_{50}} + \frac{1}{R_{15}} + sC_5 \end{bmatrix} \begin{bmatrix} T_1 \\ T_3 \\ T_4 \\ T_5 \end{bmatrix} = \begin{bmatrix} q \\ 0 \\ 0 \\ 0 \end{bmatrix}$$

(5.1)

The equations of the system are:

$$C_1 \frac{dT_1}{dt} + \left(\frac{1}{R_{13}} + \frac{1}{R_{15}}\right)T_1 - \frac{1}{R_{13}}T_3 - \frac{1}{R_{15}}T_5 = q$$

$$-\frac{1}{R_{13}}T_1 + C_3 \frac{dT_3}{dt} + \left(\frac{1}{R_{13}} + \frac{1}{R_{34}}\right)T_3 - \frac{1}{R_{34}}T_4 = 0$$

$$-\frac{1}{R_{34}}T_3 + \frac{1}{R_{34}}T_4 + C_4 \frac{dT_4}{dt} = 0$$

$$-\frac{1}{R_{15}}T_1 + C_5 \frac{dT_5}{dt} + \left(\frac{1}{R_{50}} + \frac{1}{R_{15}}\right)T_5 = 0$$

$$(5.2)$$

The differential equations of the heating system are:

$$\frac{dT_1}{dt} = \frac{1}{C_1}\left[-\left(\frac{1}{R_{13}} + \frac{1}{R_{15}}\right)T_1 + \frac{1}{R_{13}}T_3 + \frac{1}{R_{15}}T_5 + q\right]$$

$$\frac{dT_3}{dt} = \frac{1}{C_3}\left[\frac{1}{R_{13}}T_1 - \left(\frac{1}{R_{13}} + \frac{1}{R_{34}}\right)T_3 + \frac{1}{R_{34}}T_4\right]$$

$$\frac{dT_4}{dt} = \frac{1}{C_4}\left[\frac{1}{R_{34}}T_3 - \frac{1}{R_{34}}T_4\right]$$

$$\frac{dT_5}{dt} = \frac{1}{C_5}\left[\frac{1}{R_{15}}T_1 - \left(\frac{1}{R_{50}} + \frac{1}{R_{15}}\right)T_5\right]$$

$$(5.3)$$

Representation of state variables

To find the transfer function of our heating system, we suppose the state variables are $x_i = T_i$.

Then we can put the state variables into the standard matrix form:

$$\dot{\mathbf{x}} = \mathbf{A}\mathbf{x} + \mathbf{B}u \qquad (5.4)$$

with:

$$
\mathbf{A} = \begin{bmatrix} -\frac{1}{C_1}\left(\frac{1}{R_{13}} + \frac{1}{R_{15}}\right) & \frac{1}{C_1 R_{13}} & 0 & \frac{1}{C_1 R_{15}} \\ \frac{1}{C_3 R_{13}} & -\frac{1}{C_3}\left(\frac{1}{R_{13}} + \frac{1}{R_{34}}\right) & \frac{1}{C_3 R_{34}} & 0 \\ 0 & \frac{1}{C_4 R_{34}} & -\frac{1}{C_4 R_{34}} & 0 \\ \frac{1}{C_5 R_{15}} & 0 & 0 & -\frac{1}{C_5}\left(\frac{1}{R_{50}} + \frac{1}{R_{15}}\right) \end{bmatrix}
$$

$$(5.5)$$

$$
\mathbf{B} = \begin{bmatrix} \frac{1}{C_1} \\ 0 \\ 0 \\ 0 \end{bmatrix}, \qquad \mathbf{x} = \begin{bmatrix} x_1 \\ x_3 \\ x_4 \\ x_5 \end{bmatrix}, \qquad \dot{\mathbf{x}} = \begin{bmatrix} \dot{x}_1 \\ \dot{x}_3 \\ \dot{x}_4 \\ \dot{x}_5 \end{bmatrix}, \qquad u = q \qquad (5.6)
$$

Determination of the parameters in our experimental conditions

I Calculation of the parameters of the lump model

(See definitions in 1, all parameters are calculated for 1 meter length, $L = 1$ m, of a long cylindrical furnace)

a) C_1: $C_1 = \delta_1 \rho_c c_{pc} 2\pi D_1 L + \frac{d^2 \pi}{4} l' L \rho_w c_{pw} = 18.38 \, \mathrm{kJ}/^\circ\mathrm{C}$

where: δ_1 = thickness of the ceramic layer, m;

ρ_c, c_{pc} = density (kg/m^3) and specific heat (kJ/kgK) of ceramic substrate of the heater;

D_1 = mean diameter of the heater, m;

d = diameter of the heating wire, m;

l' = length of heating wire per unit length of the heater, m/m;

ρ_w, c_{pw} = density (kg/m), specific of heat (kJ/kgK) of wire.

b) C_3: $C_3 = \frac{\pi\left(D_2^2 - D_3^2\right)}{4}L\rho_2 c_{p2} = 6.9\,\text{kJ}/^\circ\text{C}$

where: D_2 = the diameter of the sample, m;

D_3 = diameter of mass m4, m;

ρ_2, c_{p2} = density (kg/m^3) and specific heat (kJ/kgK) of the sample.

c)$C_4 = \frac{\pi D_3^2}{4}L\rho_2 c_{p2} = 2.3\,\text{kJ}/^\circ\text{C}$.

d)$C_5 = \delta_5 \pi D_5 L\rho_5 c_{p5} = 10.56\,\text{kJ}/^\circ\text{C}$

where: δ_5 = thickness of the shell, m;

ρ_5, c_{p5} = density (kg/m^3) and specific heat (kJ/kgK) of the shell;

D_5 = mean diameter of the shell, m;

e) $R_{13} = R_{12rad} + R_{23} = 0.1135$ °C/W.

$$R_{12rad} = \frac{\frac{1}{\epsilon_1} + \frac{A_1}{A_2}\left(\frac{1}{\epsilon_2} - 1\right)}{\sigma_0 A_1\left(T_1^2 + T_2^2\right)(T_1 + T_2)} \tag{5.7}$$

$$R_{23} = \frac{ln\frac{D_2}{D_3}}{2\pi L k_2} \tag{5.8}$$

where: ϵ_1 = emissivity of the heater body;

ϵ_2 = emissivity of the sample;

A_1 is the area of the heater, m^2, $A_1 = \pi D_1 L$;

A_2 is the area of the sample, m^2, $A_2 = \pi D_2 L$;

k_2 = thermal conductivity of the sample, W/mK;

σ_0 is Stefan-Boltamann constant with the value of 5.669×10^{-8} W/m^{2}K^4.

f)$R_{34} = \dfrac{ln\frac{D'_3}{D_4}}{2\pi L k_2} = 0.39^\circ$C/W.

g)$R_{15} = R_{rad15} = \dfrac{\frac{1}{\epsilon_1}+\frac{A_1}{A_5}\left(\frac{1}{\epsilon_5}-1\right)}{\sigma A_1(T_1^2+T_5^2)(T_1+T_5)} = 0.0515^\circ$C/W

Where, A_5 is the area of the shell, m^2, $A_5 = D_5 \pi L$;

ϵ_5 is the emissivity of the shell.

h)$R_{50} = \dfrac{R_{rad50}R_{conv50}}{R_{rad50}+R_{conv50}} = 0.076^\circ$C/W.

where: $R_{rad50} = \dfrac{1}{\sigma A_5 \epsilon_5(T_1^2+T_5^2)(T_1+T_5)}$;

$R_{conv50} = \dfrac{1}{hA_5}$;

h = convection heat transfer coefficient, W/m^2°C.

II The summary of the material properties and calculated results

Tables 5.1 – 5.3 give the parameters of the heating system, calculated from the experimental data.

Table 5.1 Physical properties of the materials

	m1 (ceramics)	m2, m3 (coke)	m5(stainless steel)
k (W/mK)	2	1	30
ρ (kg/m^3)	2 500	1 172	7 900
c_p (J/kgK)	900	1 000	4 600
ϵ	0.6	0.65	0.6

Table 5.2 Thermal resistances in the system (°C/W)

R_{12}	R_{23}	R_{13}	R_{34}	R_{15}	R_{50}
0.0615	0.052	0.1135	0.39	0.0515	0.076

Table 5.3 Thermal capacities of the lumped masses (kJ/m°C)

C_1	C_3	C_4	C_5
18.38	6.9	2.3	10.56

III The state equation with the actual parameters

Substituting the above numerical values into matrices **A** and **B**, we have:

$$
\mathbf{A} = \begin{bmatrix}
-1.551 & 0.4946 & 0 & 1.056 \\
1.317 & -1.689 & 0.3716 & 0 \\
0 & 1.115 & -1.115 & 0 \\
1.839 & 0 & 0 & -3.085
\end{bmatrix}
\tag{5.9}
$$

$$
\mathbf{B} = \begin{bmatrix}
0.054 \\
0 \\
0 \\
0
\end{bmatrix}
\tag{5.10}
$$

So the state equation is:

$$
\begin{bmatrix}
\dot{x}_1 \\
\dot{x}_3 \\
\dot{x}_4 \\
\dot{x}_5
\end{bmatrix}
=
\begin{bmatrix}
-1.551 & 0.4946 & 0 & 1.056 \\
1.317 & -1.689 & 0.3716 & 0 \\
0 & 1.115 & -1.115 & 0 \\
1.839 & 0 & 0 & -3.085
\end{bmatrix}
\begin{bmatrix}
x_1 \\
x_3 \\
x_4 \\
x_5
\end{bmatrix}
+
\begin{bmatrix}
0.054 \\
0 \\
0 \\
0
\end{bmatrix}
u
\tag{5.11}
$$

The transformation of state variables

As we are interested in the surface temperature of the sample (T_2), we transform the matrices $\mathbf{A}$ and $\mathbf{B}$ into $\bar{\mathbf{A}}$ and $\bar{\mathbf{B}}$. The change of variables is represented by a linear transformation:

$$\mathbf{z} = \mathbf{Tx} \tag{5.12}$$

$$\mathbf{x} = \mathbf{T}^{-1}\mathbf{z} \tag{5.13}$$

$$\frac{T_1 - T_2}{R_{12}} = \frac{T_1 - T_3}{R_{13}} \tag{5.14}$$

$$T_1 = \frac{R_{13}}{R_{23}}T_2 - \frac{R_{12}}{R_{23}}T_3 = 2.18T_2 - 1.18T_3 \tag{5.15}$$

$$\begin{bmatrix} T_1 \\ T_3 \\ T_4 \\ T_5 \end{bmatrix} = \begin{bmatrix} 2.18 & -1.18 & 0 & 0 \\ 0 & 1 & 0 & 0 \\ 0 & 0 & 1 & 0 \\ 0 & 0 & 0 & 1 \end{bmatrix} \begin{bmatrix} T_2 \\ T_3 \\ T_4 \\ T_5 \end{bmatrix} \tag{5.16}$$

$$\mathbf{T}^{-1} = \begin{bmatrix} 2.18 & -1.18 & 0 & 0 \\ 0 & 1 & 0 & 0 \\ 0 & 0 & 1 & 0 \\ 0 & 0 & 0 & 1 \end{bmatrix} \tag{5.17}$$

$$\mathbf{T} = \begin{bmatrix} 0.4587 & 0.5413 & 0 & 0 \\ 0 & 1 & 0 & 0 \\ 0 & 0 & 1 & 0 \\ 0 & 0 & 0 & 1 \end{bmatrix} \tag{5.18}$$

$$\bar{\mathbf{A}} = \mathbf{TAT}^{-1} = \begin{bmatrix} 0.0031 & -0.6890 & 0.2011 & 0.4844 \\ 2.8711 & -3.2431 & 0.3716 & 0 \\ 0 & 1.1150 & -1.1150 & 0 \\ 4.0090 & -2.1700 & 0 & -3.0850 \end{bmatrix} \tag{5.19}$$

$$\bar{\mathbf{B}} = \mathbf{TB} = \begin{bmatrix} 0.0248 \\ 0 \\ 0 \\ 0 \end{bmatrix} \quad (5.20)$$

The new state equation is:

$$\begin{bmatrix} \dot{x}_2 \\ \dot{x}_3 \\ \dot{x}_4 \\ \dot{x}_5 \end{bmatrix} = \begin{bmatrix} 0.0031 & -0.6890 & 0.2011 & 0.4844 \\ 2.8711 & -3.2431 & 0.3716 & 0 \\ 0 & 1.1150 & -1.1150 & 0 \\ 4.0090 & -2.1700 & 0 & -3.0850 \end{bmatrix} \begin{bmatrix} x_2 \\ x_3 \\ x_4 \\ x_5 \end{bmatrix} + \begin{bmatrix} 0.0248 \\ 0 \\ 0 \\ 0 \end{bmatrix} u \quad (5.21)$$

Considering T_2 as the output of our system, the output matrix $\bar{\mathbf{C}}$ is:

$$\bar{\mathbf{C}} = \begin{bmatrix} 1 & 0 & 0 & 0 \end{bmatrix} \quad (5.22)$$

The observation equation is:

$$y = \bar{\mathbf{C}}\mathbf{x} = \begin{bmatrix} 1 & 0 & 0 & 0 \end{bmatrix} \begin{bmatrix} x_2 \\ x_3 \\ x_4 \\ x_5 \end{bmatrix} \quad (5.23)$$

5.1.2 Controllability and observability [22]

Controllability

The controllability of our system can be analyzed by means of the control matrix $\mathbf{Q}$ which is defined as:

$$\mathbf{Q} = \begin{bmatrix} \bar{\mathbf{B}} & \bar{\mathbf{A}}\bar{\mathbf{B}} & \bar{\mathbf{A}}^2\bar{\mathbf{B}} & \bar{\mathbf{A}}^3\bar{\mathbf{B}} \end{bmatrix} = \begin{bmatrix} 0.0248 & 0.0001 & -0.0009 & -0.0484 \\ 0 & 0.0712 & -0.2307 & 0.7751 \\ 0 & 0 & 0.0794 & -0.3458 \\ 0 & 0.0994 & -0.4609 & 1.9190 \end{bmatrix}$$

$$(5.24)$$

$$det(\mathbf{Q}) = 3.2557 \times 10^{-5} \qquad (5.25)$$

which is not zero, therefore the system is controllable.

Observability

The observability can be found by determining the observation matrix $\mathbf{N}$

$$\mathbf{N} = \begin{bmatrix} \bar{\mathbf{C}}^T & \bar{\mathbf{A}}^T\bar{\mathbf{C}}^T & \left(\bar{\mathbf{A}}^T\right)^2\bar{\mathbf{C}}^T & \left(\bar{\mathbf{A}}^T\right)^3\bar{\mathbf{C}}^T \end{bmatrix} = \begin{bmatrix} 1 & 0.0031 & -0.0362 & -1.9499 \\ 0 & -0.6890 & 1.4054 & -1.8283 \\ 0 & 0.2011 & -0.4796 & 1.0498 \\ 0 & 0.4844 & -1.4929 & 4.5880 \end{bmatrix}$$
$$(5.26)$$

$$det(\mathbf{N}) = -0.0215 \qquad (5.27)$$

which is not zero, therefore the variables of the system are observable.

5.1.3 Model in open loop

Transfer Function of the Open Loop

$$H(s) = \bar{\mathbf{C}}\Phi(s)\bar{\mathbf{B}} \qquad (5.28)$$

$$\Phi(s) = \left(s\mathbf{I} - \bar{\mathbf{A}}\right)^{-1} \qquad (5.29)$$

$$H(s) = \frac{0.0248s^3 + 0.1844s^2 + 0.4123s + 0.2447}{s^4 + 7.44s^3 + 16.6597s^2 + 12.0453s + 1.9352} \qquad (5.30)$$

From the above formula of the transfer function *H(s)*, we can conclude that this is a 4$^{\text{th}}$ order system.

Stability

By using the software package MATLAB, the poles and zeros of the system were determined.

The zeroes are:

$$z_1 = -3.389$$

$$z_2 = -3.1105$$

$$z_3 = -0.9360$$

The poles are:

$$p_1 = -3.9925$$

$$p_2 = -2.2622$$

$$p_3 = -0.9627$$

$$p_4 = -0.22256$$

Because all the four poles are on the left side of the imaginary axis of the complex plane, the system is stable.

The response of the heating system in open loop

The block diagram of the heating system of open loop including the signal generator, power supply unit and heater assembly is shown in Figure 5.4.

T=Tmin+aτ [°C] → | Signal generator K_m | → $\tilde{T}$ [mA] → | Power Supply unit K_m | → Q(s) [w] → | Heater System $H(s)$ | → T′ [°C]
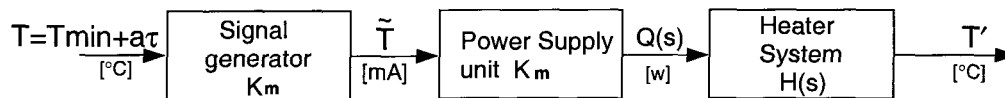
Figure 5.4 Block diagram for the entire control system

In our project the heating range is from room temperature (20°C) to 1 300°C. The maximum power of the heater is estimated as Q = 2 300 W. The rate of heating is achieved by adjusting the signal generator unit to the desired ramp value (°C/s). Also, the starting and maximum temperatures are set on this unit. The outputs of the signal generator is in the standard 4 – 20 mA current signal range (4 mA → 0% and 20 mA → 100% of the signal.)

The K_m and K_T are defined as:

$$K_m = \frac{range\ of\ signal\ generator\ output}{range\ of\ signal\ generator\ input} = \frac{20-4}{1300-20} = 0.0125\,\text{mA}/°\text{C}$$

$$(5.31)$$

$$K_T = \frac{range\ of\ heating\ energy}{range\ of\ instrument\ input} = \frac{2300}{20-4} = 143.75\,\text{W}/\text{mA} \qquad (5.32)$$

The transfer function of the system is

$$G(S) = K_m K_T H(s) = \frac{0.04456s^3 + 0.3314s^2 + 0.7409s + 0.4397}{s^4 + 7.44s^3 + 16.6597s^2 + 12.0453s + 1.9352} \qquad (5.33)$$

By using MATLAB the response in open loop of the ramp input is shown in Figure 5.5
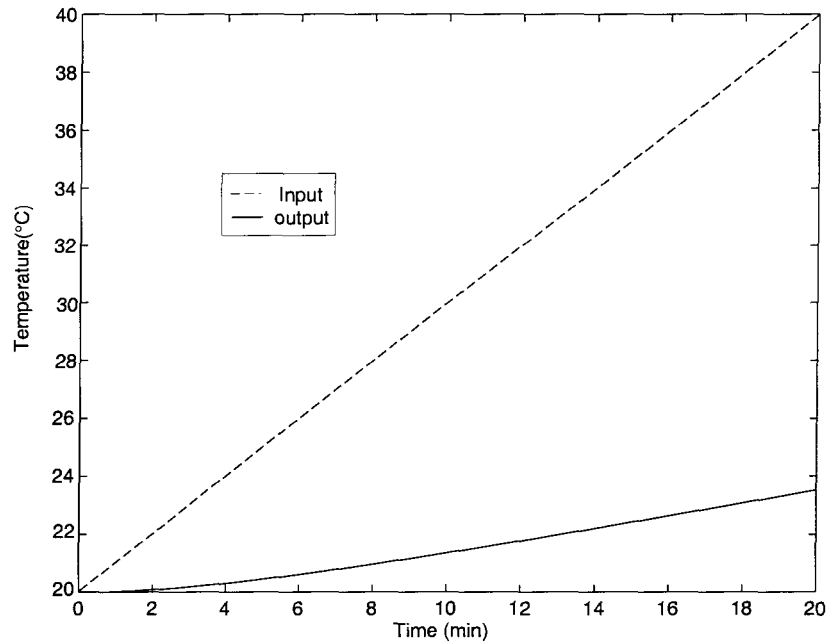
Figure 5.5 Open loop system response

From Figure 5.5, we see that the open loop response has two types of error:

1. The slope of the temperature increase does not follow the prescribed rate. The signal generator provides $1°C/min$, and the system has only $0.23°C/min$.

2. The surface temperature follows the increase of the set value with a significant time delay.

5.1.4 Feedback controller design [23]

In order to get a better control of the surface temperature of the sample during the heating, a closed loop control-system should be developed. The objectives of

applying closed loop control are:

1. The surface temperature follows the linear law as fast as possible.

2. The error in the heating rate (slope) is small.

3. The system has a good stability.

The closed-loop transfer functions

The block diagram for our feedback control system is shown in Figure 5.6
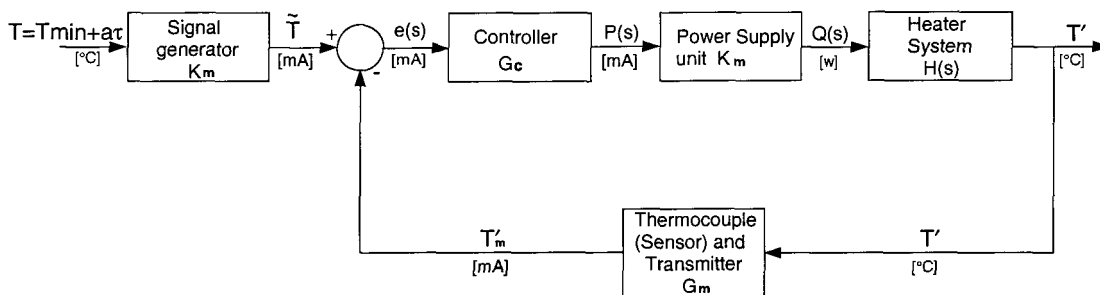
Figure 5.6 Block diagram for the entire control system

The thermocouple transmitter and controller signals are in the standard 4 −

20 mA current range.

Assuming $K_m = G_m$ and that the elements of the feedback system are linear,

the system can be put into the form of a unity feedback system as shown in

Figure 5.7.
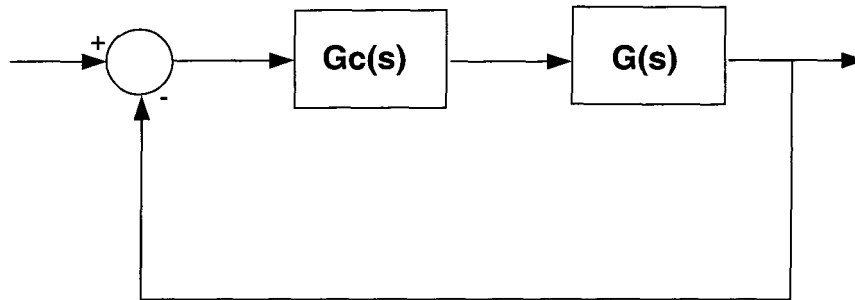
Figure 5.7 The rearranged block diagram

Here G(s) is the transfer function of the power supply, heater assembly, thermocouple and transmitter system together.

The transfer function G(s) is

$$G(s) = \frac{K_m K_\tau H(s)}{1 + K_m K_\tau H(s)} \tag{5.34}$$

$$G(s) = \frac{0.4464s^3 + 3.319s^2 + 7.4214 + 4.4046}{s^4 + 7.886s^3 + 19.98s^2 + 19.466s + 6.3402} \tag{5.35}$$

Finally, the closed-loop transfer function is

$$T(s) = \frac{G_c(s)G(s)}{1 + G_c(s)G(s)} \tag{5.36}$$

Proportional control

The proportional controller can be realized as shown in Figure 5.7 with $G_c(s) = K$, where, K is a variable. With different values of K, we can obtain

different gain of our feedback control system. The transfer function of the closed loop is:

$$T(s) = \frac{KG(s)}{1 + KG(s)} \qquad (5.37)$$

In our case, the values $K = 1, 10, 20$ were analyzed, respectively.

For $K = 1$, the system is a close loop but without the effect of a P controller.

The response of the system was obtained by using MATLAB is shown in Figures 5.8, 5.9, and 5.10. It can be noted that with $K = 10$ and $K = 20$, the output curves reached the linear ramp faster and the slopes of the curves are closer to the required rate.

The error in the case when $K = 1$ at 40°C (20°C above the initial room temperature level) is 35.5% (see the graph in Figure 5.8). By increasing the gain even further, to $K = 20$, the error at 40°C is slightly below 5% (Figure 5.10).
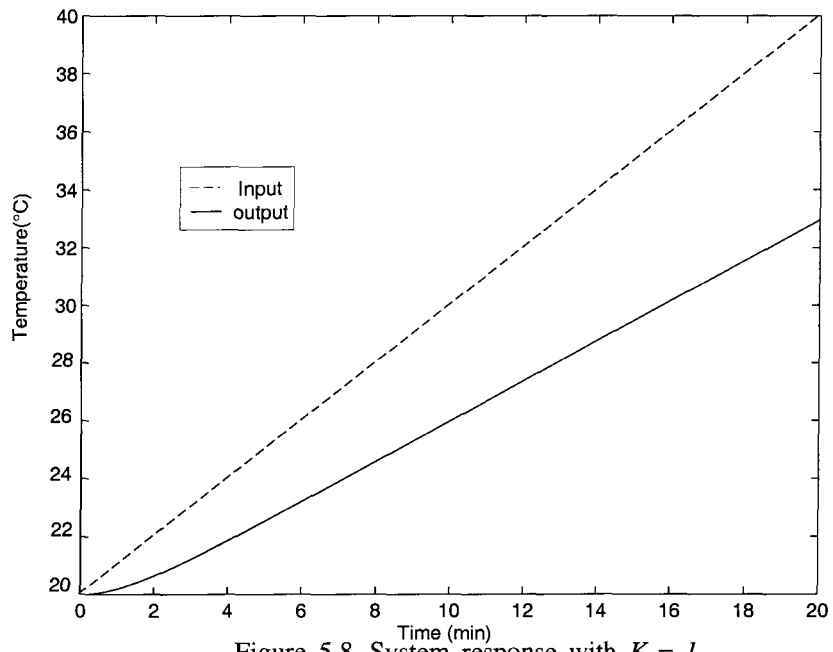
Figure 5.8 System response with $K = 1$
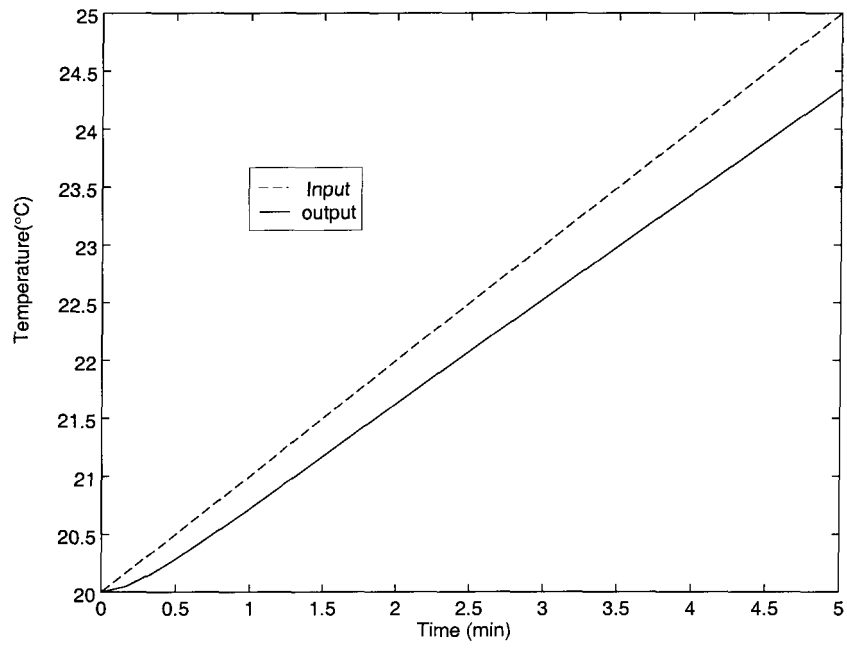
Figure 5.9 System response with P controller $K = 10$
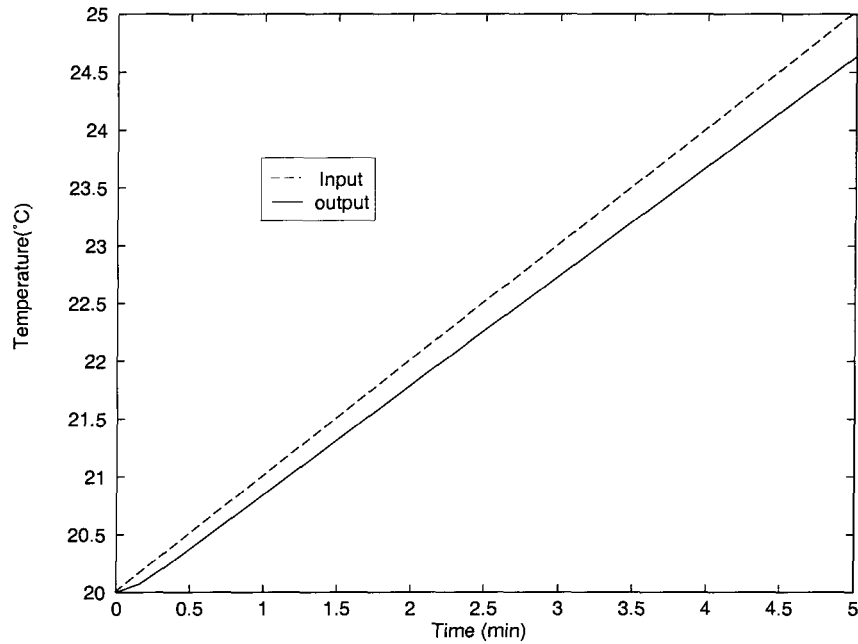
Figure 5.10 System response with P controller $K = 20$

PI control

To obtain a better response that is to follow the prescribed ramp more precisely, the proportional and integral control (PI control) concept is used. The transfer function for the PI controller is

$$G_c(s) = K_c\left(1 + \frac{1}{\tau_I s}\right) \qquad (5.38)$$

The block diagram is shown in Figure 5.7. By computing several cases, we found that with $K_c = 10$ and $\tau_I = 2$, the result (as shown in Figure 5.11) is quite satisfactory. At this condition the response curve reaches a linear increase of

temperature in less than 30 seconds and the slope of the curve after the initial 30 seconds is the same as that of the required one.

Taking into consideration that the total heating time from 20°C to 1 300°C will take more than 2 hours, the less than half a minute delay of the surface temperature does not affect the accuracy of the measurement at all. As a result of the application of the PI control, the slope of the temperature increase on the surface of the sample follows the prescribed rate with a very high precision. The initial delay is practically negligible, but if necessary, can be easily compensated by shifting the time axis by approximately 30 seconds. Even at moderate temperatures, at the beginning of the heating process, the temperature error is small, for example at 40°C it is only 1.5%.

Chapter 5
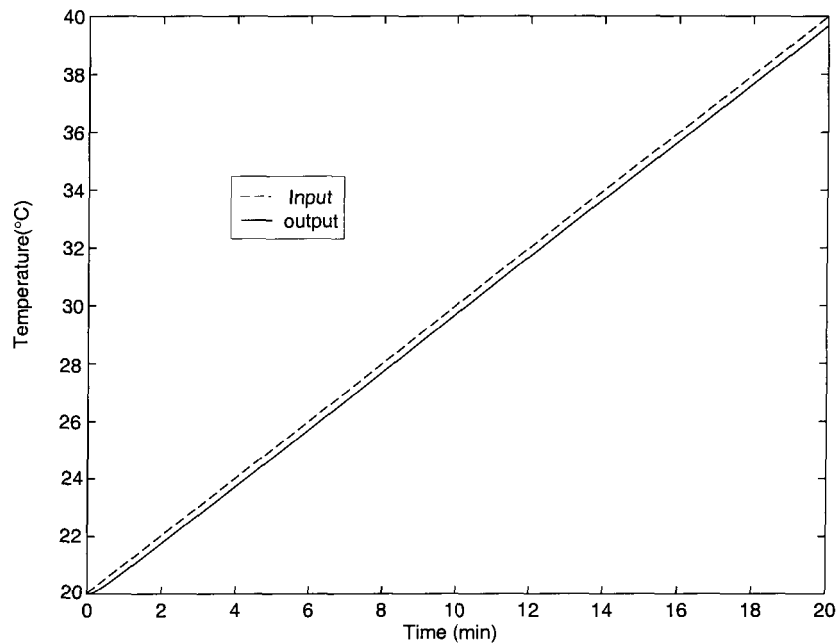
Figure 5.11 System response with PI controller ($K_c = 10 \ \tau_I = 2$)

For determining the thermal conductivity of packing coke, a model of the heating system is established. This heating system is controllable and observable.

The dynamic behavior of the system in open loop and closed loop was analyzed. In these two cases, a signal generator provides a linearly increasing set value. From the results of the analysis, we have drawn the following conclusions:

• In open loop the system response has a large error.

• The proportional control in closed loop with $K = 20$ can improve the system response but not enough.

Chapter 5

- By using the PI control with $K_c = 10$ and $\tau_I = 2$, the error of the system can be greatly reduced and easily compensated.

5.1.5 The development of the heating systems [2]

Heaters and controllers

Based on our calculation and estimation, the heating apparatus was designed and built at UQAC, using materials from several external suppliers. The heaters made by Thermcraft Inc., represent the latest technology in this field. They have a very low thermal mass and a high insulating capacity which makes possible to follow the prescribed temperature variation with a high precision and at a low heating power.

Theoretically, the tests can be performed both during heating and cooling at a constant rate. As the cooling of the sample is the result of a "natural" cooling through the walls of the apparatus, the cooling rate — except the very first few seconds — is significantly lower than the heating rate. As a consequence, the heater control can provide a linear cooling law only at low rates [2].

Three microprocessor digital controllers model 808 were installed to control the power supply of the furnace. They control the power supply to three zones of the sample separately. The temperatures are transmitted to the controllers by the thermocouple. Then the controllers send the signal to the furnace to adjust the heating power according the set points.

Heating rate and accuracy

The correct operation of the measurement system is the result of a compromise between different factors influencing the overall precision.

As the material properties are ultimately calculated from temperature differences across the diameter of the sample, it is evident that from the point view of the accuracy of temperature measurement, the biggest difference is the best. On the other hand, in the case of high temperature differences inside the sample, the heat conduction looses its linear character, and one cannot follow correctly the variation of the computed property in the studied temperature domain.

The temperature difference, heating rate, size and material of the sample are in a close correlation according to Equation 3.10. As a rule of thumb, if one sets the requirement for the precision of the temperature measurement at about 1%, the temperature difference must be at least 10°C, as it is not realistic to expect a better resolution than 0.1°C at elevated temperatures. Special attention must be paid to the measurement noise, which is introduced into the low level signal domain of the measurement system by the electric heaters (electromagnetic interference, EMI), as it can easily generate voltage fluctuations higher than the equivalent of 0.1°C. In the case of the packing coke samples, and a sample container of about 80 mm diameter, to create a temperature difference around 15 − 30°C, we need a heating rate about 2 − 8°C/minute. When the measurement results indicate a

weak temperature dependence of the diffusivity/conductivity, a higher rate of 30 – 50°C can be applied, which accelerates the measurements in a wide temperature range and the same time improves the accuracy of the temperature measurements.

Construction materials, temperature limits

One of the advantages of the monotonic heating is that the chosen measurement method itself does not limit the temperature range, the linear increase of the temperature is forced on the sample independently of the mechanism of the heat transfer. In the case of the constant flux method, the changing mechanism of the heat transfer during temperature increase (increasing role of radiation non-linearities) makes the control and compensation very difficult. The upper temperature of the measurements is determined only by the construction materials of the system.

The maximum temperature of the heaters is limited by the manufacturer to 1 100°C. There are electric heating elements for much higher temperatures, but none of them offer the ensemble of advantages that we found with the Fibercraft heaters. These resistance elements of these heaters form a uniformly distributed, complete cylindrical surface around the sample container. There is no additional thermal resistance between heater and target, the heating wires are embedded into the surface of the lightweight bonded ceramic fiber body. These features make possible to follow the commands of the control unit in a fast and precise way.

The selection of the thermocouples was the next important issue of the design. Noble metal thermocouples offer a temperature range up to 1 450°C ("R" and "S" type, platinum based alloys), while the well know "K" and "N" type nickel based alloys are applicable only up to 1 250°C. On the other hand, noble metal thermocouples are not only more expensive, but what is more important for our experiments, their sensitivity is about four times lower than K type thermocouples. The consequence of this lower sensitivity of R and S type thermocouples (about 10 μV/°C instead of 40 μV/°C for type K) means that we need to increase the temperature differentials inside the sample by a factor of four to achieve the same accuracy.

Considering all these factors we decided to use K type thermocouples, as their temperature limit just overlaps the maximum temperature of the furnace elements. First we used type 304 stainless steel sheathed, 1.6 mm external diameter, ungrounded junction thermocouples. If properly installed and grounded, these thermocouples are practically insensitive to electromagnetic noise. A complete noise rejection is impossible due to the design of the available ceramic body high-temperature thermocouple connectors which are placed inside the external shell of the apparatus.

The first series of experiments have shown that the stainless steel components (sample container, core, thermocouple sheathing) do not resist well enough the corrosive, high temperature environment in the presence of the packing coke

samples. The degradation was the fastest at the thermocouples, their sheath material became brittle and corroded and they were replaced several times. A new batch of thermocouples with Inconel 400 sheathing was then purchased to replace the ones protected by stainless steel. The experiments show a better corrosion resistance of these sensors, but it is clear that those components which are in direct contact with the coke samples need to be changed regularly after a few dozen tests.

Internal atmosphere of the test rig

The whole heater-sample container assembly is placed inside an external shell that can be hermetically sealed. The vessel is equipped with gas inlet and outlet connections in order to make possible of filling the internal space with a gas other than air. The reasons to do this are as follows:

1. Suppressing the air burning of the carbon particles. In this case the application of a nitrogen filling offers the advantage that it does not affect the equivalent conductivity measurements, because it has practically the same conductivity as air.

2. Parametric studies can be made by using different gases with different conductivities. Inert gases cover roughly a span of one order of magnitude in thermal conductivities, a variation by a factor of 10 (from the good conductor helium to argon or carbon dioxide which is poor conductor) in thermal conductivity.

As the air in the vessel can also be evacuated, the role of the intergranular gas in the heat transfer can be completely eliminated, leaving only conduction and radiation as players in the equivalent conductivity.

Data acquisition and evaluation

Fundamentally, the evaluation is based on distance, time and temperature measurements. The distance between the temperature measurement points is determined by the size of the sample container and that of the core. Theoretically, we can formulate the determination of the thermal diffusivity as the measurement of the time which is necessary for a given isotherm to propagate from the surface to the second measurement point (centre of sample or surface of the core). In practice, by using the quartz clock of the controllers, the time is not measured directly but calculated from the heating rate and the temperature increase ΔT.

During the experiments, the quantities directly measured are the temperatures. As a minimal requirement, the temperatures on the surface and in the centre of the sample are to be measured. Optionally we install a third thermocouple in between the two points to extract more information from the experiments which will be discussed in 5.2.3. There are other thermocouples installed for diagnostic purposes.

During the first tests, we connected the thermocouples to the computer (PC) controlled laboratory data acquisition system, but the quality of the temperature

signals was not satisfactory. The data acquisition cards picked up noise from the electric network and from the PC itself. By using a battery operated, microprocessor controlled six-channel data logger, and separating the measurement system galvanically from the network, we achieved a better noise rejection. The temperature histories in the characteristic points of the sample are collected and stored in the battery operated logger and are transferred to the PC for analysis only after the measurement is finished.

Even with this technique, the noise is not perfectly eliminated, so before the evaluation of the material properties from the heating curves, those are smoothed by a numerical filter.

5.2 Description of the Experiments and the Method of Evaluation

To have precise measurement results, we should make a good experiment plan and set a suitable program.

5.2.1 Control system programing

Set a program

The programmer/controller generates a fixed-format, 4–segment program: ramp, dwell, ramp, dwell. The 4 segments are executed in succession; when the first is finished, the second is automatically started and so on until the fourth segment is executed. The program can be executed between 1 and 200 times or

continuously. Examples of various programs following this format are given in Figure 5.12.
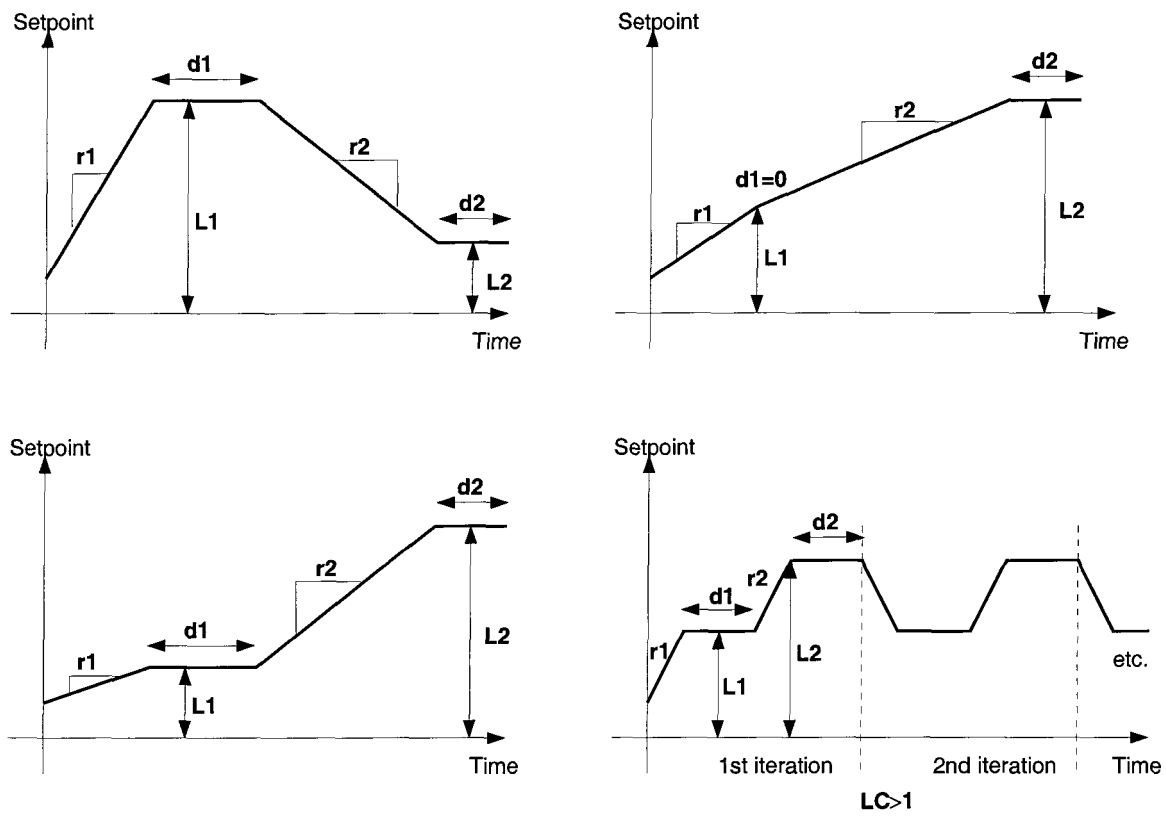
Figure 5.12 Examples of 4–segment programs (2 ramp/dwell pairs)

In Figure 5.12, r1 is the first ramp rate (heating rate), °C/min, L1 is the first dwell level (temperature), °C, d1 is the first dwell time, min, r2 is the second ramp rate, °C/min, L2 is the second dwell level, °C, d2 is the second dwell time, min, LC is the loop counter.

Self tuning

To have a good control of the program, a suitable set of PID parameters can be obtained and set by self-tuning option. The procedure is:

1. Set the program to "idle".

2. Put the set point to desired temperature (usually the maximum temperature of the measurement).

3. Go to the tune parameter and select "on".

After a period of time the self-tuning is done. Some PID parameters of coke and anthracite samples are listed in Table 5.4

Table 5.4 The PID parameters

	P			I			D
zone	1	2	3	1	2	3	—
coke	3	3	3	31	32	33	—
anthracite	3	3	2	21	23	24	—

The PID parameters obtained by "self tuning" are different with the estimated results in 5.1.4. Because PID changes with different kind of samples and heating systems. To get good control effect we should set "self tuning" every time when the size or the sort of the sample is changed.

5.2.2 Two temperature points measurement

Thermal diffusivity can be determined by measuring the two points of temperature history at the surface and center of the sample. In order to control and measure the temperature in surface of the sample, thermocouples were inserted in a stainless steel vessel. To measure the temperature in center of the sample a thin stainless steel rod was put in the centre with a thermocouple fixed into the surface of the rod.
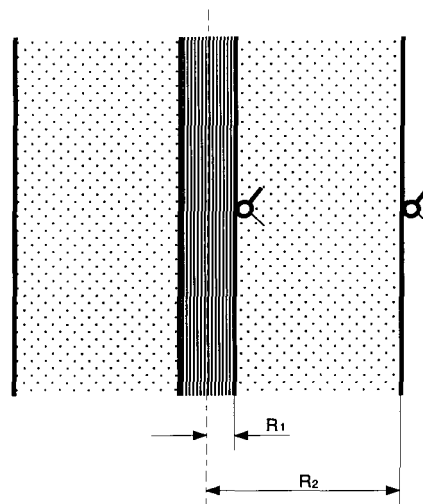
Figure 5.13 Two temperature points measurement

For the hollow sample with a metallic rod inside with constant temperature increase on the surface, the boundary condition at $r = R_1$:

$$q = \pi R_1^2 (\rho_1 c_{p1}) \frac{dT_1}{d\tau}$$ (5.39)

where R_1 is the radius of stainless steel core, m, ρ_1 is the density of the core, kg/m^3, c_{p1} is the specific heat of the core, kJ/kg°C and T_1 is the temperature of the core, °C.

$$q = -2k\pi R_1 \frac{dT}{dr}\bigg|_{r=R_1} \tag{5.40}$$

$$\frac{dT}{dr} = \alpha\left[\frac{1}{r}\frac{d}{dr}\left(r\frac{dT}{dr}\right)\right] \tag{5.41}$$

$$\frac{dT}{d\tau}\bigg|_{R_1} \approx \frac{dT}{d\tau}\bigg|_{R_2} = b \tag{5.42}$$

$$\frac{dT}{d\tau} = \frac{b}{2\alpha}r + \frac{C_1}{r} \tag{5.43}$$

$$T = \frac{b}{4\alpha}r^2 + C_1 lnr + C_2 \tag{5.44}$$

$$\Delta T_{21} = \frac{b}{4\alpha}\left(R_2^2 - R_1^2\right) + C_1 ln\frac{R_2}{R_1} \tag{5.45}$$

$$\alpha = \frac{k}{\rho c_p} \tag{5.46}$$

From Equation 5.39, 5.40, 5.42 and 5.46 we can know that

$$C_1 = \frac{R_1^2}{2k}\left[(\rho_1 c_{p1}) - (\rho c_p)\right] \tag{5.47}$$

hence

$$\Delta T_{21} = \frac{b}{4k}\left(R_2^2 - R_1^2\right)(\rho c_p) + \frac{bR_1^2}{2k}[(\rho_1 c_{p1}) - (\rho c_p)]ln\frac{R_2}{R_1} \tag{5.48}$$

Chapter 5

5.2.3 Three temperature points measurement

If we measure the temperature of the sample not only at its boundaries but in a third point inside, this additional information creates the possibility to determine two independent thermophysical properties simultaneously.
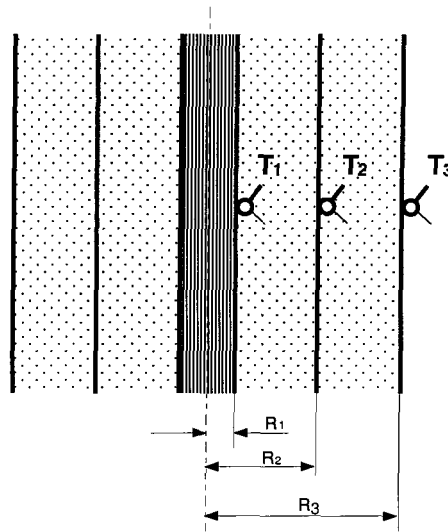
Figure 5.14 Three temperature points measurement

The temperature difference between point 3 and 1 is

$$\Delta T_{31} = \frac{b}{4k}\left(R_3^2 - R_1^2\right)(\rho c_p) + C_1 ln\frac{R_3}{R_1}$$
(5.49)

and the one between point 3 and 2 is

$$\Delta T_{32} = \frac{b}{4k}\left(R_3^2 - R_2^2\right)(\rho c_p) + C_1 ln\frac{R_3}{R_2}$$
(5.50)

By measuring the temperatures in three points according to Figure 5.14 and after some algebraic steps, we arrive to the expressions to calculate the heat capacity and conductivity as follows

$$(\rho c) = \frac{2R_1^2(\rho_1 c_{p1})\left[(T_3 - T_2)ln\frac{R_3}{R_1} - (T_3 - T_1)ln\frac{R_3}{R_2}\right]}{(T_3 - T_2)\left(2R_1^2 ln\frac{R_3}{R_1} + R_1^2 - R_3^2\right) - (T_3 - T_1)\left(2R_1^2 ln\frac{R_3}{R_2} + R_2^2 - R_3^2\right)}$$

(5.51)

and the thermal conductivity is

$$k = \frac{bR_1^2(\rho_1 c_{p1})\left[(R_2^2 - R_3^2)ln\frac{R_3}{R_1} - (R_1^2 - R_3^2)ln\frac{R_3}{R_2}\right]}{2(T_3 - T_1)\left(2R_1^2 ln\frac{R_3}{R_2} + R_2^2 - R_3^2\right) - 2(T_3 - T_2)\left(2R_1^2 ln\frac{R_3}{R_1} + R_1^2 - R_3^2\right)}$$

(5.52)

Chapter 6 ANALYSIS OF THE THEORETICAL MODELS FOR THE DESCRIPTION OF THE EQUIVALENT THERMAL CONDUCTIVITY OF THE GRANULAR MATERIALS

One of the main objectives of the project is to develop a theoretical model for the determination of the thermal conductivity as a function of temperature and granulometry. There is no theoretical model in the literature which can cover such complicated structure and wide temperature range. Our theoretical models are based on the Krischer model [24] and on the model developed by Zehner-Bauer [25].

6.1 Input Data for Equivalent Conductivity Models

6.1.1 Gas conductivity k_g

Figure 6.1 is the thermal conductivity of air at different temperatures [26]. An approximating equation for k_g (W/m°C) as function of T (°C) was set up..

$$k_g = a_0 + a_1 T + a_2 T^2 + a_3 T^3 \tag{6.1}$$

where: $a_0 = -7 \times 10^{-5}$, $a_1 = 0.0001$, $a_2 = 5 \times 10^{-8}$, $a_3 = 2 \times 10^{-11}$.
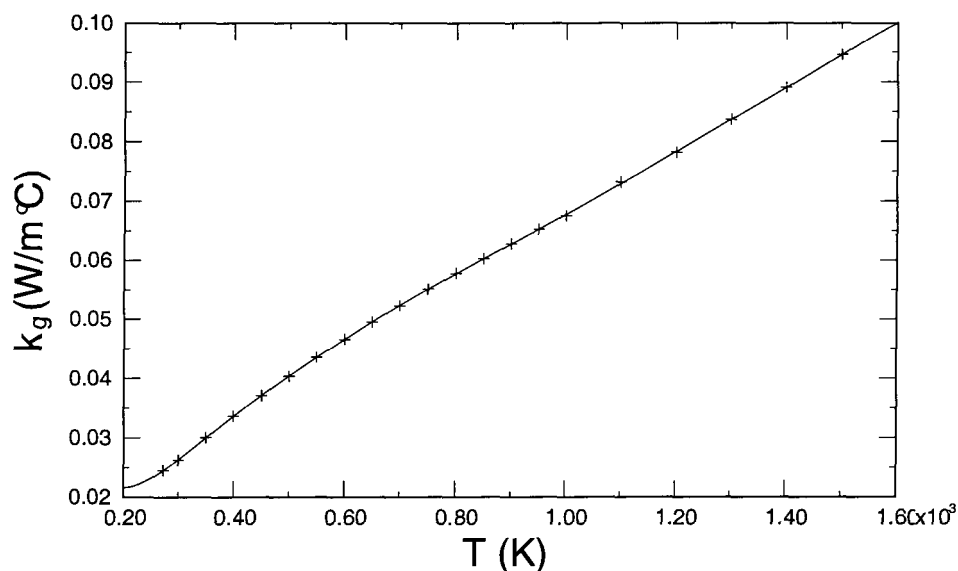
Figure 6.1 Thermal conductivity of gas

6.1.2 Solid conductivity k_s

There are not enough data published or reported on the thermal conductivity of solid coke although it is an important basic physical property in the study of the equivalent conductivity of coke. The experimental values and the temperature dependency vary greatly among the literature sources. We assume that an important source of the uncertainties in this field is that the notion of the solid conductivity is ambiguous in the literature. Some sources give conductivity data for "coke", without specifying whether it is bulk conductivity, particle conductivity or even "real" solid conductivity (compact solid with near zero porosity). The real solid conductivity of carbon materials is at least one order of magnitude higher than it is in the case of the porous particles. In connection

with the equivalent conductivity models, we always use the expression "solid conductivity (k_s)" as the conductivity of the disperse — but porous — solid component, i.e. as a synonym to particle conductivity $(k_{particle})$.

In Reference [27], reproduced in Appendix C, the thermal conductivity k_s, W/mK, of the metallurgical coke was measured by flash method. The result for zero porosity is a linear function of temperature, given by Equation 6.2.

$$k_s = 0.973 + 6.34 \times 10^{-3}(T - 273) \ (373 \ K \leq T \leq 1\,673\,K) \qquad (6.2)$$

In Reference [28], the thermal conductivity of coke is in the range of 2.91 – 3.49 W/mK at 100°C. It is not specified what kind of coke.

6.2 Analysis of Equivalent Conductivity of Packing Coke Using Simple Porosity Models

The equivalent conductivity can be determined by using some equivalent conductivity models, for example some of the simplest models which use rectangular grain and cavity shapes. In this section we use a method based on the Krischer model to calculate the simplest unit cells.

6.2.1 The formulas of model A and model B

In Figure 6.3 inhomogeneous materials with porosity P are represented as idealized cubic particles in the unit cell. The unit cell is a translational symmetry element of the inhomogeneous material. The surfaces are either isothermal or insulated. An equivalent resistance network is then developed and the thermal

conductivity of the system is obtained from the thermal-electrical analogy. For a given porosity there are two extremes. The estimate of the minimum equivalent conductivity is given by the "serial cell" (Figure 6.2 a). The maximum case is given by the "parallel cell" (Figure 6.2 b). The more realistic equivalent conductivity models may be illustrated by a combination of the two extreme cases as model A [24] or model B [21] [29] (Figure 6.3). For model A the serial sub-cell and the parallel sub-cell are in series in respect to the heat flow through the cell. In the case of model B the two sub-cells are parallel in respect to the heat flow.
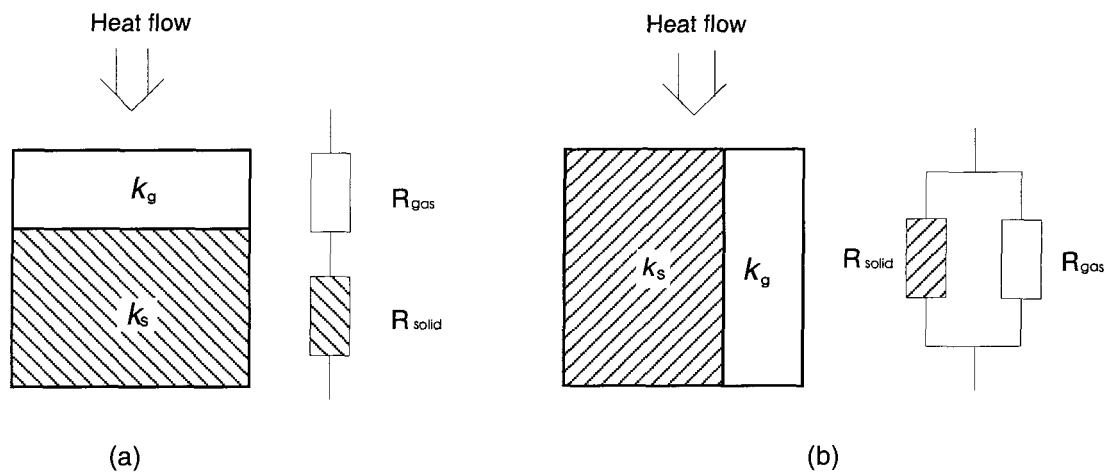
Figure 6.2 The notions of "serial" and "parallel" cells
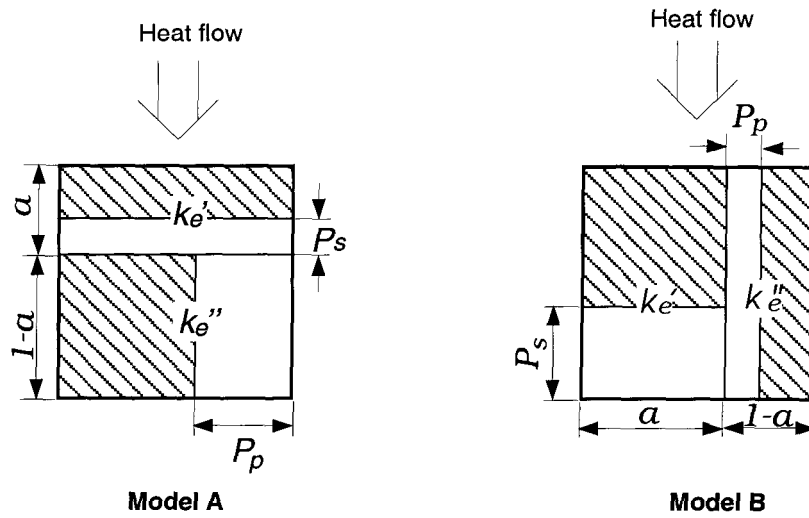
Figure 6.3 The unit cell of model A and model B

The input parameters for the calculation are the thermal conductivities of the gas and solid phase and the porosity. The models are first verified against the measurement results at room temperature and the temperature effects will be incorporated into the model thereafter. The parameter a characterizes the microgeometry of the granular material as the ratio of the serial and parallel component inside the unit cell, and serves as a fitting parameter for the equivalent conductivity model.

The formulas of equivalent conductivity for model A and model B are:

Model A

$$k_e' = \frac{1}{\frac{1-P_s}{k_s} + \frac{P_s}{k_g}} \tag{6.3}$$

$$k_e'' = P_p k_g + (1 - P_p)k_s \tag{6.4}$$

$$k_e = \frac{1}{\frac{a}{k_e'} + \frac{1-a}{k_e''}} \qquad (6.5)$$

Where k_e is the equivalent conductivity of the unit cell, W/m°C, P_s is the

porosity of the serial sub-cell, P_p is the porosity of the parallel sub-cell, k_g is the

conductivity of gas, W/m°C, k_s is the conductivity of solid component (particle

conductivity), W/m°C, a is the part of the serial sub-cell, k_e' is the equivalent

conductivity of the serial sub-cell, W/m°C, k_e'' is the equivalent conductivity of

the parallel sub-cell W/m°C.

Model B

$$k_e' = \frac{1}{\frac{1-P_s}{k_s} + \frac{P_s}{k_g}} \qquad (6.6)$$

$$k_e'' = P_p k_g + (1 - P_p)k_s \qquad (6.7)$$

$$k_e = a k_e' + (1 - a)k_e'' \qquad (6.8)$$

6.2.2 Analysis of k_e as the function of the structural parameters P, a, P_s/P_p

The above outlined simple equivalent conductivity models concentrate all the

information about the structure of the granular material into the P porosity and

into the a "seriality" factor. There is another, hidden geometrical parameter inside

the model in the form of the P_s/P_p ratio of the porosity in the serial and parallel

elements — which describes how the total porosity of the bulk is distributed

between the two subcells.

Case 1: $P_s = P_p = P$

Model A:

$$k'_e = \frac{1}{\frac{1-P}{k_s} + \frac{P}{k_g}}$$ (6.9)

$$k''_e = Pk_g + (1-P)k_s$$ (6.10)

$$k_e = \frac{1}{\frac{a}{k'_e} + \frac{1-a}{k''_e}}$$ (6.11)

Model B:

$$k'_e = \frac{1}{\frac{1-P}{k_s} + \frac{P}{k_g}}$$ (6.12)

$$k''_e = Pk_g + (1-P)k_s$$ (6.13)

$$k_e = ak'_e + (1-a)k''_e$$ (6.14)

We have selected a set of conductivity values on the basis of the literature survey. These values are estimations and we used them to feed into our k_e models. The physical properties of air [26], coke (Equation 6.2 [27]) and anthracite [30] are listed in Table 6.1, for three temperatures. the values quoted seem to be very low with respect to our measurements (see Figure 7.6).

Table 6.1 Physical properties of air, coke and anthracite

Temperature (K)	k (W/m K)		
	air	anthracite	coke
293	0.02603	0.238	-

Table 6.1 (Continued)   Physical properties of air, coke and anthracite

373	0.03181	-	1.607
1273	0.0768	0.250	7.313

Figures 6.4, 6.5, 6.6 and 6.7 are the curves of k_e of porous materials of anthracite and coke at different values of a.
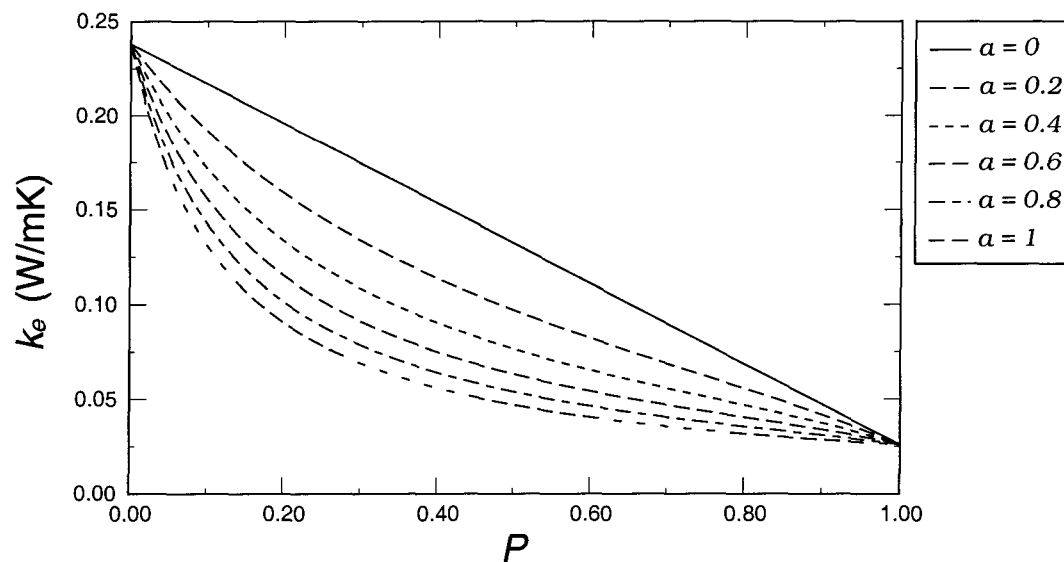
Figure 6.4 The $k_e - P$ curves of model A for anthracite at 293 K
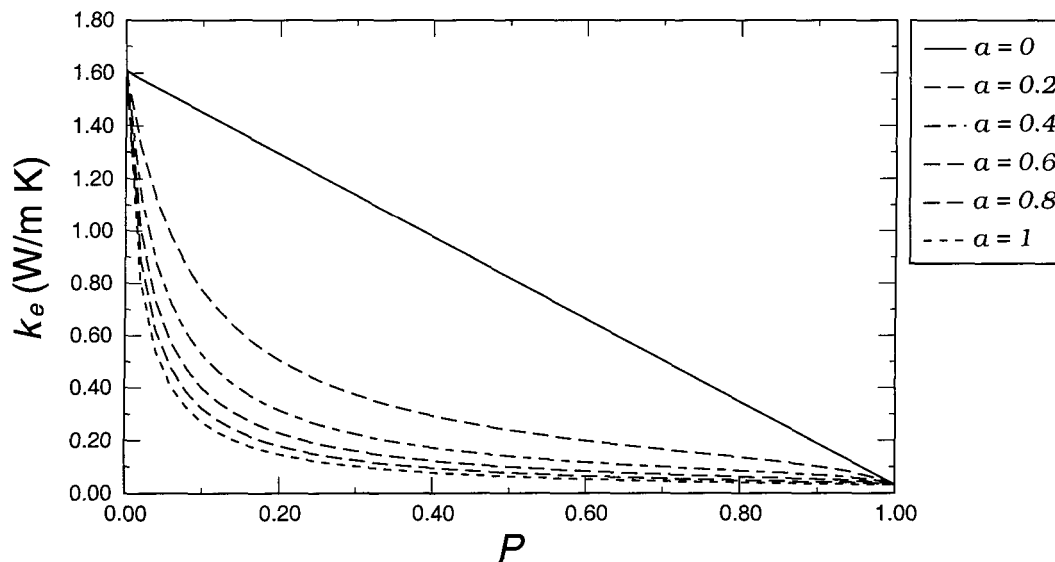
Figure 6.5 The $k_e - P$ curves of model A for coke at 373 K

The influence of P

As $k_s > k_g$, k_e decreases for increasing P. When $P = 0$, it means that the unit cell is only solid, $k_e = k_s$. When $P = 1$, the cell is 100% of gas, so $k_e = k_g$.

The influence of a

In both model A and model B when $a = 0$ the unit cell is purely parallel and the k_e curve is a straight line (Figures 6.4, 6.5, 6.6 and 6.7) corresponding to mixing rule representing the equivalent conductivity as an average, weighted by the porosity. With increasing a, the $k_e - P$ curve shows more and more a concave character.
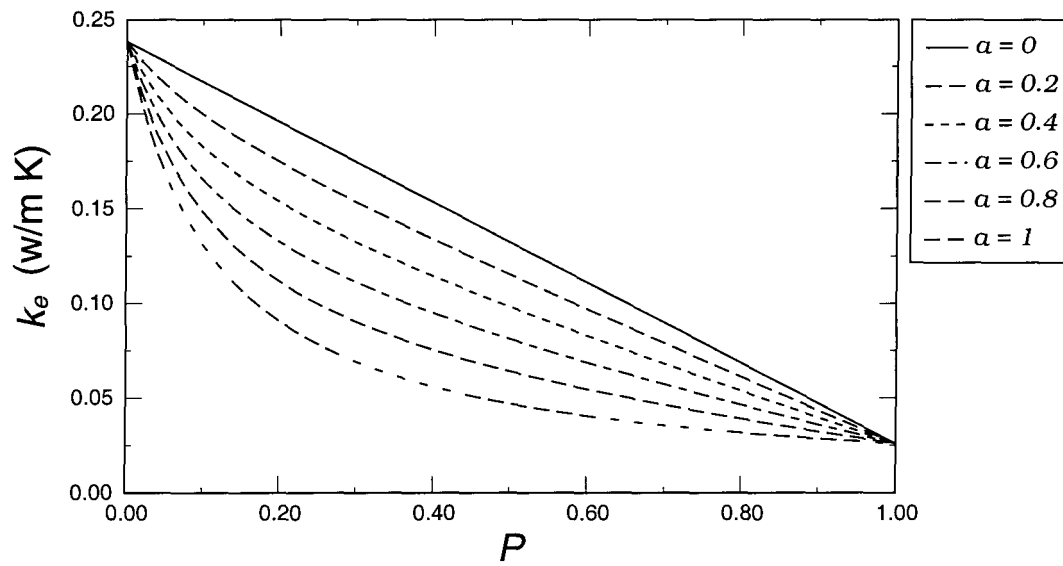
Figure 6.6 The $k_e - P$ curves of model B for anthracite at 293 K
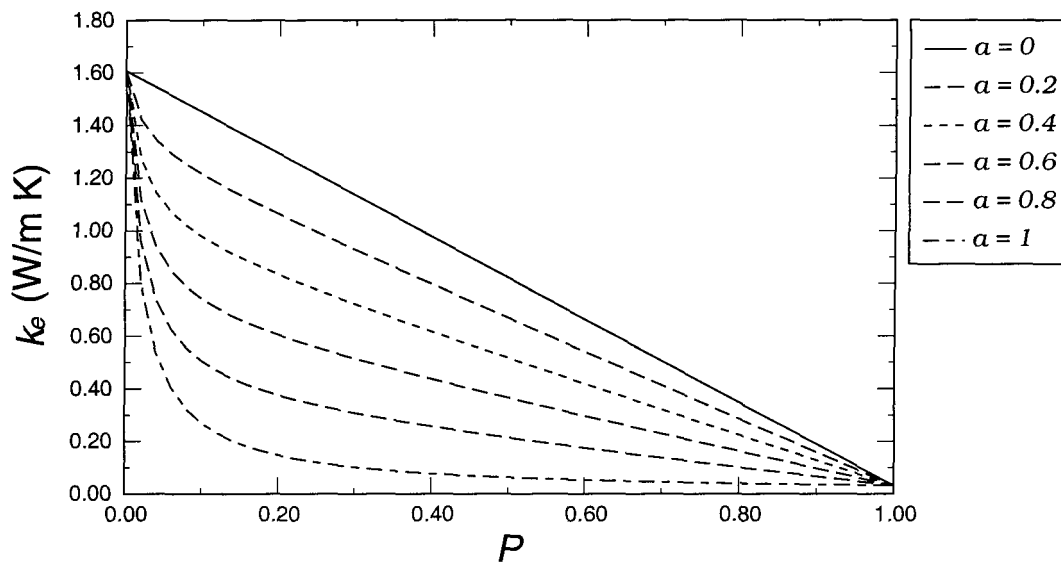
Figure 6.7 The $k_e - P$ curves of model B for coke 373 K

The Curves of k_e as the function of a

Figures 6.8, 6.9, 6.10 and 6.11 show the curves of k_e as the function of the geometrical parameter a.
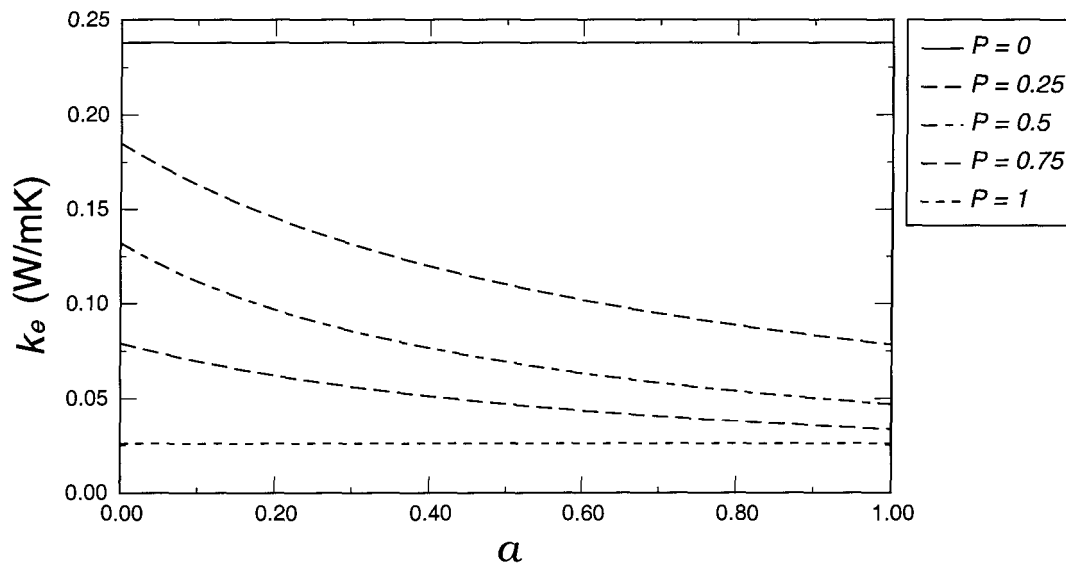
Figure 6.8 The k_e—a curves of model A for anthracite at 293 K
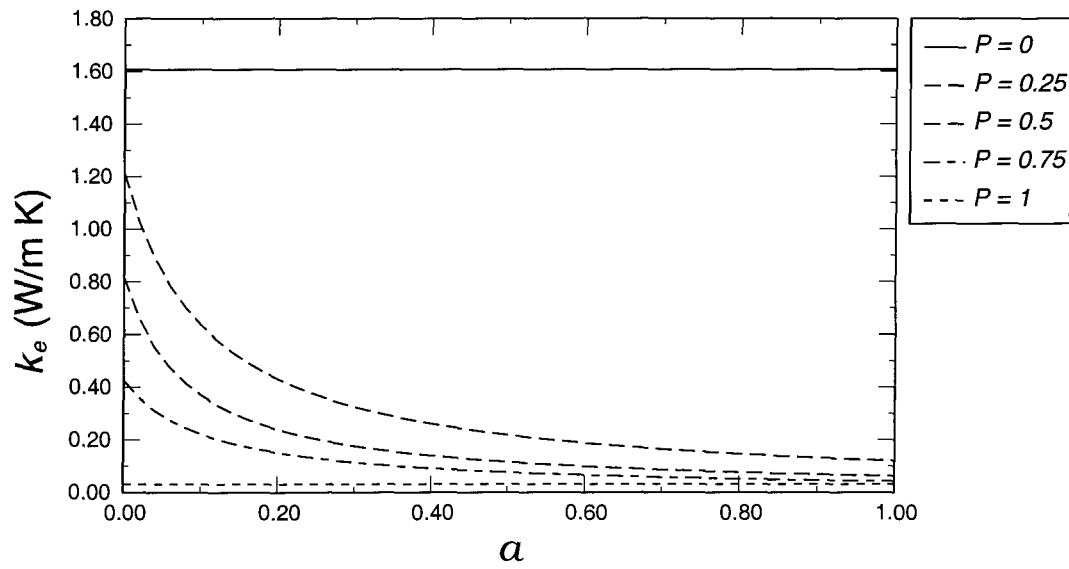
Figure 6.9 The $k_e - a$ curves of model A (coke)
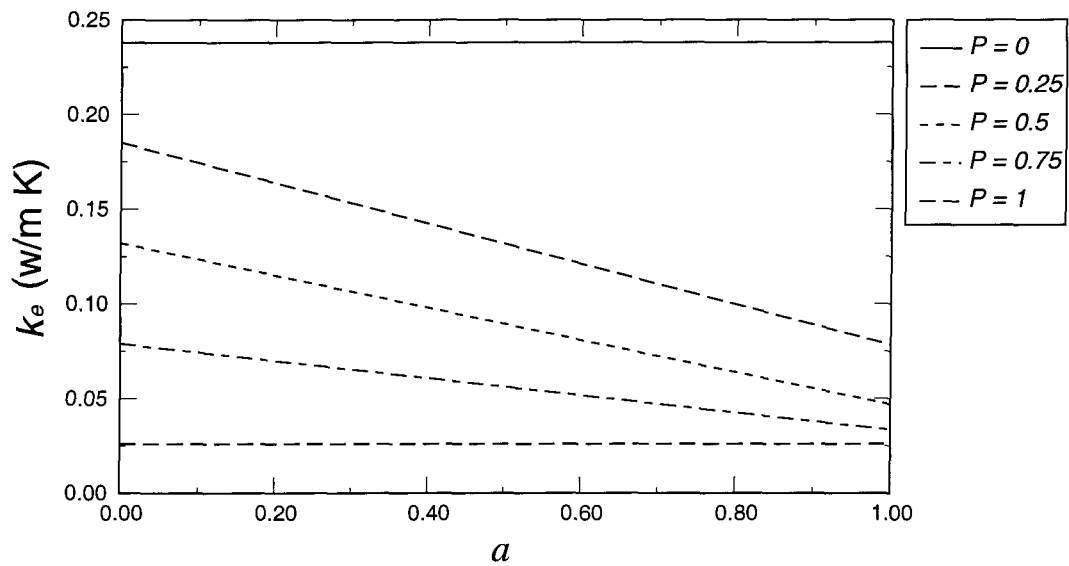
Figure 6.10 The $k_e - a$ curves of model B for anthracite at 293K
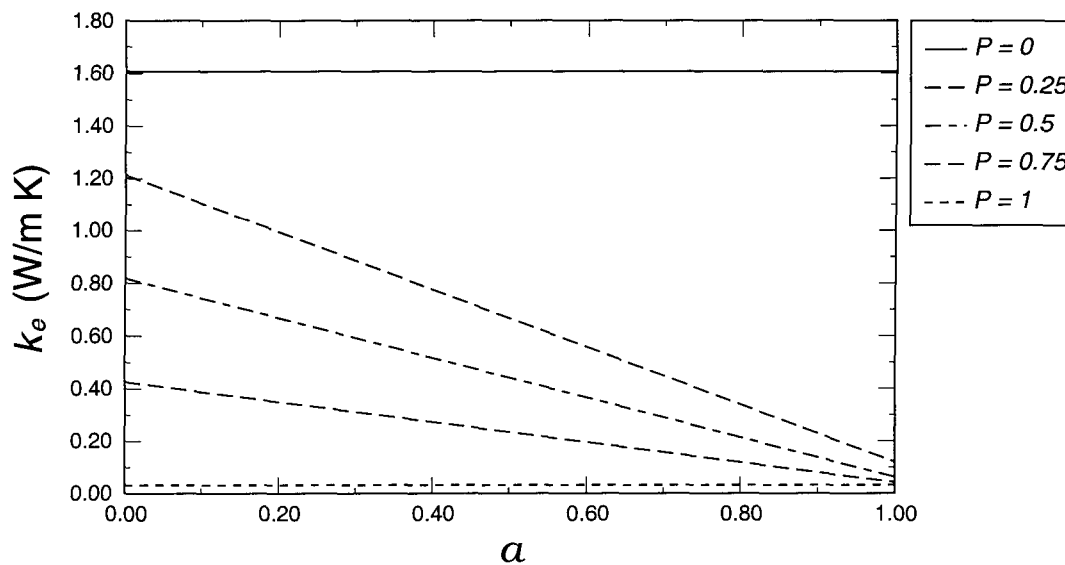
Figure 6.11 The $k_e - a$ curves of model B for coke at 373 K

The influence of temperature dependent conductivities (without radiation)

Here we study the increase of the equivalent conductivity due to the increase in the thermal conductivities of the composite phases (solid grains and air) at two temperatures. The effect of the radiation, which is the most important mechanism of the heat transmission inside the packing coke, will be analyzed separately.

Figure 6.12 shows the curves of k_e of anthracite at room temperature (293 K) and at high temperature (1 273 K). Because the conductivity of the gas increases faster than that of the solid, the curves become flatter at the higher temperature.
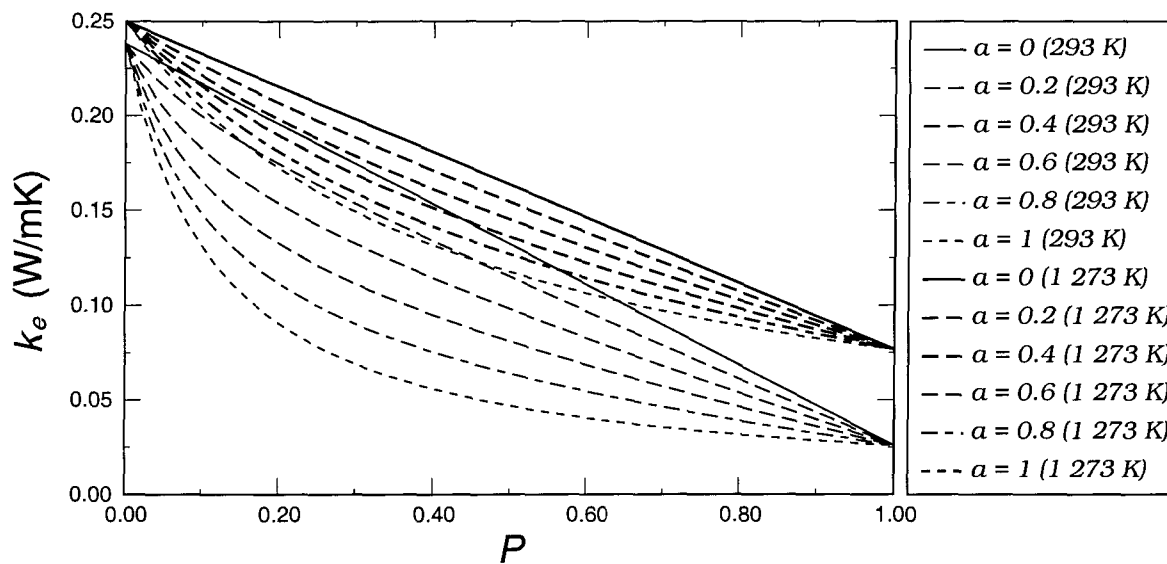
Figure 6.12 The $k_e - P$ curves of model B for anthracite at temperature of 293 K and 1 273 K
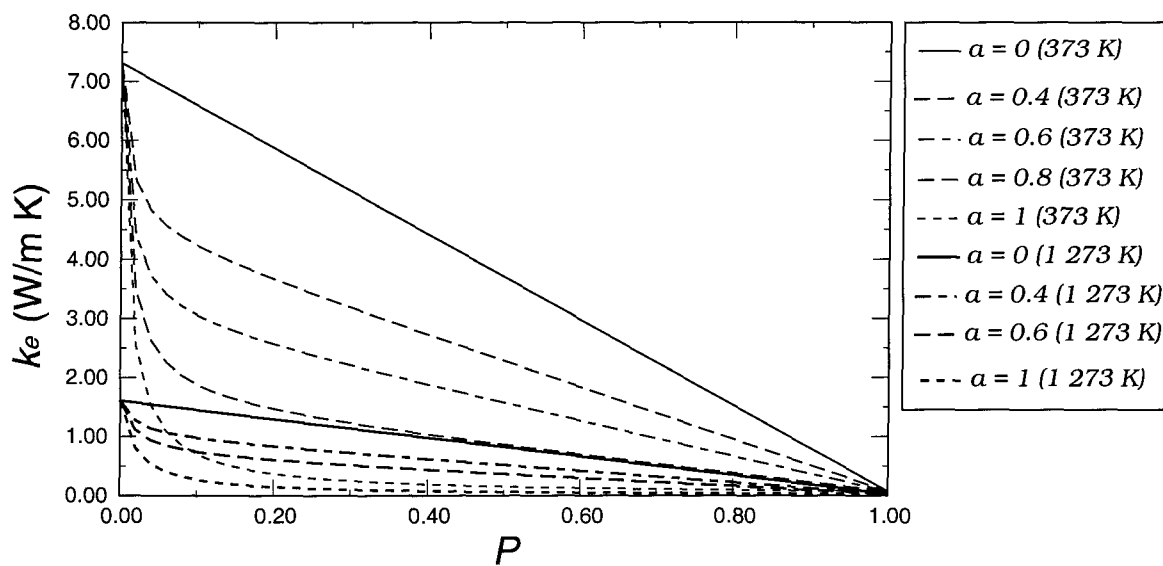
Figure 6.13 The $k_e - P$ curves of model B for coke at temperature of 373 K and 1 273 K

Contradictorily, from Figure 6.13 we can see that because the k_e of coke changes more with temperature, the curves are flatter at a lower temperature.

Case 2: $Ps \neq P_p$

If we give up the identical distribution of the total porosity between the serial and parallel subcells, the models become more complex.

The relation between the total porosity P and P_s, P_p, and a can be written :

$$P = aP_s + (1 - a)P_p \tag{6.15}$$

The equivalent thermal conductivity consequently depends upon two independent parameters, an arbitrary pairing of P_s and P_p and a.

Figures 6.14, 6.15 and 6.16 illustrate the influence of the porosity ratio, P_s/P_p, on the equivalent conductivity.

The equivalent conductivity curves in these diagrams were calculated using model A. The upper envelope of the curves is the purely parallel connection unit cell ($a = 0$), with the linear dependence on the porosity. The lower envelope for the family of curves with a constant value of a, is the characteristic of a pure serial connected cell (both $P_p = 1$ and $P_p = 0$ correspond to pure serially connected cells). with a total porosity of $(1-a) \leq P \leq 1.0$. (These envelopes coincide with the corresponding curves in Figure 6.4.)

Chapter 6
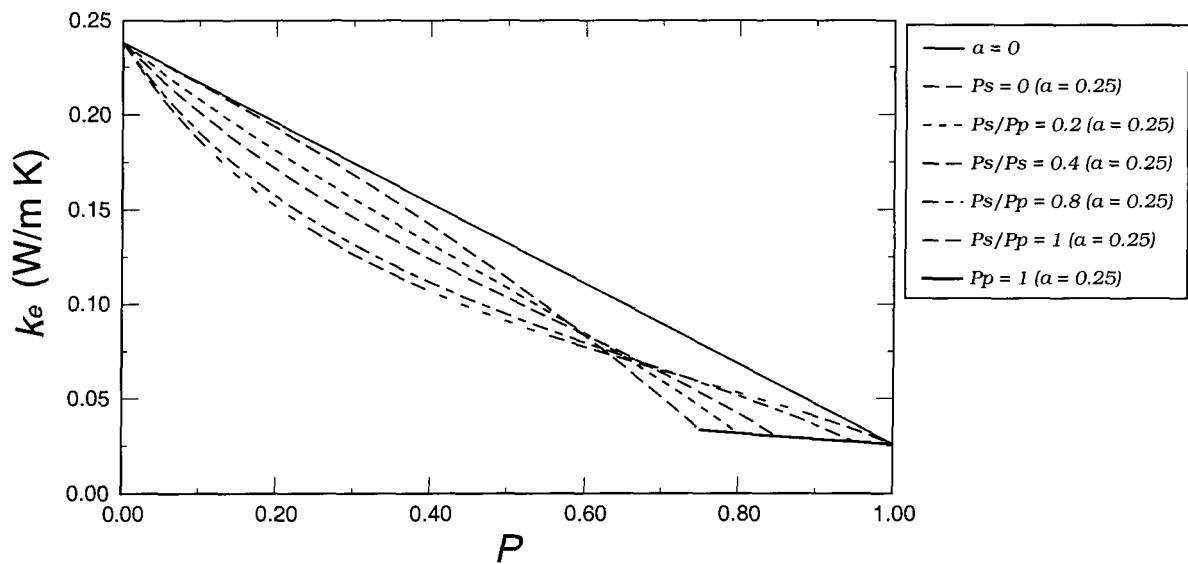
Figure 6.14 The $k_e - P$ curves for different ratio of P_s/P_p of model A $(a = 0, a = 0.25)$
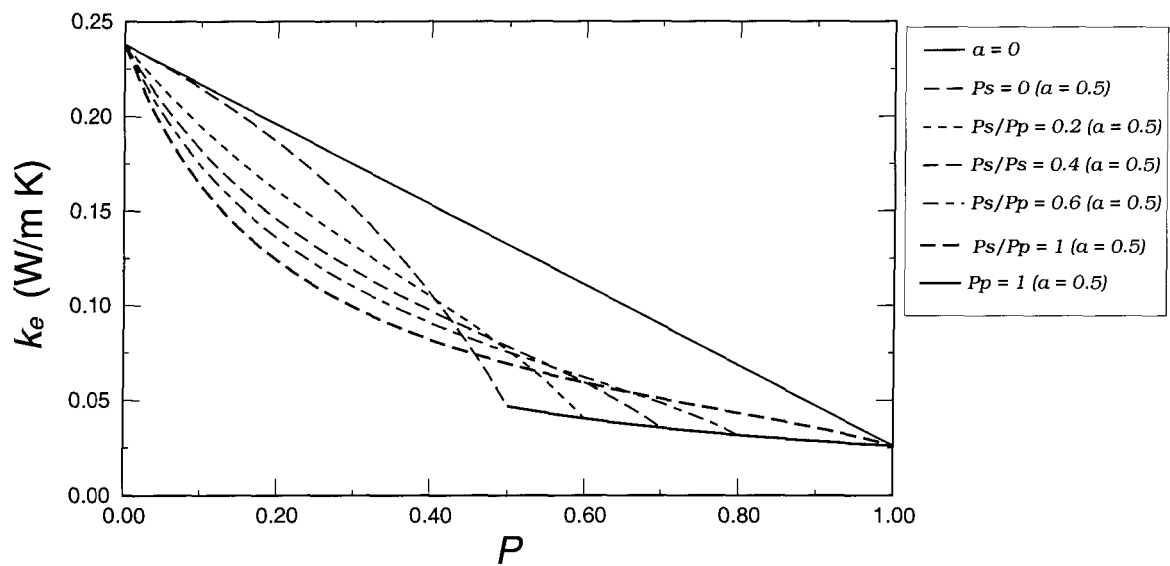
Figure 6.15 The $k_e - P$ curves for different ratio of P_s/P_p of model A $(a = 0, a = 0.5)$
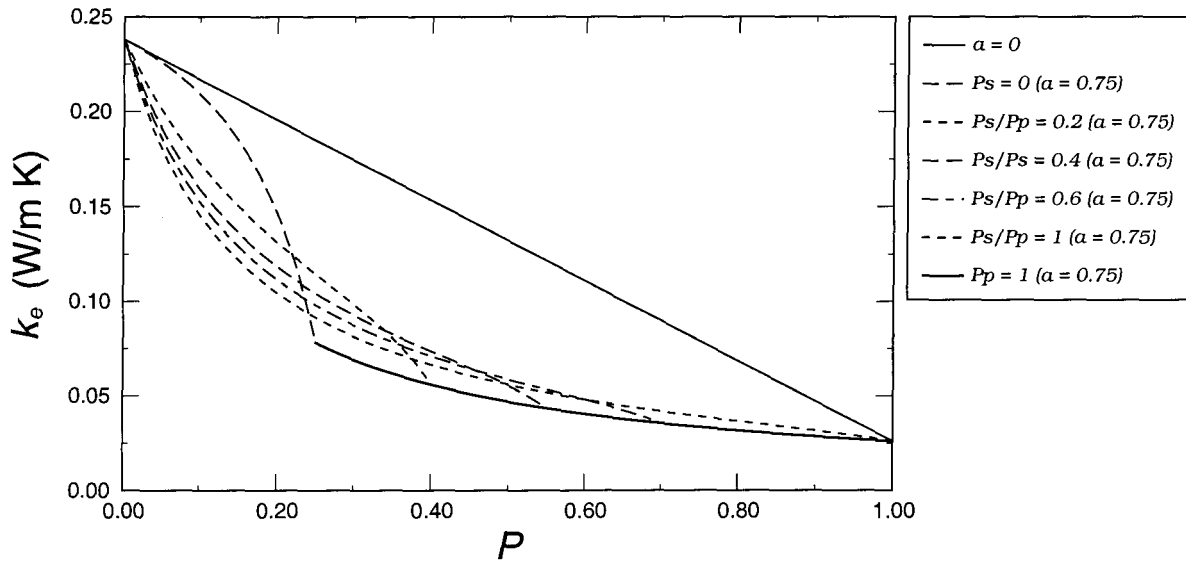
Figure 6.16 The $k_e - P$ curves for different ratio of P_s/P_p of model A $(a = 0, a = 0.75)$

- **$P_s = 0$**

(i). $a = 0$

Purely parallel connection character, the curve is a straight line same as Figure 6.4.

(ii). $a \neq 0$

$$k'_e = k_s \tag{6.16}$$

$$k''_e = P_p k_g + (1 - P_p)ks \tag{6.17}$$

$$P = (1 - a)P_p \tag{6.18}$$

$$k_e = \frac{1}{\frac{a}{k_s} + \frac{1-a}{k''_e}} \tag{6.19}$$

Chapter 6

- $P_s/P_p\ =\ 1$

$P_s = P_p = P$ the curve is same as case 1, discussed above.

- $P_p\ =\ 1$

$$k_e = \cfrac{1}{\frac{a}{k_e'} + \frac{1-a}{k_g}} \qquad (6.20)$$

Model A becomes purely serial in this case so the curve is same as Figure 6.4 when $a = 1$. Each curve in Figures 6.14, 6.15 and 6.16 ends on the enveloping curve of $P_p = 1$

So all the curves are also between the two extreme cases, $a = 0$ and $a = 1$.

It can be seen in the previous graphs that the introduction of the new structural parameter P_s/P_p opens up new possibilities to describe equivalent conductivity variations of different nature. The stronger is the serial character, either due to the increasing a, or due to the higher P_s/P_p value, the faster decreases the equivalent conductivity, specially in the lower porosity range. It is also clear that if the serial subcell is completely solid $(P_s/P_p = 0)$, the decrease of the equivalent conductivity in the low porosity range is weak. This behavior approximates the case of a continuous solid phase with gas filled pores inside. In our case, the solid phase is disperse, the role of the gas filled, serially connected elements is

important. Granular materials like the packing coke are better described by a higher value of the porosity ratio, generally $P_s/P_p \geq 1.0$.

For the reliable identification of the two structural parameters, a series of measurements at room temperature, using the same type of coke but with different porosity (granulometry) will be necessary. As we tested the samples in their original state, without changing their granulometry, in the analysis we used always as first hypothesis, an estimated value of the porosity ratio: $P_s/P_p = 1$. As further analysis has shown, the $P_s/P_p = 1$ factor together with the a "seriality" parameter play an important role in the above described simple equivalent conductivity models specially if we include the radiation effects.

6.3 Analysis of Equivalent Conductivity of Packing Coke Using the Zehner–Bauer Model

6.3.1 Zehner-Bauer model

The Zehner-Bauer model uses a more complex description of the grain geometry and of the different heat transfer modes between the particles. The unit cell is illustrated in Figure 6.17 (based on references [25] and [24]).

In the figure, $1 - \sqrt{1 - P}$ is the fluid phase, $\sqrt{1 - P}$ is the solid phase.

Where P is the porosity.

One of the main characteristics of the model is the use of a model particle with "deformable" shape according to the equation

$$r^2 + \frac{z^2}{[B - (B-1)z]^2} = 1 \tag{6.21}$$

Where, B is the deformation factor. For $B = 1$ the particle (disperse phase) surface is a sphere. For $B < 1$ more or less prolongated needles and for $B > 1$ barrel-like bodies are obtained (see Figure 6.17).

B<1   B>1
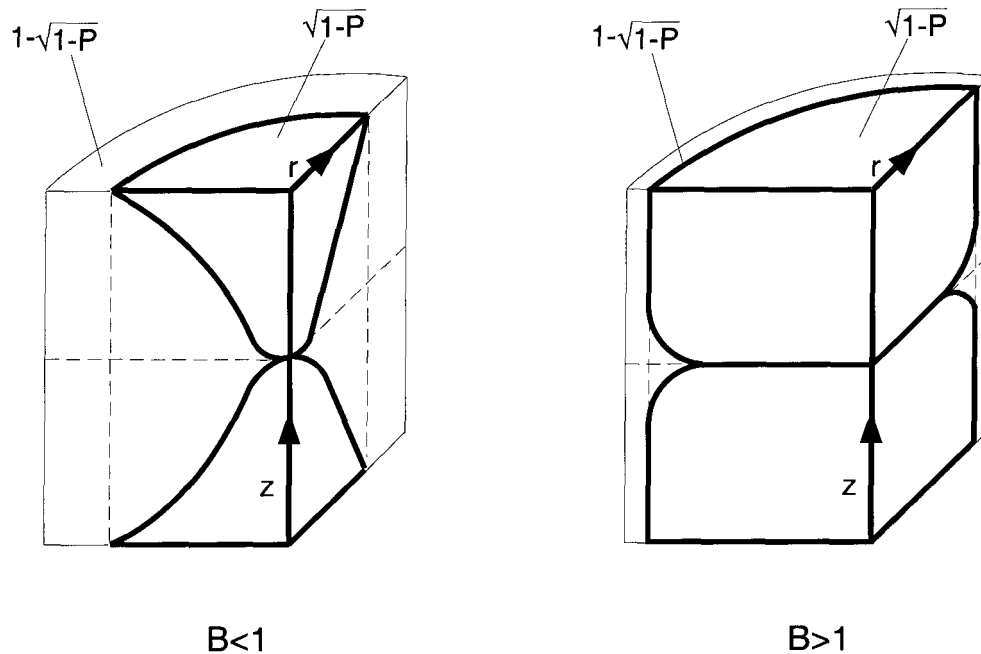
Figure 6.17 The unit cell of the Zehner-Bauer model

The unit cell is divided into core region and into an annular, gas filled space. These parts (subcells) are connected in parallel. As the division ratio between the two parts is fixed by the porosity, P and B are correlated:

$$P = 1 - \left[\frac{B}{(B-1)^3}(3 - 4B + B^2 + 2lnB)\right]^2 \qquad (6.22)$$

A good explicit approximation of Equation 6.22 is

$$B = 1.25\left(\frac{1-P}{P}\right)^{\frac{10}{9}} \qquad (6.23)$$

The final formula for the conductivity of the unit cell is

$$\frac{k_e}{k_g} = 1 - \sqrt{1-P} + \chi_c\sqrt{1-P} \qquad (6.24)$$

where, k_e is the equivalent conductivity of the unit cell, k_g is the conductivity

of gas, and

$$\chi_c = \frac{2}{N}\left(\frac{B}{N^2}\frac{\chi_p - 1}{\chi_p}ln\left(\frac{\chi_p}{B}\right) - \frac{B+1}{2} - \frac{B-1}{N}\right) \qquad (6.25)$$

$$\chi_p = \frac{k_s}{k_g} \qquad \chi_c = \frac{k_{core}}{k_g} \qquad (6.26)$$

$$N = 1 - \frac{B}{\chi_p} \qquad (6.27)$$

Here k_s is the conductivity of solid phase, k_{core} is the conductivity of the core

of the unit cell.

6.3.2 The influence of secondary parameters

An extension of Equation 6.24 accounts for such secondary parameters as

thermal radiation, particle flattening, shape and size distribution. The generalized

equations are as follows [12], [24]:

$$\frac{k_e}{k_g} = \left(1 - \sqrt{1-P}\right)(1 + P\chi_r) + \sqrt{1-P}\left[\varphi\chi_p + (1-\varphi)\chi_c\right] \qquad (6.28)$$

with

$$\chi_c = \frac{2}{N}\left[\left(\frac{B(\chi_p + \chi_r - 1)}{N^2\chi_p}\right)\ln\left(\frac{\chi_p + \chi_r}{B}\right) + \frac{B+1}{2B}(\chi_r - B) - \frac{B-1}{N}\right]$$

$$(6.29)$$

$$N = 1 + \frac{\chi_r - B}{\chi_p} \qquad (6.30)$$

$$B = C_f\left[\frac{(1-P)}{P}\right]^{\frac{10}{9}} f(\zeta) \qquad (6.31)$$

C_f is the form factor, and φ is the flattening coefficient.

$$\chi_r = \frac{k_r}{k_g} = \frac{4\sigma_0}{\frac{2}{\varepsilon} - 1}T^3\frac{d}{k_g} \qquad (6.32)$$

σ_0 is the Stefan-Boltamann constant ($\sigma_0 = 5.67 \times 10^{-8}\,\mathrm{Wm^{-2}K^{-4}}$), k_r is the effective conductivity for thermal radiation, d is the mean particle diameter.

For polydisperse packing or granular materials

$$d = \left(\sum \frac{Q_i}{d_i}\right)^{-1} \qquad (6.33)$$

where Q_i is the volumetric fraction and d_i is the particle diameter of the ith fraction in the multigranuler bed.

The distribution function $f(\zeta)$ is

$$f(\zeta) = 1 + 3\zeta \qquad (6.34)$$

with

$$\zeta = \left[\frac{\sum \frac{Q_i}{d_i^2}}{\left(\sum \frac{Q_i}{d_i} \right)^2} - 1 \right]^{0.5}$$

(6.35)

6.3.3 Application to our measurements

In the application of the Zehner-Bauer model to our measurements, d_i is obtained from Section 4.14, where $d_i = x_i$. The problem is Q_i the relative volumetric fraction of component i in the mixture, since it is usually not measured as a standard parameter for particle distribution characterization. It was thus not measured in the present study. Instead, $d\phi_i$, weight fraction distribution, is usually measured and so it was in Section 4.14. It was then assumed that $dQ_i = d\phi_i$ for the purpose of evaluating the performance of Zehner-Bauer model in our context. Only too late it was realized that this assumption might be too rough for making definite conclusions about the applicability of the Zehner-Bauer model to the packing coke. Since this model is recommended in Reference [24] as the best, an effort should be made in the continuation of the present work to measure Q_i directly and to verify once again how the measurements fit the model.

Table 6.2 gives the input parameters for the Zehner-Bauer model, using our measurements for four types of coke with the assumption that $dQ_i = d\phi_i$ in Equations 6.33 and 6.34 as discussed above.

Table 6.2 Summary of the measured and calculated parameters for samples
1ARGVERT, 2FCUNEUF, 3FCNEUF, and 4FCUSAGE at 315 K

Sample		1ARGVERT	2FCUNEUF	3FCNEUF	4FCUSAGE
P (measured)		0.65	0.32	0.34	0.33
d (mm) (measured)		1.87	0.37	0.68	3.26
$f(\zeta)$ (Equation 6.34)		1	3.68	3.16	3.66
ϵ (from [28])		0.8	0.8	0.8	0.8
C_f (from [24])		1.25	1.40	1.40	1.40
φ (from [24])		0.007	0.0010	0.0010	0.0010
k_e (W/mK) (calculated by Equation 6.28)	$k_s = 3.489$ W/mK [28]	0.14	0.82	0.68	0.76
	$k_s = 1.607$ W/mK (Equation 6.2)	0.11	0.55	0.49	0.52
k_e (W/mK) (measured by guarded heating method)		0.22	0.89	0.64	0.72

6.3.4 The sensitivity factors

To analyze the contribution of the individual parameters such as solid conductivity, gas conductivity, grain emissivity, porosity, temperature etc. to the value of the equivalent conductivity, we have determined the so-called sensitivity factors.

These factors characterize quantitatively the relative influence of the properties of the constituents of the packing coke on its bulk (equivalent) conductivity. The Zehner-Bauer equivalent conductivity model, according to Equation 6.28, served as basis for these calculations. The input parameters are given in Table 6.2.

The sensitivity of k_e to the variation of k_s

Table 6.3 k_e of 2FCUNEUF at the temperature of 315 K by increasing and decreasing of k_s

k_S (W/mK)	3.389	3.489	3.589
k_e (W/mK)	0.810	0.820	0.829

At the temperature of 315 K increasing and decreasing of k_s by 0.1 W/mK, the equivalent conductivity of sample 2FCUNEUF increases by 0.01 W/mK and decreases by 0.009 W/mK. This can be expressed in form of derivatives:

$$\frac{\partial k_e}{\partial k_s} \bigg|_{-} = 0.1 \tag{6.36}$$

$$\frac{\partial k_e}{\partial k_s} \bigg|_{+} = 0.09 \tag{6.37}$$

and finally the sensitivity factor can be determined as the mean value of the derivatives

$$S_{k_s} = \frac{\partial k_e}{\partial k_s} = 0.095 \tag{6.38}$$

This result shows that if the solid conductivity is changed by 100%, the equivalent conductivity variation is only 9.5%.

The sensitivity of k_e for variations in k_g

The next factor analyzed is the contribution of the gas conductivity to the equivalent conductivity of the granular material.

Table 6.4 k_e by increasing and decreasing of k_g

k_g (W/mK)	0.02637	0.02737	0.02837
k_e (W/mK)	0.803	0.820	0.836

At temperature of 315 K increasing and decreasing of k_g by 0.001W/mK the equivalent conductivity of sample 2FCUNEUF increases 0.017 W/mK and decreases 0.016 W/mK.

$$\frac{\partial k_e}{\partial k_g}\Big|_{0.2738-} = 16 \qquad (6.39)$$

$$\frac{\partial k_e}{\partial k_g}\Big|_{0.2738+} = 17 \qquad (6.40)$$

The sensitivity of k_e to variations of k_g is

$$S_{k_g} = \frac{\partial k_e}{\partial k_g} = 16.5 \qquad (6.41)$$

This means that a unit increase in the gas conductivity brings a tenfold increase in the equivalent conductivity. This result is not surprising if we take into account that as the gas phase represents the bigger resistance in the system, it dominates the overall heat transfer rate.

The sensitivity of k_e to temperature variations

Figure 6.18 is the temperature dependence of the thermal conductivity of coke (sample 2FCUNEUF) calculated according to Equation 6.28. With increasing temperature an increase in the thermal conductivity is observed, but the character of the increase is to be proved by the monotonic heating method.
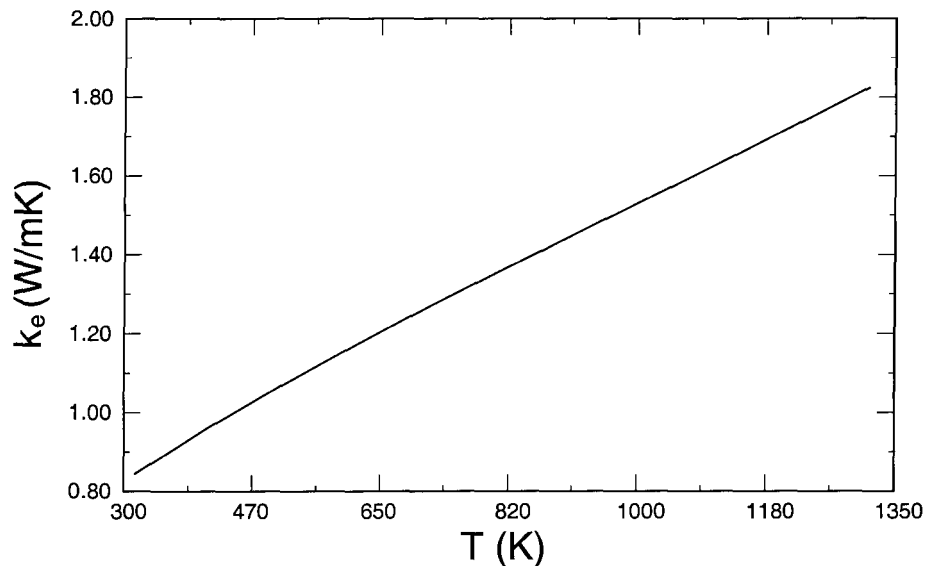
Figure 6.18 The $k_e - T$ curve of sample 2FCUNEUF calculated according to Equation 6.28

Table 6.5 k_e by increasing and decreasing of temperature

Temperature (K)	315	365	415
k_e (W/mK)	0.820	0.889	0.953

In Table 6.5, increasing and decreasing the temperature by 50°C at T = 365 K increases k_e by 0.064 W/mK and decreases it by 0.069 W/mK.

$$\frac{\partial k_e}{\partial T}\bigg|_- = 1.38 \times 10^{-3} \frac{W/mK}{K} \tag{6.42}$$

$$\frac{\partial k_e}{\partial T}\bigg|_+ = 1.28 \times 10^{-3} \frac{W/mK}{K} \tag{6.43}$$

The sensitivity of k_e to of temperature variations around this temperature is

$$S_T = \frac{\partial k_e}{\partial T} = 1.33 \times 10^{-3} \frac{W/mK}{K} \tag{6.44}$$

which means that about a 70°C temperature increase brings 0.1 W/mK increase in equivalent conductivity.

The sensitivity of the equivalent conductivity k_e to porosity variations

Table 6.6 k_e by increasing and decreasing the porosity at 315 K

Porosity	0.314	0.324	0.334
k_e (W/mK)	0.848	0.820	0.793

At 315 K, if the porosity of the sample 2FCUNEUF is increased and decreased by 1%, the equivalent conductivity decreases by 0.027 W/mK and increases by 0.028 W/mK.

$$\frac{\partial k_e}{\partial P}\bigg|_- = -2.8\,W/mK \tag{6.45}$$

$$\frac{\partial k_e}{\partial P}\bigg|_+ = -2.7\,W/mK \tag{6.46}$$

The sensitivity of the equivalent conductivity for variations in the porosity is

$$S_P = \frac{\partial k_e}{\partial P} = -2.75\,\mathrm{W/mK} \tag{6.47}$$

The sensitivity of k_e to variations of the ϵ emissivity of the solid particles

Figure 6.19 shows the $k_e\text{--}\epsilon$ curves in different temperatures. In high temperature (1 300 K) a rather rapid increase of the thermal conductivity occurs when the emissivity is also high.
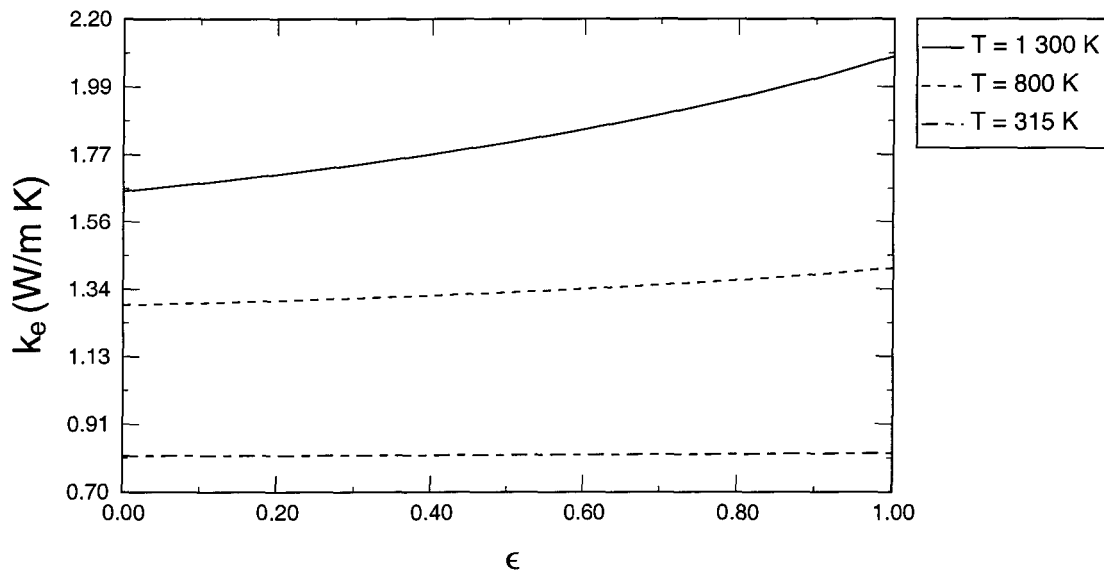
Figure 6.19 The $k_e\text{--}\epsilon$ curves

Table 6.7 k_e by increasing and decreasing of ϵ and temperature

Temperature	ϵ		
(K)	0.7	0.8	0.9
315	0.8186	0.8197	0.8211

Table 6.7 (Continued) k_e by increasing and decreasing of ϵ and temperature

| 800 | 1.3562 | 1.3710 | 1.3884 |
| 1 300 | 1.8980 | 1.9511 | 2.0119 |

From Table 6.7, we obtain:

(a) $T = 315$ K

$$\frac{\partial k_e}{\partial \epsilon}\bigg|_{\epsilon=0.8-} = 0.011\,\mathrm{W/mK} \tag{6.48}$$

$$\frac{\partial k_e}{\partial \epsilon}\bigg|_{\epsilon=0.8+} = 0.014\,\mathrm{W/mK} \tag{6.49}$$

The sensitivity of k_e for ϵ variations is

$$S_\epsilon = \frac{\partial k_e}{\partial \epsilon} = 0.0125\,\mathrm{W/mK} \tag{6.50}$$

(b) $T = 800$ K

$$\frac{\partial k_e}{\partial \epsilon}\bigg|_{\epsilon=0.8-} = 0.148\,\mathrm{W/mK} \tag{6.51}$$

$$\frac{\partial k_e}{\partial \epsilon}\bigg|_{\epsilon=0.8+} = 0.174\,\mathrm{W/mK} \tag{6.52}$$

The sensitivity of k_e for ϵ variations is

$$S_\varepsilon = \frac{\partial k_e}{\partial \varepsilon} = 0.161\,\mathrm{W/mK} \tag{6.53}$$

(c) $T = 1\ 300$ K

$$\frac{\partial k_e}{\partial \epsilon}\bigg|_{\epsilon=0.8-} = 0.531 \text{ W/mK} \tag{6.54}$$

$$\frac{\partial k_e}{\partial \epsilon}\bigg|_{\epsilon=0.8+} = 0.608 \text{ W/mK} \tag{6.55}$$

$$S_\epsilon = \frac{\partial k_e}{\partial \varepsilon} = 0.570 \text{ W/mK} \tag{6.56}$$

Figure 6.19, and the values for the variations in ϵ show that the sensitivity of k_e for ϵ variations S_ϵ increases with increasing temperature.

The effect of the mean particle diameter (d) on the equivalent conductivity

Table 6.8 Effect of the particle diameter on k_e

d (mm)	0.185	0.195	0.205
k_e (W/mK)	0.8194	0.8197	0.8200

From Table 6.8, we obtain:

$$\frac{\partial k_e}{\partial d}\bigg|_{d=0.195-} = 0.03 \frac{\text{W/mK}}{\text{mm}} \tag{6.57}$$

$$\frac{\partial k_e}{\partial d}\bigg|_{d=0.195+} = 0.03 \frac{\text{W/mK}}{\text{mm}} \tag{6.58}$$

The sensitivity for the particle diameter d is

$$S_d = \frac{\partial k_e}{\partial d} = 0.03 \frac{\text{W/mK}}{\text{mm}} \tag{6.59}$$

In conclusion, the equivalent conductivity of packing materials depends strongly on the conductivity of the gas phase, temperature and porosity. Although there is also a strong dependence on emissivity at higher temperatures,

this does not have practical importance, as all literature sources suggest that the emissivity of the coke particles does not show a great variance and it already has a relatively high value (> 0.8).

The contribution of the particle conductivity is relatively weak, but it is the only factor — besides the porosity and grain size — that can be changed, by replacing one type of coke with another. The right values of $k_{particle}$ and k_g are very important for the calculation of k_e by using the Zehner model.

The numerical values of the sensitivity factors must be taken with caution because of the assumption that $dQ_i = d\phi_i$. In future work, when Q_i is measured these factors should be recalculated.

Chapter 7 RESULTS AND DISCUSSION

7.1 Guard Heating Method

We measured conductivity of packing coke with the guarded hot plate method. For the development of the equivalent conductivity models, we need the volume fraction of the intergranular air, i.e. bulk porosity, P_{bulk} given by Equation 4.14. For this purpose, a single particle density of 1 678 kg/m^3, which is the mean value of our four measured particle densities (see Table 4.2), is used for all the samples (see Table 7.1). The reason for using mean particle density was to include the effect of the open pore air inside the particles, so the particle density can be correlated later physically with the equivalent conductivity of the grains.

The conductivities listed are the mean values from numerous measurements in the 25°C to 80°C temperature range. Each sample was tested at least three different heat flux values and at least three different thicknesses of the layer of the granular material.

Table 7.1 Conductivity of coke measured by guarded heating method and bulk porosity
of the samples, calculated by using a single particle density value of 1 678 kg/m^3

Sample	ρ_{bulk} (kg/m^3)	P	k (W/m K)
1ARGVERT	584	0.65	0.22
2FCUNEUF	1 134	0.32	0.89
3FCNEUF	1 106	0.34	0.64
4FCUSAGE	1 127	0.33	0.72
5PEUSAGE	978	0.42	0.72
6RHUSAGE	743	0.56	0.74
7RHUSAGE	644	0.62	0.50
8RHNEUF	677	0.60	0.49
9RHUSAGE	683	0.59	0.53
10PENEUF	720	0.57	0.53
11PEUSAG	1 076	0.36	0.78
12PEUSAG	1 084	0.35	0.82
13PEUSAG	1 121	0.33	0.74
14RHUSAG	713	0.58	0.59

The most important general tendency is that with increasing porosity the bulk
conductivity is decreasing. This is in agreement with our preliminary expectations
and can be explained by the insulating role of the intergranular gas, which
increases with increasing porosity.

The dependence of the equivalent conductivity on the bulk porosity is shown
later in this chapter, in Figure 7.7. The interpretation of these results is based on
the equivalent conductivity models.

Chapter 7

7.2 Flash Method

Due to the difficulties to obtain appropriate size samples for the tests, only few of the biggest grains from samples 6RHUSAGE and 8RHNEUF were selected and measured by the flash method. The results are given in Table 7.2. Where conductivity was calculated by Equation 3.10, ρ and c_p were obtained from Tables 7.1 and 4.3, respectively. The measurements were made at 26°C. The results characterize the conductivity (particle conductivity) of the big particles, and include the effects of the porosity inside the grains. For the same sample, the diffusivity and conductivity are different with the particles as the particles' shape of granular materials are not the same.

Table 7.2 Particle diffusivity and conductivity at room temperature by flash method

Sample		α (m^2/s)	k (W/m°C)
6RHUSAGE	1	1.127×10^{-6}	0.73
	2	8.66×10^{-7}	0.56
8RHNEUF		7.30×10^{-7}	0.43

The equivalent conductivities of the coke samples measured by using flash method are similar to those measured by guarded heating method.

7.3 Monotonic Heating Method

All high temperature measurements were done in the newly developed test rig using the monotonic heating method. In the first series of measurements we

used the two-point temperature measurement arrangement. Some of the measured temperature histories during the tests are shown in Figures 7.1 and 7.2. The diffusivities and conductivities were calculated from these curves according the formulas derived in the previous chapters. Each measurement was repeated 3 – 4 times for each sample. To evaluate the thermal conductivity from the diffusivity, a mean specific heat from 20°C to 1 000°C, c_p = 1 193 J/kgK, is taken from literature [28]. Figure 7.3 gives the measurements for 11PEUSAG. Sample 12PEUSAG was measured with the two-point and three-point temperature measurement methods. We found there is big difference between the two methods in the case of sample 12PEUSAG (see comparison in Figure 7.5). Note that for a better visualization of the differences, we used a bigger vertical scaling factor in this diagram than in the summary of the measurement results, Figure 7.4. Samples 13PEUSAG and 7RHUSAGE were measured with three-point measurement method. Samples 11PEUASG, 12PEUSAG and 13PEUSAG come from the same furnace and are all used packing coke (poussiers usagés Pechiney). It is therefore not suprising that they have similar structure, a relatively high bulk density and also similar low temperature thermal conductivity. The results are shown in Table 7.3. The bulk (equivalent) conductivity is around 0.7 – 0.8 W/mK at 200°C, — close enough to the values measured by the steady state method — and shows a nearly linear increase of 40 – 50% from 200°C to 1 000°C.

Seeing that these three samples show a very similar behavior, we selected

another sample with a significantly different structure. Sample 7RHUSAGE (poussier usagé Riedhammer) has the lowest bulk density, and we found also the biggest particles in this sample. The measured bulk density curve versus temperature is also shown in the same graph, Figure 7.4. This sample shows a very different behavior from the previous ones. The low temperature value, extrapolated from the high temperature measurements, is not very different than the conductivity measured at near room temperature by the guarded hot plate method (see Table 7.5, and Figure 7.15). However, the extrapolated cuvre of Sample 7RHUSAGE goes down from room temperture to 200°C. There is a fourfold increase of the thermal conductivity from 200°C to 1 000°C. This tendency is explained by the presence of the larger particles. The role that porosity plays, changes dramatically as temperature increase, specially in the presence of big particles. We cannot draw conclusions purely by evaluating the role of porosity alone, particle size, granulometry are nearly independent players in the overall effect.

Figure 7.6 is the equivalent conductivity of anthracite whose particle size is larger (about 10 – 15 mm). It shows also a strong temperature dependence. The variation from 150°C to 1 000°C is about fivefold increase.
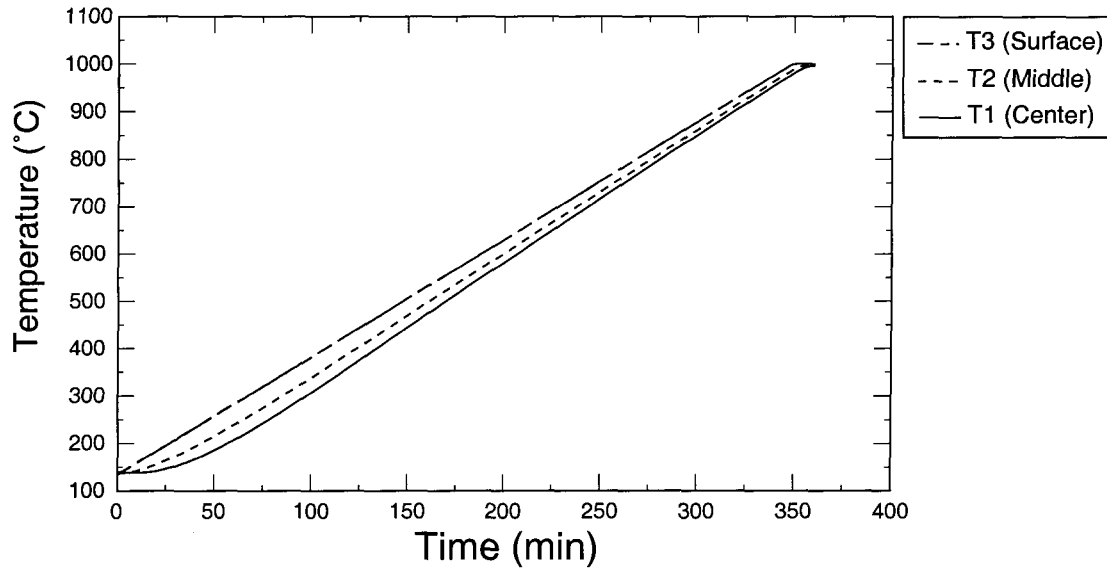
Figure 7.1 The temperature history of 7RHUSAGE (three points method)
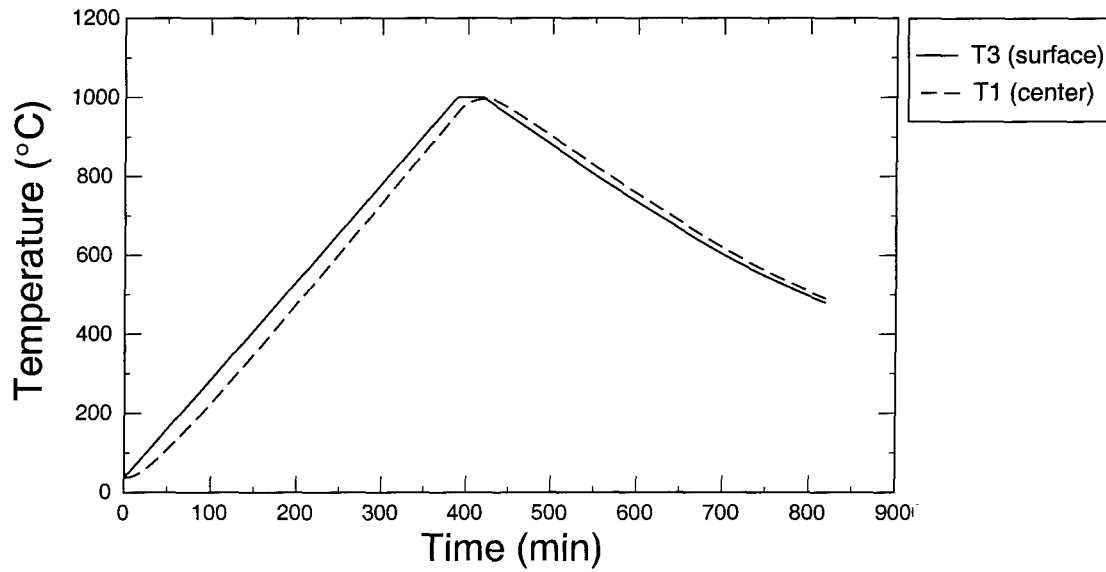
Figure 7.2 The temperature history of 11PEUSAG (two points method)
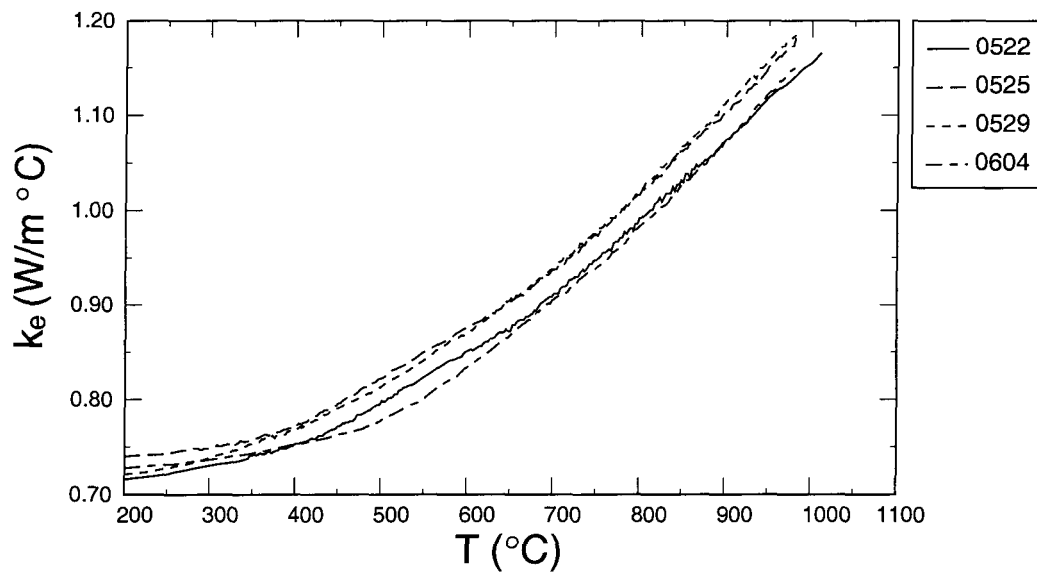
Figure 7.3 The experimental results of 11PEUSAG
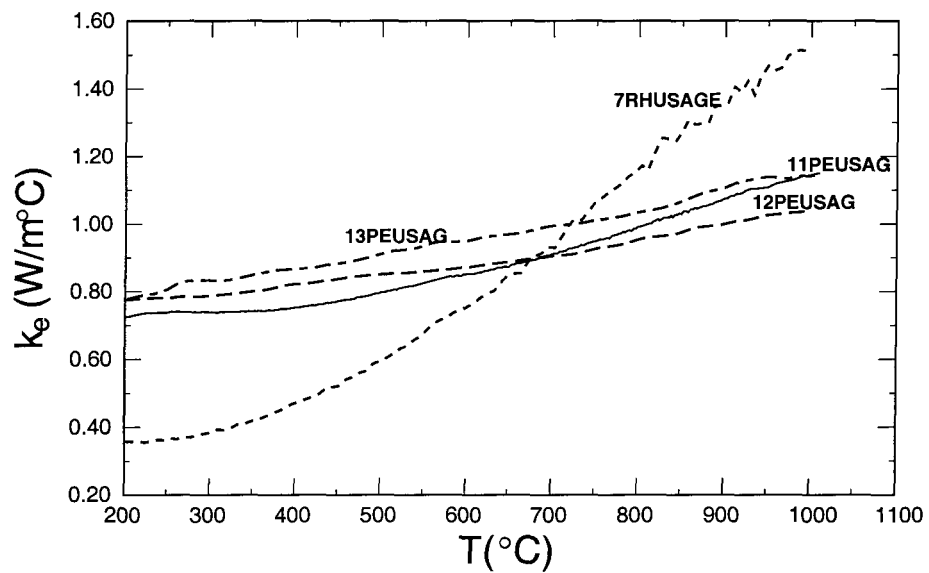
Figure 7.4 The equivalent conductivity of coke

Table 7.3 Conductivity of coke

| Temperature (°C)	Conductivity (W/m°C)			
	7RHUSAGE	11PEUSAG	12PEUSAG	13PEUSAG
200	0.36	0.73	0.78	0.78
250	0.36	0.74	0.79	0.81
300	0.38	0.74	0.79	0.83
350	0.42	0.74	0.79	0.85
400	0.47	0.75	0.82	0.87
450	0.52	0.77	0.82	0.88
500	0.59	0.80	0.82	0.91
550	0.68	0.82	0.86	0.94
600	0.75	0.85	0.87	0.95
650	0.85	0.87	0.89	0.97
700	0.93	0.91	0.90	0.97
750	1.07	0.95	0.93	1.01
800	1.16	0.99	0.95	1.03
850	1.27	1.03	0.98	1.07
900	1.35	1.07	0.99	1.11
950	1.47	1.11	1.00	1.14
1 000	1.51	1.15	1.04	1.14
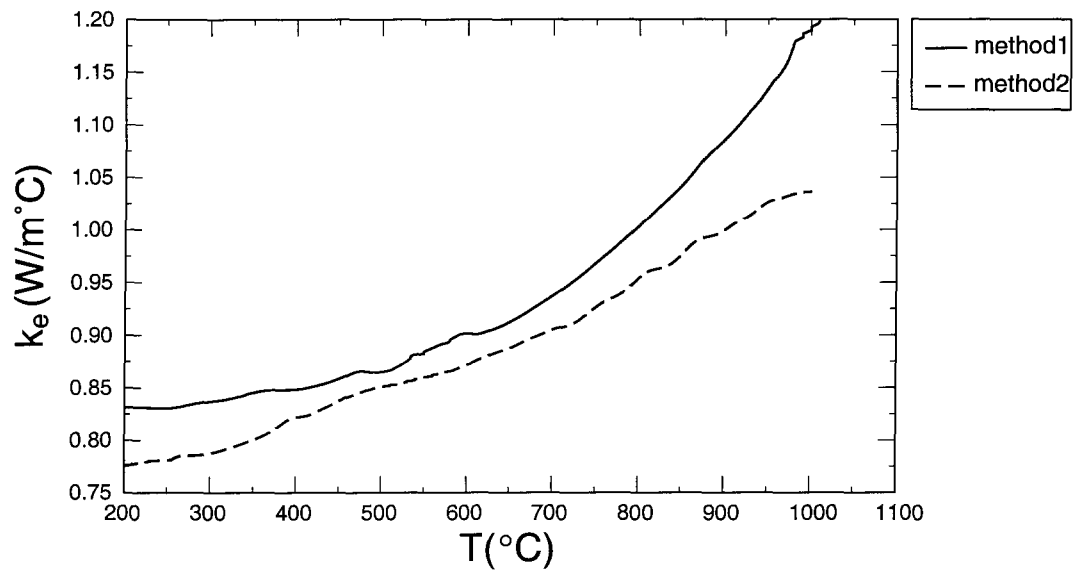
Figure 7.5 The conductivity of 12PEUSAG measured by two methods, method 1 is two-point and method 2 three-point temperature measurement
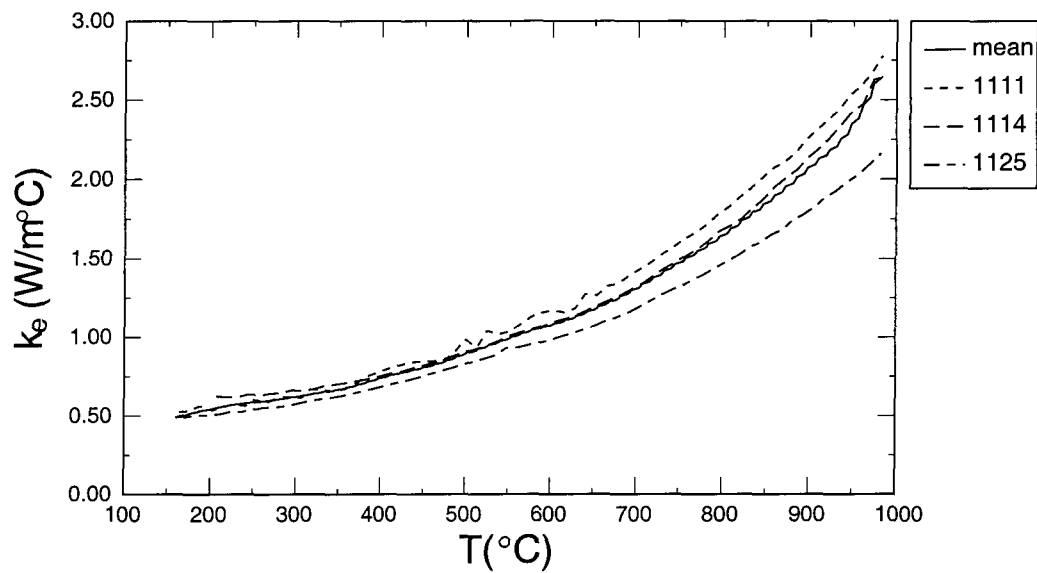

Figure 7.6 The equivalent conductivity of anthracite

Table 7.4 Conductivity of anthracite

Temperature (°C)	Conductivity (W/m°C)			
	No.1111	No.1114	No.1125	Mean
150	0.51	0.65	0.49	0.55
200	0.54	0.63	0.51	0.56
250	0.60	0.63	0.54	0.59
300	0.62	0.66	0.58	0.62
350	0.66	0.70	0.62	0.66
400	0.78	0.75	0.68	0.74
450	0.85	0.82	0.75	0.81
500	0.98	0.91	0.83	0.91
550	1.03	1.00	0.93	0.99
600	1.17	1.09	0.98	1.08
650	1.27	1.19	1.07	1.18
700	1.42	1.32	1.18	1.31
750	1.60	1.49	1.32	1.47
800	1.80	1.69	1.47	1.65
850	2.04	1.90	1.63	1.85
900	2.27	2.15	1.80	2.07
950	2.55	2.43	2.01	2.33
1 000	2.92	2.67	2.26	2.62

7.4 Comparison of Models with the Experimental Results

7.4.1 Model A (Krischer model) and model B

In order to compare the predictions of the equivalent conductivity values,

we plotted all the measured room temperature results into the $k_e - P$ graph of model A and model B respectively. Here the conductivities are equal to the individually determined values given above in Table 7.1, but the bulk porosities of the samples are approximate as they were calculated from the individually measured bulk densities by using a single estimated particle density value of $1\,678\,\text{kg/m}^3$. Another common value we used for all the samples in the equivalent conductivity model is the particle conductivity of 1.607 W/mK, obtained from Equation 6.2 for 100°C.

The comparison of experimental data to $k_e - P$ curve of model A is shown in Figures 7.7 and 7.8. We can see the $k_e - P$ curve of model A with $a = 0.03$ and model B with $a = 0.25$ agree well with most of the experimental results. Granular materials with open pores may be better described by model B.
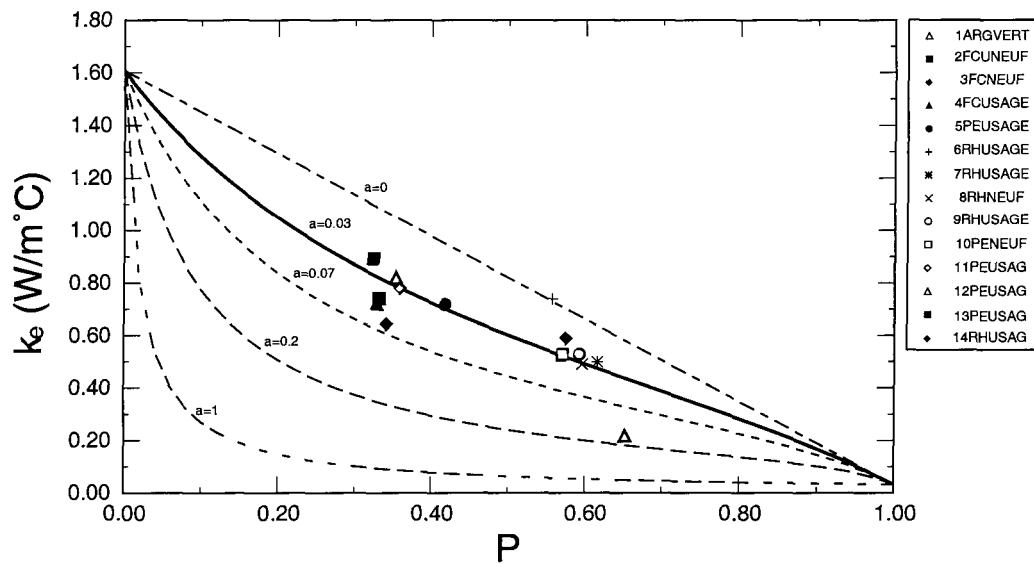
Figure 7.7 Comparison of model A and experimental
results for the conductivity of coke for k_s = 1.607 W/mK
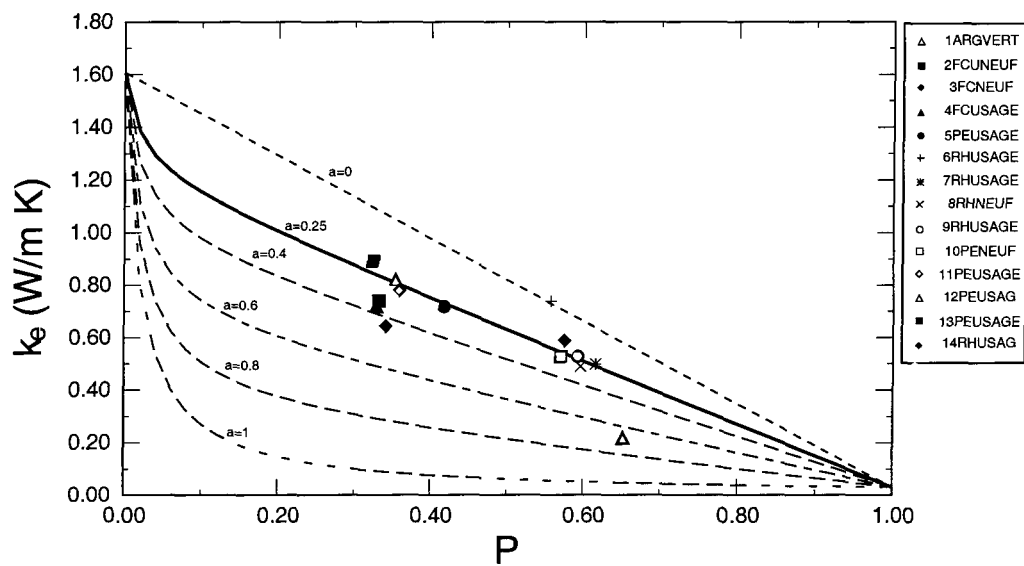
Figure 7.8 Comparison of model B and experimental
results for the conductivity of coke for k_s = 1.607 W/mK

In Reference [28], the thermal conductivity of coke is 2.908 – 3.489 W/mK.

So we input the value of 3.489 W/mK to the model A and B to compare the two

models with our experimental results (see Figures 7.9 and 7.10). From Figures

7.9 and 7.10, we see that the k_e – P curve of model A with a = 0.07 and model

B with a = 0.67 agree very well with most experimental results. The comparison

with Figures 7.7 and 7.8 shows that the solid conductivity influences greatly the

value of a.
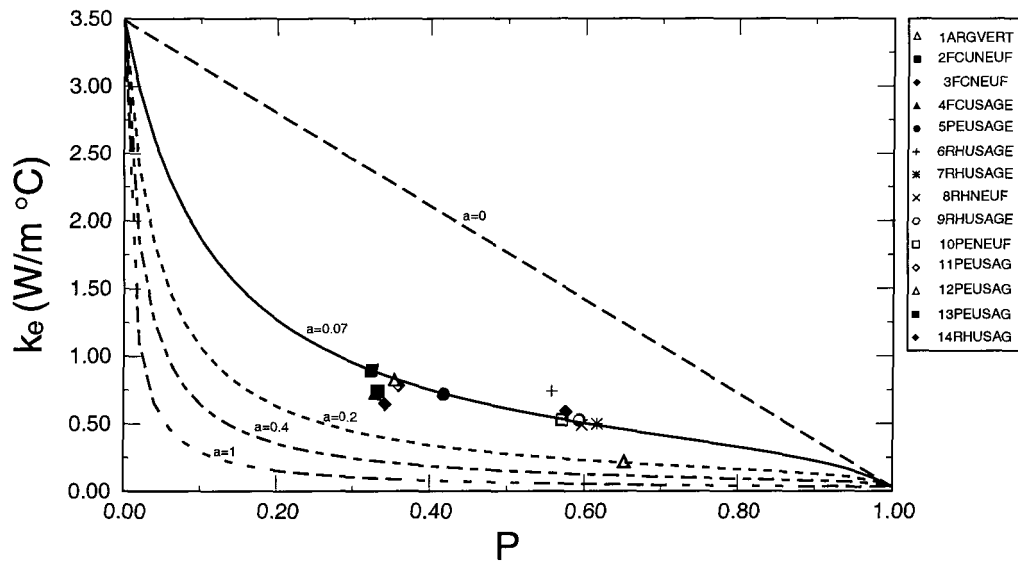
Figure 7.9 Comparison of model A and experimental
results for the conductivity of coke for k_s = 3.489 W/mK

Chapter 7
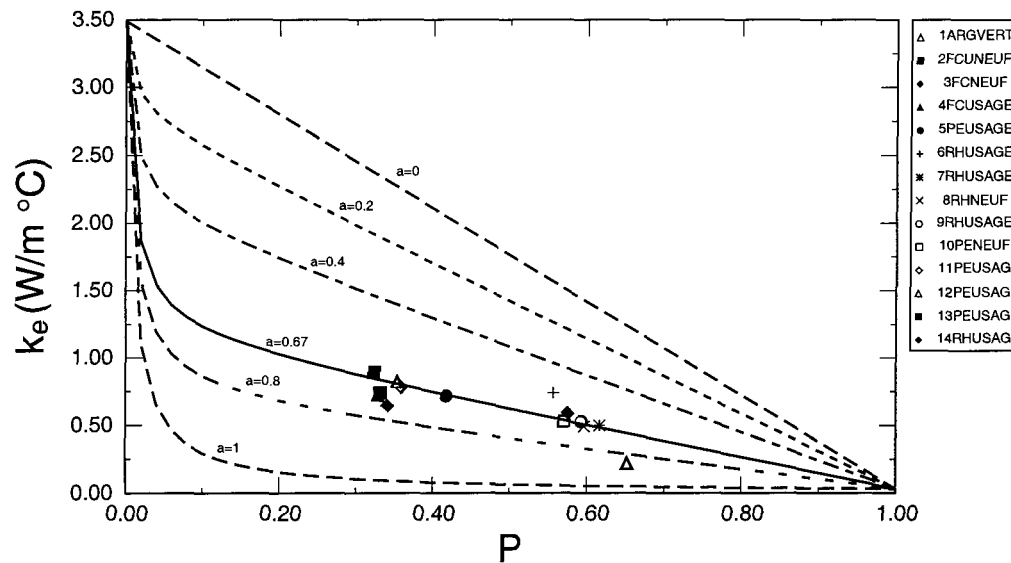
Figure 7.10 Comparison of model B and experimental
results for the conductivity of coke for k_s = 3.489 W/mK

In this comparison, the individual differences among the different packing
cokes are characterized solely by the variations in the bulk density. Considering
that this simplified approach cannot take into account the differences in the
composition of the solid component, in its emissivity, in particle shape and size
distribution the variations — the relatively small scattering is rather surprising.
This comparison gives further indication that the solid conductivity (particle
conductivity) has a weaker effect on the equivalent conductivity of the packing
coke than the structural parameters like porosity, structure of the unit cell (parallel-
serial relations), particle size. The parametric analysis by the mathematical
models of the equivalent conductivity provide further support for the mentioned
tendencies.

Chapter 7

Even the simple equivalent conductivity models, which describe the topological properties of the unit cell by a combination of serial and parallel connected elements and different porosities, provide enough room to adjust the model to the real behavior of the packing coke. The character of the temperature dependence is strongly affected by the selection of these structural parameters (the seriality factor a, the porosities of the serial and parallel sub-cells P_s and P_p). Unfortunately we do not have enough experimental data to be able to identify these geometrical parameters together with the other important factors like the conductivity of the grains $k_{particle}$ or k_{grain} and the radiation coefficient. The only way to obtain sufficient data is to make a series of measurements on the same type of coke but with different particle sizes and bulk densities. Also a series of measurements with different intergranular gases, having different gas conductivities would help identify the model parameters by changing an internal variable and at the same time keeping others like particle size, particle conductivity, granulometry, radiative transfer constant.

7.4.2 Zehner-Bauer model

Using the equations of the Zehner-Bauer model, we have computed and plotted the k_e–P curve of the packing coke. Lacking more detailed information about the individual differences among the solid conductivities of the various cokes, we tried two solid conductivity values of each sample for all different

porosities. The comparison between the experimental results (Table 7.1) and the

Zehner-Bauer model are illustrated in Figure 7.11.
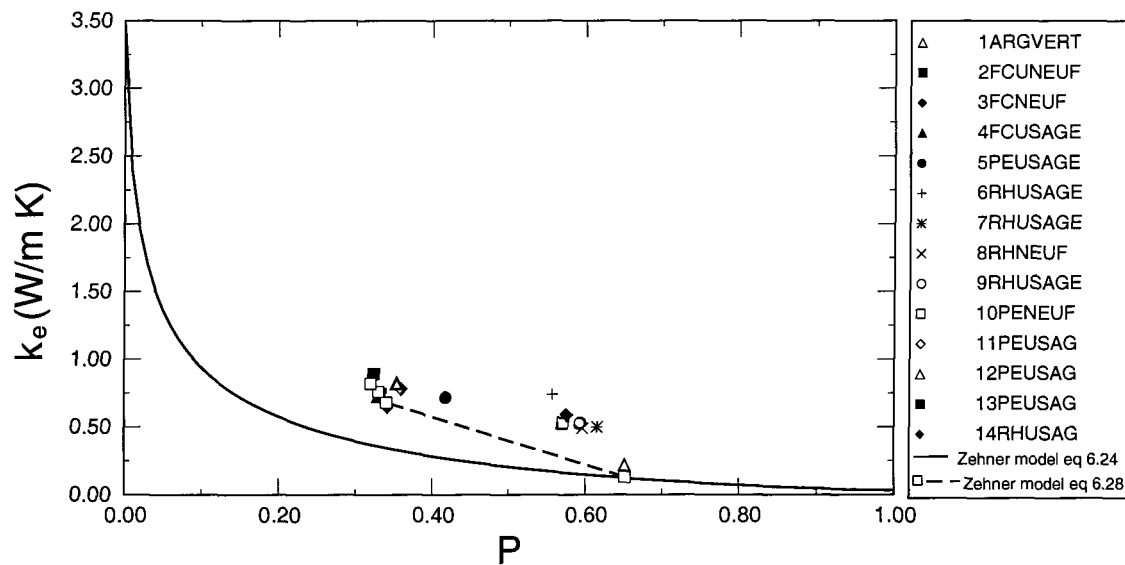
Figure 7.11 Comparison of experimental results with
the model of Zehner–Bauer for k_s = 3.489 W/mK

Two fitting curves are shown: The first curve is obtained with the basic model

described by Equation 6.24 and Table 6.4. The fitting is not good. The second

curve is obtained with the extended model described by Equation 6.28. This model

requires particle distribution parameters d_i and Q_i. This curve was calculated for

four samples only whose particle distribution and porosity were measured (see

Chapter 4). Howerer, the particle distribution was measured on the basis of weight

fraction only, and we assumed that $Q_i = d\phi_i$. This assumption may have affected

the goodness of fit. Nevertheless, we can cautiously conclude that the secondary

parameters of the Zehner model such as form factor C_f, flattening coefficient and granulometry distribution, etc. also play an important role. Particle analysis, including the measurement of Q_i, should be done on many more samples in the future research in order to draw definite conclusions.

7.4.3 Other references

The data for the thermal conductivity of petroleum coke reported previously are shown in Figure 7.12 and Equation 7.1 [27]. All references in Figure 7.12 show an increase with increasing temperature.
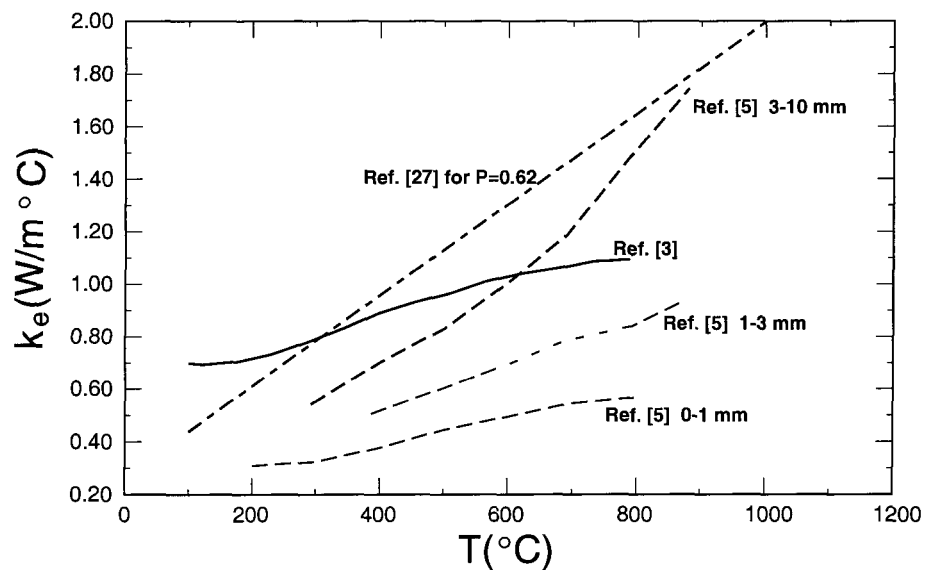

Figure 7.12 Thermal conductivity of coke

Equation 7.1 is the thermal conductivity of coke as a function of porosity and temperature reported in Reference [27] which were measured in the temperature

range from 100 to 1 400°C by using the laser flash method. Their results show that the effect of radiation in coke pores on the value of equivalent thermal conductivity of coke was very small. The following empirical equation was obtained for equivalent thermal conductivity k_e, W/mK, as a function of temperature T, K, and porosity P, for all kinds of coke.

$$k_e = \left[0.973 + 6.34 \times 10^{-3}(T - 273)\right]\left(1 - P^{\frac{2}{3}}\right) \tag{7.1}$$

The thermal diffusivity and conductivity of the coke particles was also determined by ourselves for certain samples, using the flash method at room temperature level, as it was described earlier in this chapter. Our measured results of equivalent conductivity lie in the range given by [3] and [5] for the same particle diameter. The measurements of Reference [5], given in Appendix B, are of particular significance for us since the same kind of coke, the packing coke for anode furnaces, was measured.

We compared our measured k_e with Equation 7.1 near room temperature, using porosity values from Table 7.1 in Equation 7.1, and at high temperatures. We found it is close to our results measured by guarded heating method near room temperature (Figure 7.13). But big differences were found between the curves calculated from Equation 7.1 by using the porosities of the four samples at higher temperature and our experimental results obtained with the monotonic heating method (see Figure 7.14). Furthermore the slope of the calculated curve using the

porosity of sample 7RHUSAGE is smaller than the others (from Equation 7.1 the slope decreases with increasing porosity) which is contrary to our results. One of the reasons is that in Reference [27] the influence of the radiation on the effective thermal conductivity of coke was concluded to be negligibly small. Another reason may be the type of coke: we measured petroleum coke, whereas Equation 7.1 [27] is for metallurgical coke. Also, the mean particle diameter of Reference [27] was not specified and may have been quite different with our cokes.
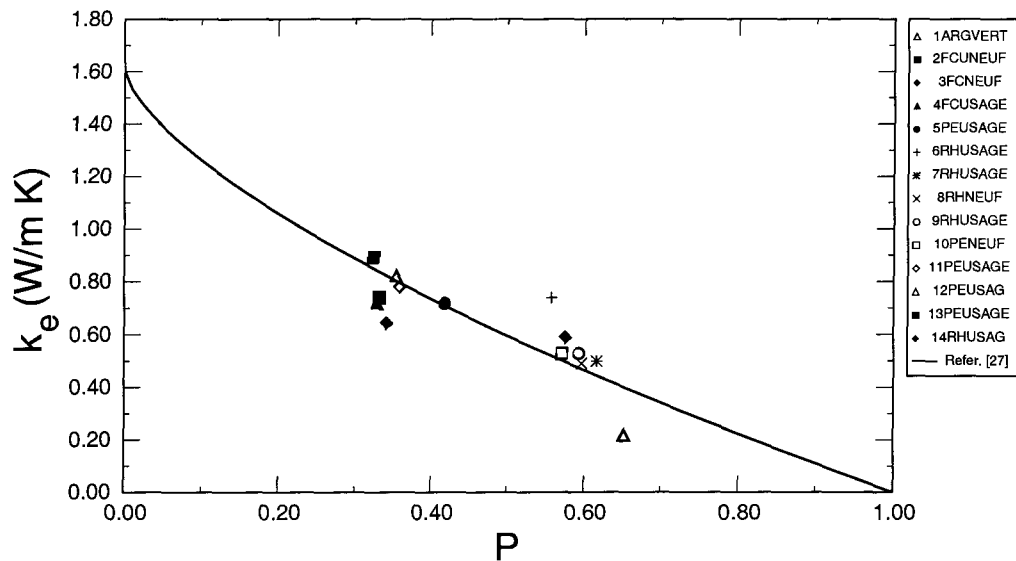

Figure 7.13 Comparison of the experimental results near room temperature with Equation 7.1
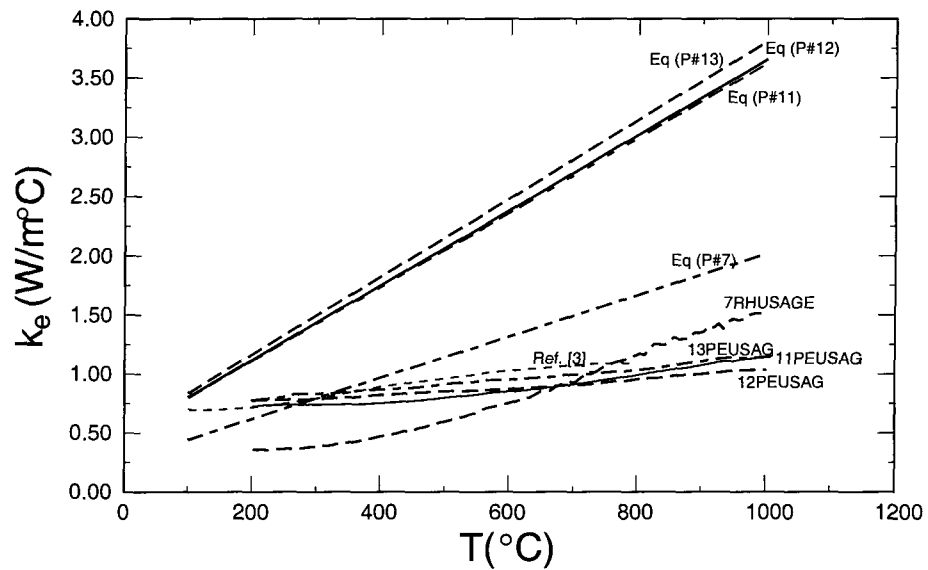
Figure 7.14 Comparison of the experimental results measured by monotonic heating method with Reference [3] and Equation 7.1 [27] (Eq(P#7): $k_e - T$ calculated from Equation 7.1 by using the porosity of 7RHUSAGE; Eq(P#11): $k_e - T$ calculated from Equation 7.1 by using the porosity of 11PEUSAG; Eq(P#12): $k_e - T$ calculated from Equation 7.1 by using the porosity of 12PEUASG; Eq(P#13): $k_e - T$ calculated from Equation 7.1 by using the porosity of 13PEUASG

7.5 Modelling of the Relationship Between Temperature and the Conductivity

In order to analyze the relationship between the conductivity and the temperature of coke, we have tried to find the fitting curves to the measured results by using an empirical formula for the conductivity in form of

$$k(T) = b_0 + b_1 T + b_2 T^2 + b_3 T^3 \qquad (7.2)$$

or

$$k(T) = b_0 + b_1 T + b_2 T^2 \qquad (7.3)$$

Chapter 7

The fitting curves are given to temperatures in °C and K. The polynomial curves (Equation 7.2) of the third order show good fitting to the experimental results of the sample 7RHUSAGE, quadratic fitting gives best fit for the samples 11PEUSAG, 12PEUSAG and 13PEUSAG. The fitting curves and the original data are shown in Figure 7.15. Note that the curve of sample 7RHUSAGE is more curved than the others. We explain this with the fact that 7RHUSAGE contains much larger particles and less fines than the other three tested cokes. The stronger temperature dependence is probably due to the more important role of radiation inside the packing coke, which is attenuated by the presence of the numerous solid-gas interfaces in the samples with small particles.
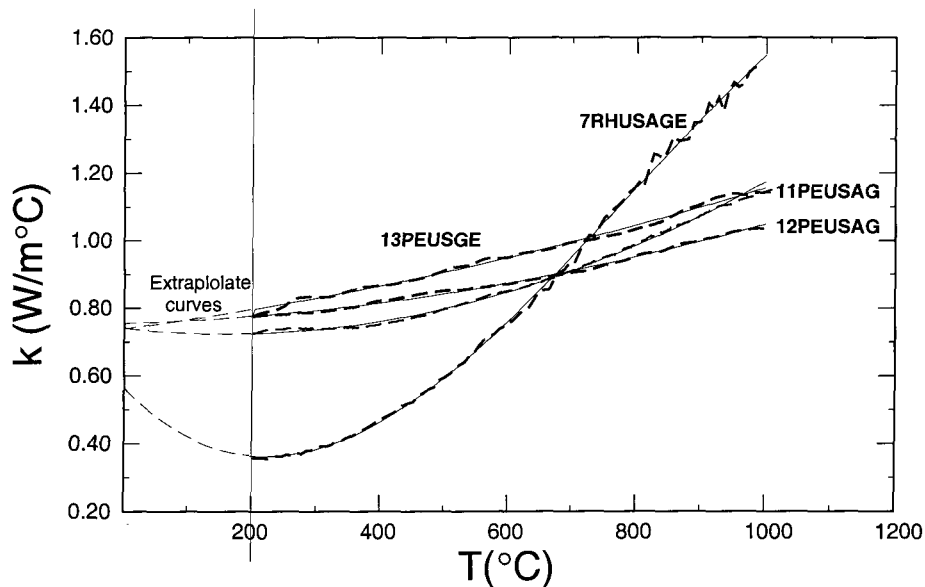

Figure 7.15 The fitting curves of $k_e - T$ curve

The fitting equations are listed as follows:

11PEUSAG

for T in °C, $200^o C \leq T \leq 1000^o C$

$$k = 0.74 - 2.15 \times 10^{-4}T + 6.48 \times 10^{-7}T^2 \qquad (7.4a)$$

for T in K, $473\,K \leq T \leq 1273\,K$

$$k = 0.85 - 5.68 \times 10^{-4}T + 6.48 \times 10^{-7}T^2 \qquad (7.4b)$$

12PEUSAG

for T in °C, $200^o C \leq T \leq 1000^o C$

$$k = 0.76 + 5.30 \times 10^{-5}T + 2.43 \times 10^{-7}T^2 \qquad (7.5a)$$

for T in K, $473\,K \leq T \leq 1273\,K$

$$k = 0.76 - 8.28 \times 10^{-5}T + 2.43 \times 10^{-7}T^2 \qquad (7.5b)$$

13PEUSAG

for T in °C, $200^o C \leq T \leq 1000^o C$

$$k = 0.74 + 2.50 \times 10^{-4}T + 1.66 \times 10^{-7}T^2 \qquad (7.6a)$$

for T in K, $473\,K \leq T \leq 1273\,K$

$$k = 0.68 + 1.59 \times 10^{-4}T + 1.66 \times 10^{-7}T^2 \qquad (7.6b)$$

7RHUSAGE

for T in °C, $200^{o}C \leq T \leq 1000^{o}C$

$$k = 0.57 - 1.99 \times 10^{-3}T + 5.15 \times 10^{-6}T^2 - 2.19 \times 10^{-9}T^3 \qquad (7.7a)$$

for T in K, $473\,K \leq T \leq 1273\,K$

$$k = 1.55 - 5.29 \times 10^{-3}T + 6.95 \times 10^{-6}T^2 - 2.19 \times 10^{-9}T^3 \qquad (7.7b)$$

In order to compare the results of the monotonic heating method and guarded hot plate method, the fitting curves were extrapolated to the temperature of the guarded hot plate method for each sample. The results are shown in Table 7.5. We can see that the results of the two methods correspond well. However, it has to be noted that the extrapolated curve for the sample 7RHUSAGE shows a decrease of conductivity between the room temperature and 200°C, which seems unusual.

Table 7.5 Comparison of guard heating method and monotonic heating method

Sample	Guard heating method		Monotonic heating method
	k_e	T°C	k_e extrapolated
11PEUSAG	0.78	39.1	0.7349
12PEUSAG	0.821	40.2	0.7577
13PEUSAG	0.74	40.5	0.7495
7RHUSAGE	0.498	42.1	0.34

The fitting equation for anthracite is:

for T in °C, $150^o C \leq T \leq 1000^o C$

$$k = 0.2216 + 1.9738 \times 10^{-3}T - 3.068 \times 10^{-6}T^2 + 3.5 \times 10^{-9}T^3 \qquad \text{(7.8a)}$$

for T in K, $473\,K \leq T \leq 1273\,K$

$$k = -0.6179 + 4.4401 \times 10^{-3}T - 5.966 \times 10^{-6}T^2 + 3.5 \times 10^{-9}T^3 \qquad \text{(7.8b)}$$

Chapter 8 CONCLUSIONS AND SUGGESTIONS FOR FUTURE WORK

8.1 Conclusions

1. The methodology was developed and successfully applied for the experimental determination of the thermophysical properties of packing coke and anthracite up to 1 000 – 1 200°C.

2. We modified the classical monotonic heating method by measuring temperature histories in three points instead of two, making possible the simultaneous determination of thermal conductivity and diffusivity without the need to use heat capacity data from literature sources. We compared the two methods using the same coke samples, and we found a physically reasonable behavior of the 3 point method, the results from it being consistent with data from other measurements.

3. The equivalent thermal conductivity of all the 14 packing coke samples was determined experimentally in 25 – 80°C range. These values were then correlated with the porosities of the samples, and were used to verify the predictions of the equivalent conductivity models. Also, this data measured by the guarded hot plate method served the verification of the low temperature conductivities given by the monotonic heating method.

4. The equivalent thermal conductivity of four different packing coke samples was determined in the 200 – 1 000°C range. Three of these samples show a similar behavior, while the fourth (7RHUSAGE) is very different. It has lower conductivity at room temperature, but around 700°C its conductivity becomes equal to the others and at higher temperatures it is much higher than others. This finding warns us about the potential errors when room temperature data are used to compare the conductivities of different packing cokes.

    It is also evident from these graphs that the structure of the packing coke (particle size, granulometry, the presence of fine fractions) has a very strong influence on the bulk conductivity.

5. The influencing factors on the equivalent thermal conductivity of packing cokes were analyzed by using equivalent conductivity models. Without such a model that describes the dominant physical effects inside the granular material, one cannot interpret the differences between the packing cokes. Also, a well built and validated equivalent conductivity model can predict tendencies like the effect of crushing (changing granulometry) on the thermal conductivity and its temperature dependence.

    We found that the simple porosity models (model A and B in Chapter 6) offer ample opportunities to match the behavior of the real packing cokes. With four parameters (ratio of serial and parallel subcells, porosity in the parallel and serial subcells, particle conductivity), a wide range of bulk conductivity-

temperature functions can be simulated. To identify these parameters for the packing coke, we need further measurements, including measurements of bulk conductivity of the same coke but with different granulometry.

6. We found that the structural parameters (porosity, mean particle size, granulometry, geometry of topology of the unit cell) have a very strong influence on the equivalent conductivity of the packing coke, — even stronger than the conductivity of the solid component. With the reduction of the particle size, the conductivity is also reduced. The reasons are multiple: the radiative transfer is attenuated by the insertion of more "radiation shields", the number of contact points with serially connected contact resistances is increased, the size of the air spaces is effectively reduced, suppressing gas motion. The conductivity of the interstitial gas has also a strong influence on the bulk conductivity according to the simulations with the equivalent conductivity models.

7. The character of the temperature function of the equivalent conductivity is different for the different samples, but all measured results show higher than linear increase. The equivalent conductivity models can reproduce these tendencies by either the variation of the structural parameters or the temperature.

8. The comparison of our measurements with the Zehner-Bauer model was inconclusive, possibly because of our assumption that the volumetric fraction distribution required the model is equal to mass fraction distribution which

was measured.

8.2 Suggestions for future work

1. Test the remaining 10 samples at elevated temperatures.

2. Replace the recent sample container by another one made from Inconel, in order to be able continuing the tests up to 1 100–1 200°C.

3. Make measurements with the same samples, but with different gas atmospheres to be able to separate the contribution of the gas to the total equivalent thermal conductivity.

4. Measure the different particle size fractions of the same type of packing coke, in order to determine the role of the fines in the bulk as well as to identify a more realistic and reliable value of the thermal conductivity of the grains.

5. Measure the volumetric fraction distribution of the samples in order to test the Zehner-Bauer model appropriately.

BIBLIOGRAPHY

[1] L. I. Kiss, André Charette, Vinko Potocnik, and André Proulx. Measurement of the thermal conductivity and diffusivity of granular materials. Proposal, August, 1994.

[2] L. I. Kiss, Weixia Chen André Charette, and Vinko Potocnik. Thermophysical properties of granular carbon products. Report No. GRIPS-70, December, 1997.

[3] A. Schack, editor. *Industrial Heat Transfer*. John Wiley & Sons Inc., 1965.

[4] D. Q. Kern. *Process Heat Transfer*. McGraw-Hill Book Company, 1950.

[5] M. Fernández, J. Marletto, and H. Martirena. Combined mathematical simulation and experimental studies on a closed baking furnace. *Light Metals*, pages 805–817, 1983.

[6] R. L. Gorring and S. W. Churchill. Thermal conductivity of heterogeneous materials. *Chemical Engineering Progress*, 57(7):53–59, 1961.

[7] Y-M. Lee, A. Haji-sheikg, L. S. Fletcher, and G. P. Peterson. Effective thermal conductivity in multidimensional bodies. *Journal of Heat Transfer*, 116:1727, 1994.

[8] A. B. Duncan, G. P. Peterson, and L. S. Fletcher. Effective thermal conductivity within packed beds of spherical particles. *Journal of Heat Transfer*, 111:830–836, 1989.

[9] M. G. Laganer. Contact heat transfer in granular material under vacuum. *J. of Eng. Physics*, 11(1):30–36, 1966.

[10] J. C. Chen and S. W. Churchill. Radiate heat transfer in packed beds. *A.I.Ch.E. Journal*, 9(1):35–41, 1963.

[11] N. Wakao and D. Vortmeyer. Pressure dependency of effective thermal conductivity of packed beds. *Chemical Engineering Science*, 26:1753–1765, 1971.

[12] K. Nasr, R. Viskanta, and S. Ramadhyaani. An experimental evaluation of the effective thermal conductivities of packed beds at high temperatures. *J. of Heat Transfer*, 116:829–837, 1994.

[13] L. I. Kiss. Sujets speciaux (1). 1995.

[14] K. D. Maglic, A. Cezairliyan, and V. E. Peletsky. *Compendium of Thermophysic Property Measurement Methods*. Vol. 1 Plenum Press, 1984.

[15] H. S. Carslaw and J. C. Jaeger. *Conduction of Heat in Solids*. Oxford at Clarendon Press, 2nd edition, 1967.

[16] L. I. Kiss, B. Fall, A. Charette, and R. T. Bui. Experimental study of the thermophysical properties of solids. *Proceedings Intl. Symp. Dev. & Appl. Ceramics. CIM*, pages 143–154, 1993.

[17] W. J. Parker and Al. Flash method of determining thermal diffusivity, heat capacity and thermal conductivity. *J. of Applied Physics*, 332(9):1679, 1961.

[18] Loran S. O'Bannon. *Dictionary of Ceramic Science and Engineering*. Plenum Press, 1984.

[19] M. Jakob. *Heat Transfer*. John Wiley & Sons, Inc., 1967.

[20] T. Allen. *Particle Size Measurement*. Powder Technology Series. Chapman and Hall, third edition, 1981.

[21] L. I. Kiss. Thermophysical properties in heat conduction. Short course LTAS Université de Liège, March 18–26, 1996.

[22] B. Friedland. *Control System Design*. McGraw-Hill Book Co., 1986.

[23] D. E. Seborg, T. F. Edgar, and D. A. Mellichamp. *Process Dynamics and Control*. John Wiley & Sons, Inc., 1989.

[24] E. Tsotsas and H. Martin. Thermal conductivity of packed beds: a review. *Chem. Eng. Process.*, 22:19–37, 1987.

[25] P. Zehner and E. U. Schlünder. Wärmeleitfähigkeit von schüttungen bei mässigen temperature. *Chem.-Ing.-Tech.*, 42:933–941, 1970.

[26] J. P. Holman. *Heat Transfer*. McGraw-Hill Publishing Company, 7th edition, 1990.

[27] Akito Kasai, Takeaki Murayama, and Yoichi Ono. Measurement of effective thermal conductivity of coke. *ISIJ International*, 33(6):697–702, 1993.

[28] Kuzman Ražnjević. *Handbook of Thermodynamic Tables and Charts*. Hemisphere publishing corporation, 1976.

[29] L. I. Kiss. Sujets speciaux (2). 1996.

[30] Y. S. Touloukian, R. W. Powell, C. Y. Ho, and P. G. Klemens. *Thermophysical Properties of Materials The TPRC Date Series*, volume 2. IFI/Plenum Data Corporation, 1972.

BIBLIOGRAPHY

APPENDIX A   PICTURES OF THE COKE SAMPLES

1ARGVERT

2FCUNEUF

APPENDIX A

3FCNEUF

4FCUSAGE

APPENDIX A

mm 1 cm 2 3 4 5
5PEUSAGE

mm 1 cm 2 3 4 5
6RHUSAGE

APPENDIX A

7RHUSAGE

8RHNEUF

APPENDIX A

11PEUSAG

12RHUSAG

APPENDIX A

13PEUSAG

14RHUSAG
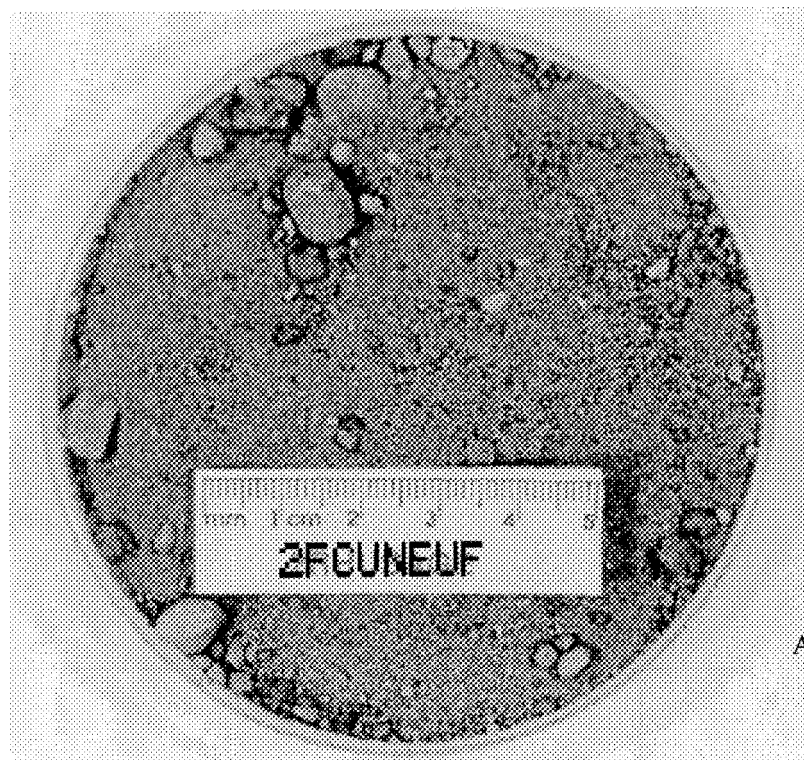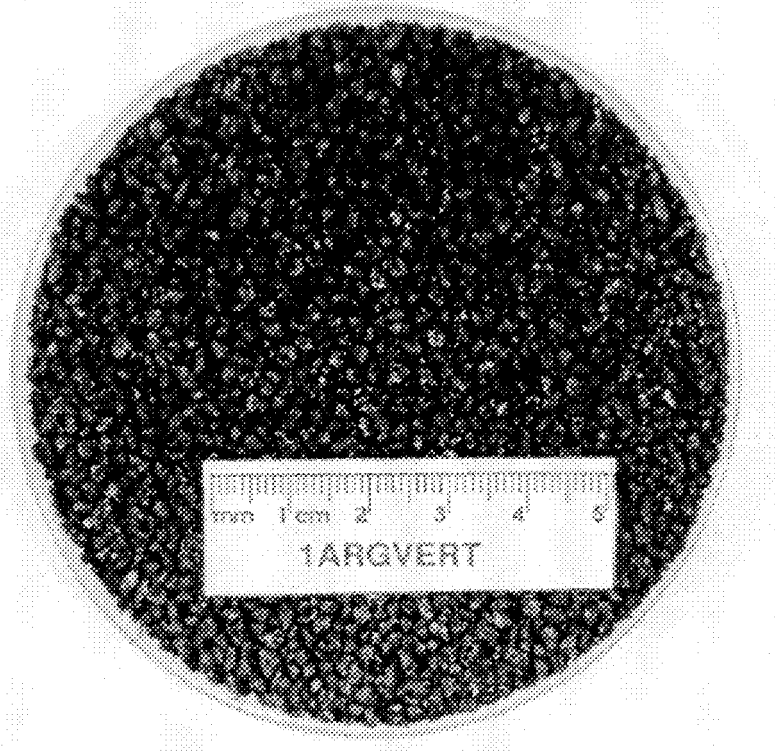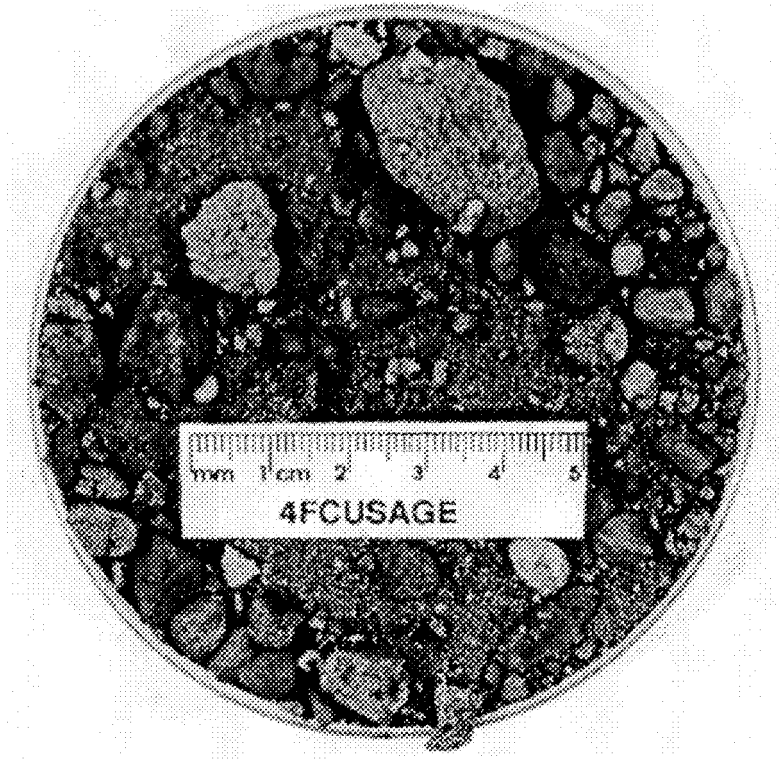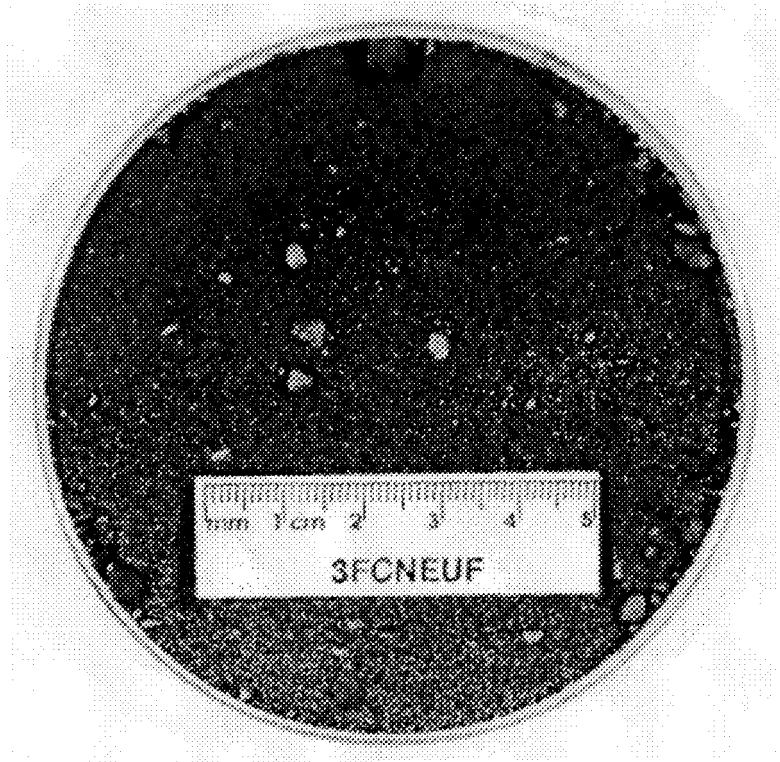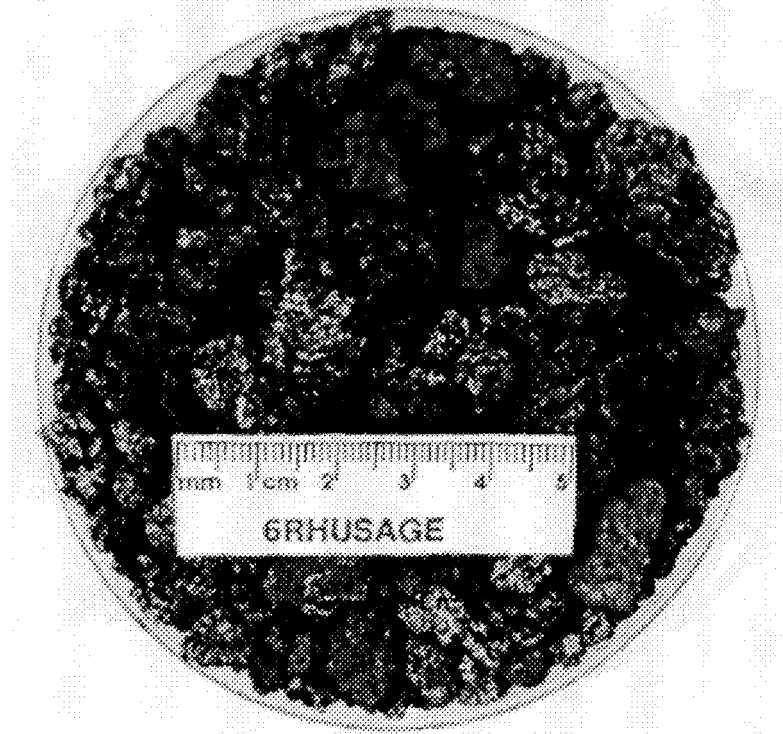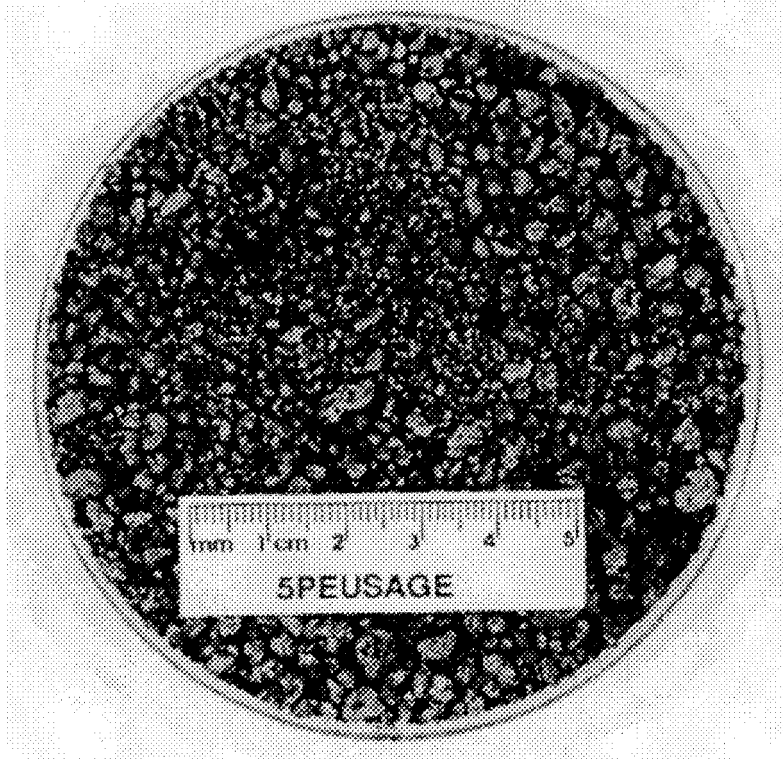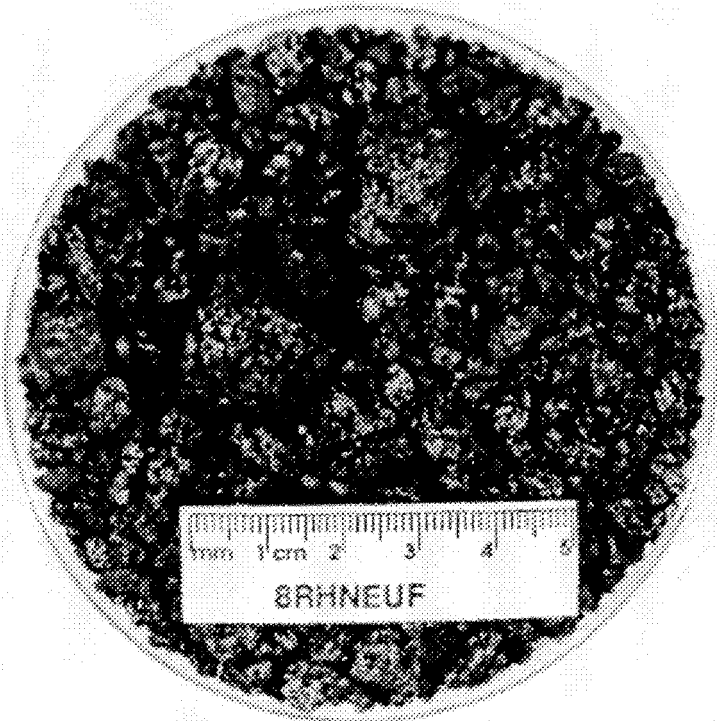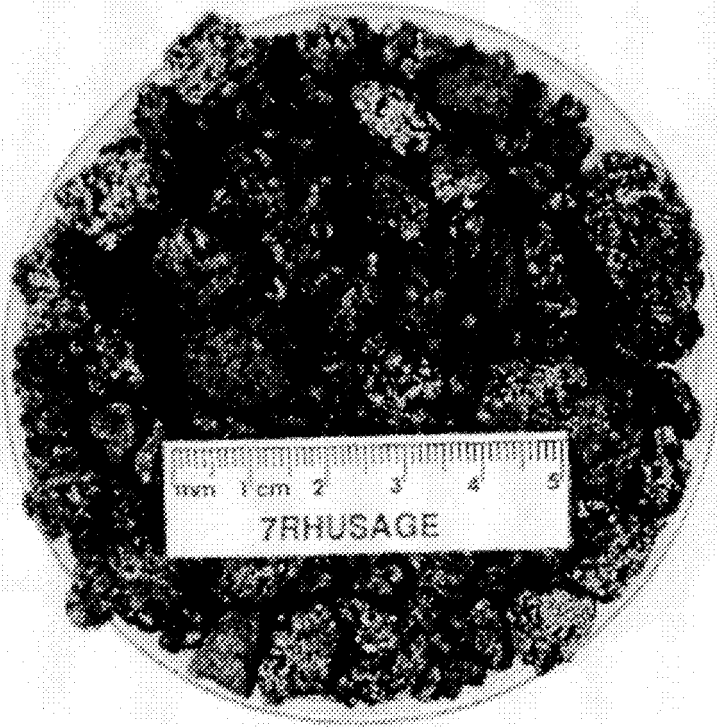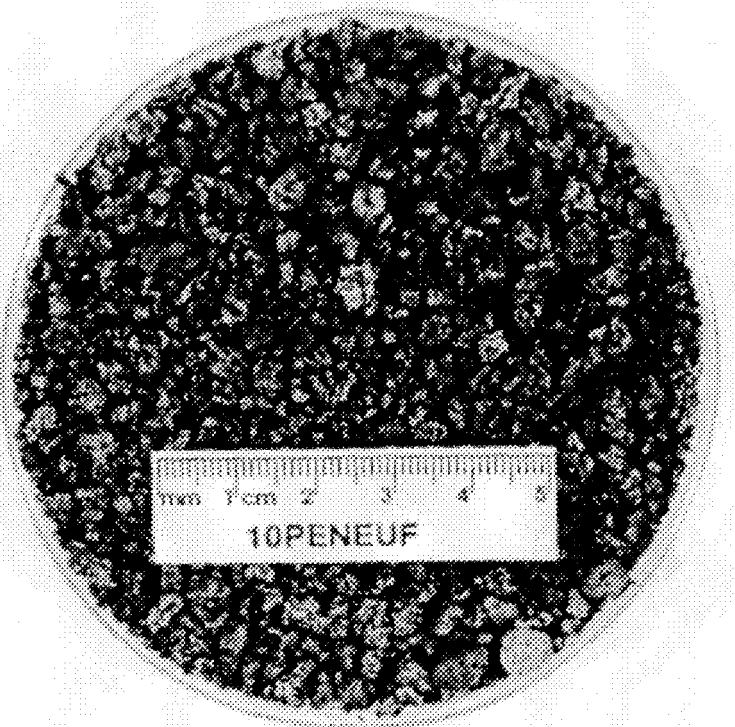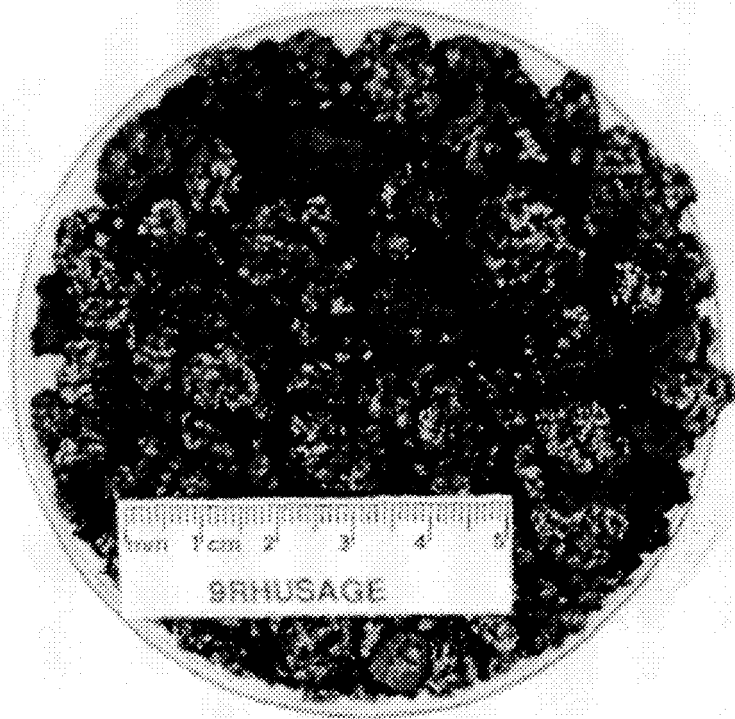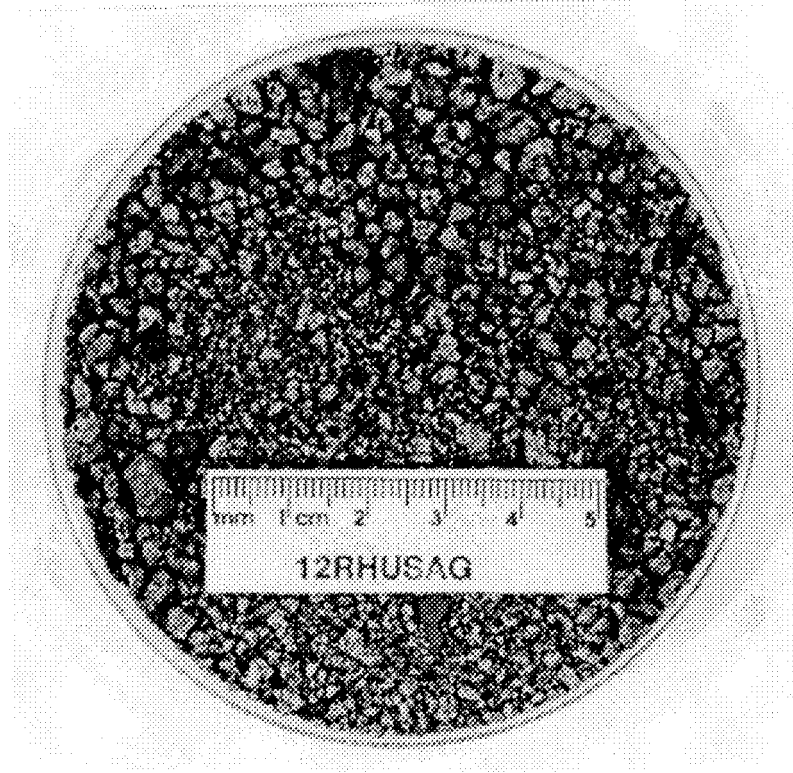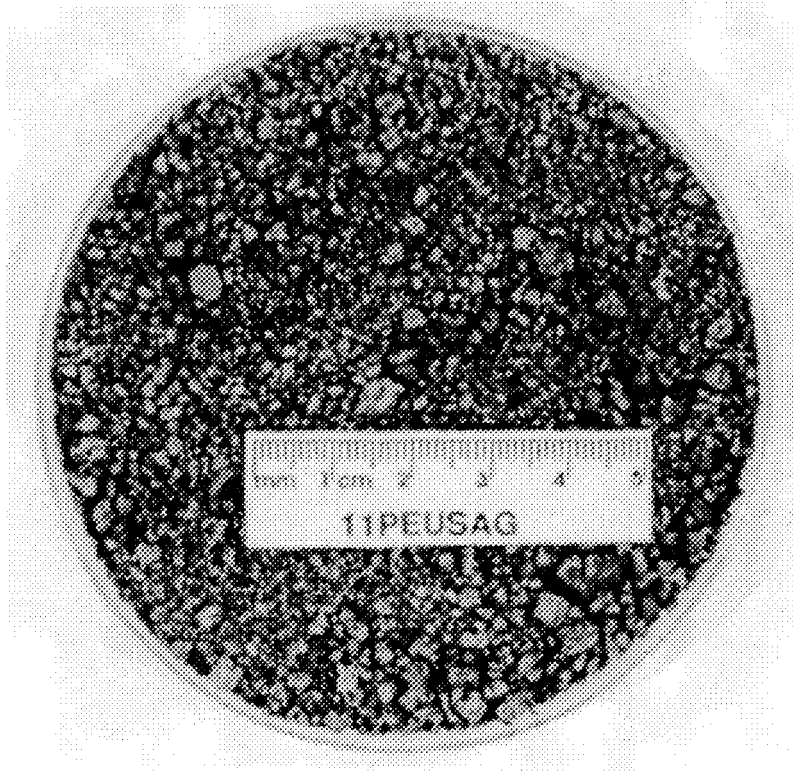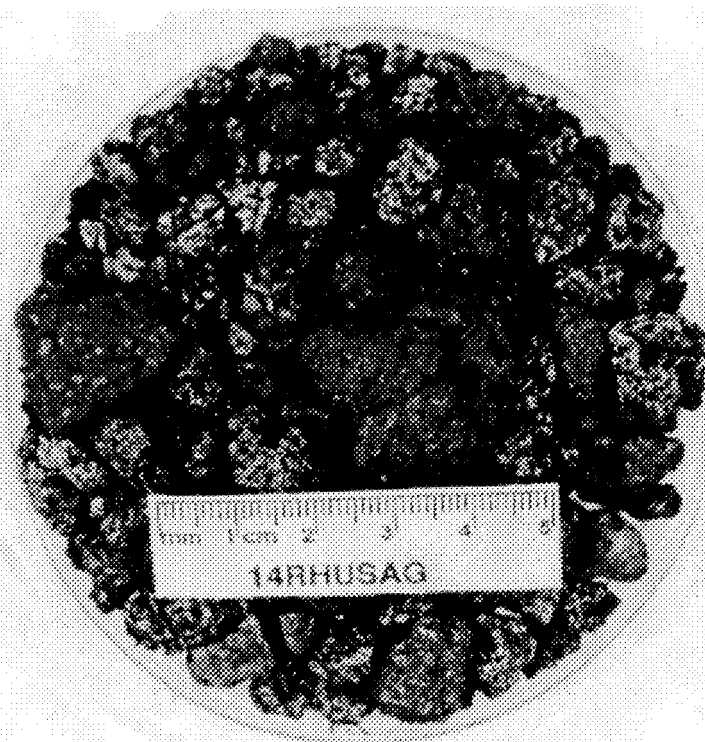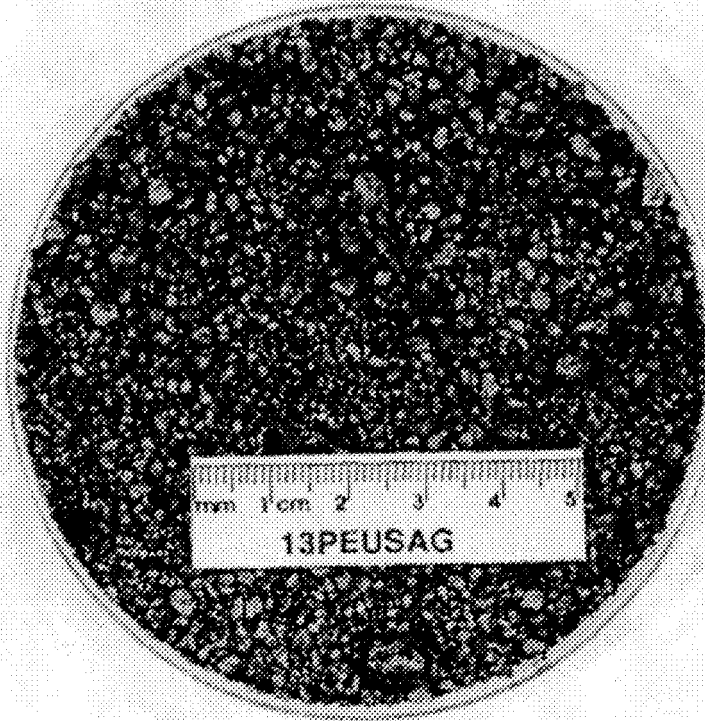
APPENDIX A

APPENDIX B   COMBINED MATHEMATICAL SIMULATION AND EXPERIMENTAL STUDIES ON A CLOSED BAKING FURNACE [5]

COMBINED MATHEMATICAL SIMULATION AND EXPERIMENTAL

STUDIES ON A CLOSED BAKING FURNACE

**Mónica E.de Fernández,*Juan Marletto,*Horacio Martírena

**Electrochemical Processes Dept.   *Carbon Dept.
Research & Development
ALUAR Aluminio Argentino SA
Puerto Madryn-Chubut
ARGENTINA

A mathematical simulation model was developed to detect the relevant mechanisms of heat and mass flow in the performance of a closed baking furnace. The existence of cold zones were predicted and, simultaneously, verified experimentally.

. The analysis of the factors responsible for low anode temperatures provided hints to guide the experimental efforts to overcome the problem. Poor horizontal heat conduction and non-homogeneous vertical gas flow along the pit walls seem to be the main factors affecting the furnace performance.

vertical flue ring furnace"
Light Metals, 569 (1981)

9) P.Dumortier "Le traitement des fumées emises par les fours à cuire les
   anodes"
   Revue de l'aluminium, 243 (Juin 1981)

10) A.Serra, A.Murgia, S.Cherchi "Improvements in the operation of a closed-
    type furnace for baking anodes"
    Light Metals, 765 (1982)

11) D.N.Holdner et.al. "Water additions to the cooling sections of horizontal-
    flue ring furnaces"
    Light Metals, 597, (1971)

Appendix

Thermal Conductivity of Packing Coke

Most of the data needed to feed into the program related to the mate-
rials properties was available in the literature, except the thermal con -
ductivity of a green anode and of the packing coke. Both properties were
measured in the Laboratory, using a method suggested by Huttinger (A1). The
experimental values for the green anode conductivity agree with those
determined by other authors (A2, A3). In this Appendix, the results related
to the packing coke will be detailed, since it was detected that its thermal
conductivity is strongly particle size dependent.

In Fig. 1A the results are summarized for 3 different particle sizes
and compared with results obtained elsewhere (A4, A5); the agreement is quite
satisfactory.
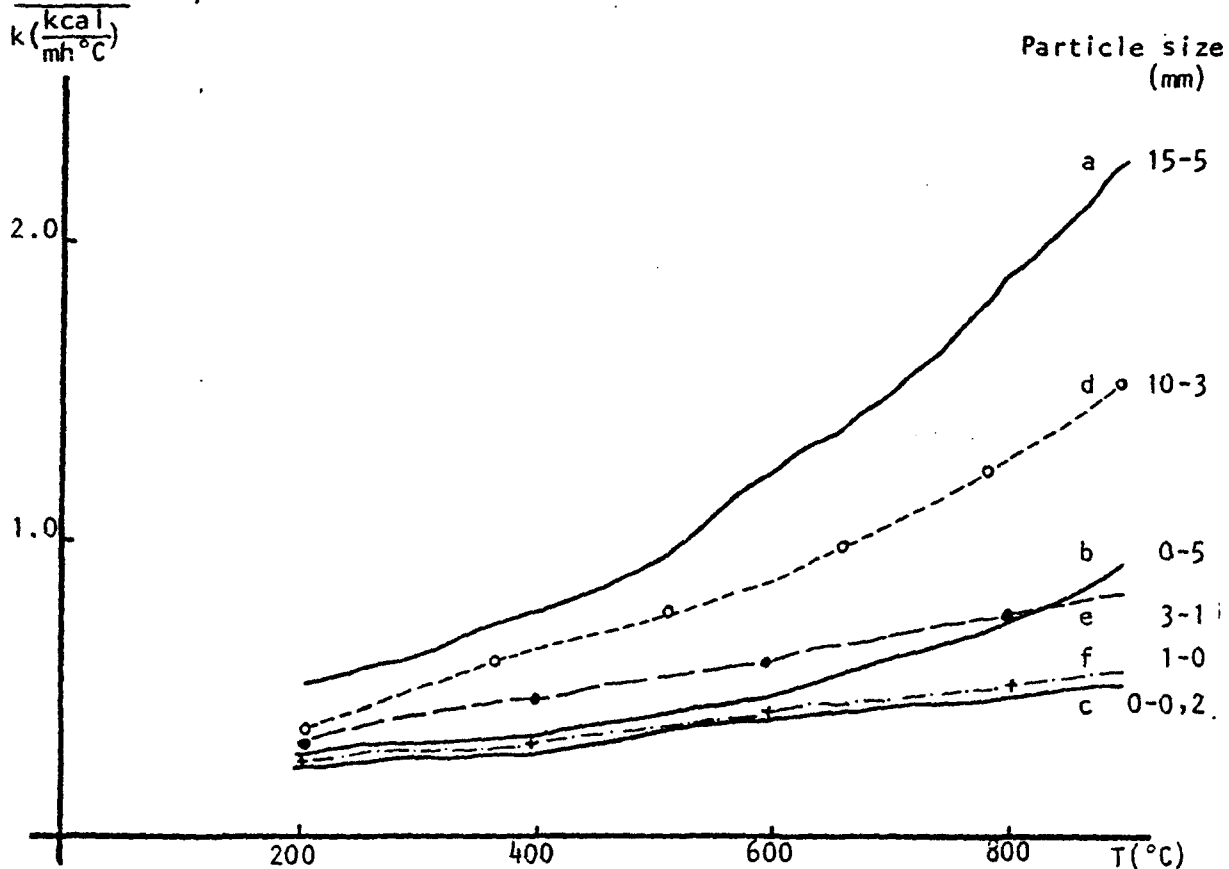
Figure 1A

Particle Size dependence of k
a,b: Reference (A4); c: Reference (A5); d,e,f: Present work

This behaviour can be explained theoretically considering the granular coke as a 2 phase material: coke and air. In this case, the combined conductivity k_{GC} can be calculated using the following formula (A6):

$$k_{GC} = (k_C)^v \cdot (k_a)^{1-v}$$

where k_C is the actual conductivity of each individual grain of coke, k_{air} is the air conductivity and v is the volume fraction of the solid phase (i.e. coke).

Values of k_C (and its temperature dependence) can be obtained from the literature (A7). The air conductivity k_a has a conduction and a radiation component:

$$k_a = k_{ac} + k_{aR}$$

The radiation component can be estimated considering the air phase as formed by cavities of dp average size (A8):(the air phase as formed by cavities of dp average size (A8):)

$$k_{aR} = 4 \ dp \ n^2 \ E \ T^3$$

where

n = index of refraction
E = total emissivity of coke
σ = radiation constant
T = average temperature of the cavity
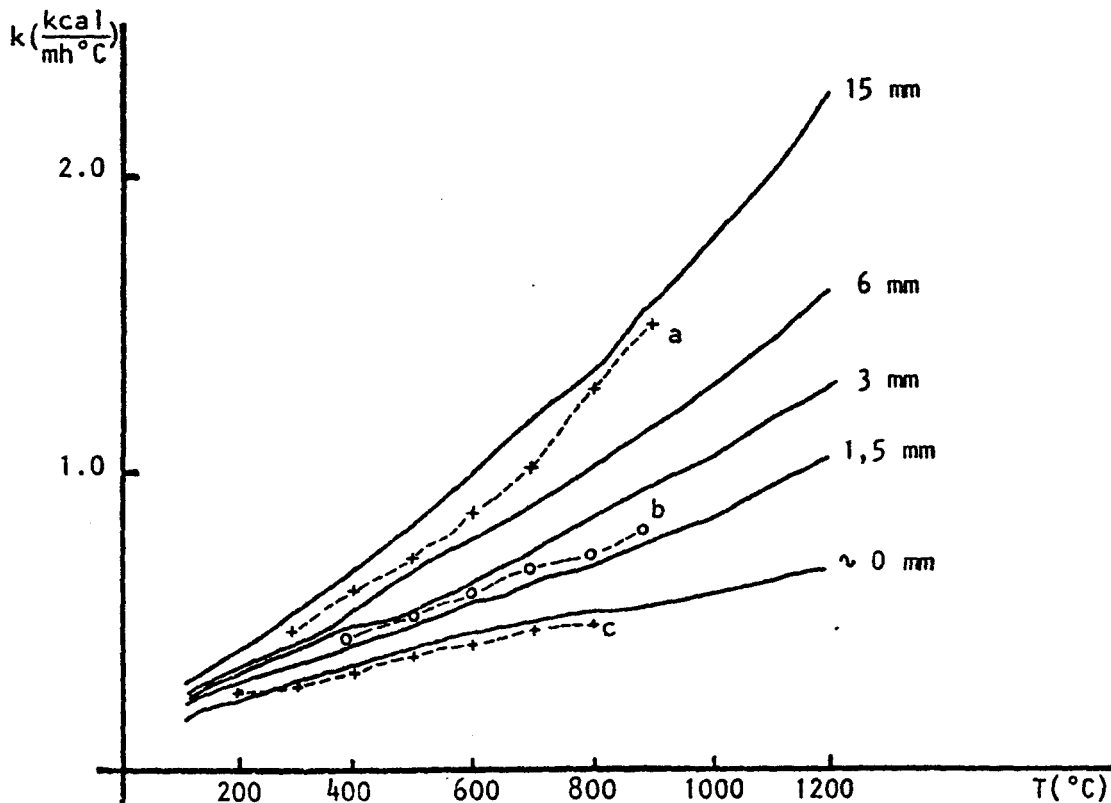
Figure 2A

Comparison of calculated (———) and experimental values of k (a: 10-3mm; b: 3-1mm; c: 1-0mm)

Figure 2A shows the calculated values of k_{GC} for different particle sizes; the agreement with the measured values is remarkably good, taking into account the simplicity of the model.

The phenomenon is well known to ceramists: the conductivity of a brick (with a given total porosity) will decrease as the pores get smaller.

It is worthwile to notice that the difference is significant at high temperatures, where the radiation mechanism plays a decisive role. Related to the calculations of the main text COKE 1 and COKE 2 had large and small particle size respectively.

The conclusion of this subject would be, then, that in order to contribute to the optimization of the baking furnace, the packing coke granulometry should be as large as possibly compatible with potential problems of sticking and anode deformation.

References

A1) K.Huttinger, "Temperaturverteilung in hotlenstoff-bindemittel-korpern bei gesteuerter brennbehandlung"
        Carbon, 7, 459 (1966)
A2) R.Bruski, Kaiser Aluminium, Pleasanton, Ca.
        Private communication, 1980
A3) J.E.Hardin et.al. "Thermal conductivity of Carbon paste shapes"
        Light Metals, 635 (1982)
A4) A.Lutkov et.al. '"Thermal conductivity and electrical conductivity of filler materials used in graphitizing"
        Tsvet.Met. (5) 41 (1975)
A5) A.Agroskin et.al. "Thermophysical properties of petroleum coke"
        Tsvet.Met. (2), 46, (1979)
A6) A.W.Pratt "Heat transmission in low conductivity materials"
        Chapter 6 of "Thermal Conductivity" Edition: R.Tye
        Academic Press, 1969
A7) Le Groupe francais d'etude des Carbones, "Les Carbones" Ed.Masson (1965)
        Vol.1, page 710
A8) W.Kingery "Introduction to Ceramics", page 504
        J.Wiley (1960)

APPENDIX C   MEASUREMENT OF EFFECTIVE THERMAL CONDUCTIVITY OF COKE [27]

Measurement of Effective Thermal Conductivity of Coke

Akito KASAI,[1] Takeaki MURAYAMA and Yoichi ONO

Department of Materials Science and Engineering, Faculty of Engineering, Kyushu University, Hakozaki, Higashi-ku, Fukuoka, Fukuoka-ken, 812 Japan.   1) Formerly Graduate School, Kyushu University. Now Ironmaking Research Laboratory, Iron & Steel Research Laboratories, Kobe Steel, Ltd., Ikeda, Onoe-cho, Kakogawa, Hyogo-ken, 675 Japan.

Effective thermal conductivity of metallurgical coke was measured in the temperature range from 100 to 1 400°C by using the laser flash method. Effective thermal conductivity k of coke increased with a rise of temperature, and decreased with an increase of porosity of coke. The effect of radiation in the pore of coke on the value of effective thermal conductivity of coke was very small. The following empirical equation was obtained for the determination of effective thermal conductivity k (W/m K) as a function of temperature T(K) and porosity ε(−) of coke.

$$k = \{0.973 + 6.34 \times 10^{-3}(T - 273)\}(1 - \varepsilon^{2/3})$$

KEY WORDS: ironmaking; coke; effective thermal conductivity; thermal diffusivity; laser flash method; porosity.

1. Introduction

The effective thermal conductivity or the thermal diffusivity of metallurgical coke has not been reported so much,[1-3] although those are important basic physical properties in the analysis of the temperature distribution in the blast furnace. The values of the thermal diffusivity reported previously are shown in Fig. 1. Y. Tadokoro and N. Oda[1] measured the effective thermal conductivity up to 645°C and extrapolated the measured values up to 850°C. The values of effective thermal conductivity reported by Y. Tadokoro and N. Oda lightly increased with temperature as shown in Fig. 1. Sato et al.[2] and Suzuki et al.[3] measured the thermal diffusivity with the high-temperature thermal shock testing apparatus. However, the values of effective thermal conductivity were uncertain due to the insufficiency of the information on properties of the coke used in their experiments. Sato et al.[2] measured the thermal diffusivity up to 1 500°C. Their experimental values

decreased with a rise of temperature from about 9×10^{-6} m²/s at room temperature to a minimum (about 2×10^{-6} m²/s) at 400°C and then increased up to 1 000°C. The values fluctuated near 5×10^{-6} m²/s over 1 000°C. Suzuki et al.[3] also measured the thermal diffusivity up to 1 800°C. Their values decreased with a rise of temperature from about 14×10^{-6} m²/s at room temperature to a minimum (about 6×10^{-6} m²/s) at 1 400°C and increased over 1 400°C. The values of thermal diffusivity converted from the values of thermal conductivity reported by Y. Tadokoro and N. Oda[1] were in the range of 1×10^{-6}–2×10^{-6} m²/s. Their values were smaller than the ones reported by the former two groups and had different temperature dependency from the former. The effective thermal conductivity of coal measured by Miura et al.[4,5] should be referred to. The values obtained by Miura et al. were one order of magnitude smaller than the values by Y. Tadokoro and N. Oda,[1] because Miura et al. used coal powder packed bed. However, the values reported by Miura et al. were almost the same values as the values by Y. Tadokoro and N. Oda[1] at about 700°C, because coal became coke.

As mentioned above, the experimental values and the temperature dependency varied largely among the investigators.

The amount of graphite crystal in coke varies depending on the career temperature.[6] As temperature rises, the graphitization advances more easily and the amount of graphite crystal in coke increases. The value of the effective thermal conductivity of graphite is large (130–170 W/m K) at room temperature and decreases with a rise of temperature.[7] With an increase of the amount of graphite crystal in coke, the influence on the value and the temperature dependency of effective thermal conductivity of coke is supposed to become
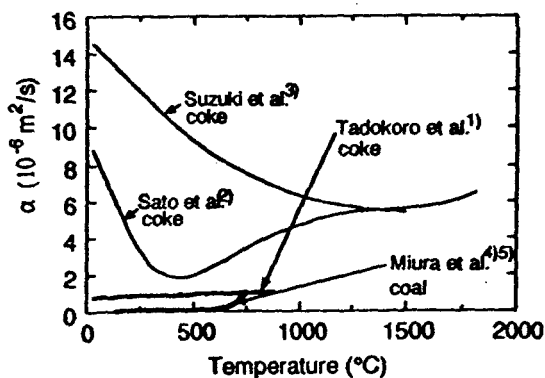

Fig. 1.   Thermal diffusivities of coke and coal.

significant.

Moreover, the value of the effective thermal conductivity is thought to vary with the pore structure of coke, because coke is porous.

The effects of the porosity of coke and the graphitization on the effective thermal conductivity of coke were investigated in this research by using the laser flash method.[8,9]

2. Sample and Experimental Method

2.1. Principle of Measurement[10,11]

The principle of the measurement of the thermal diffusivity by the laser flash method is as follows. The sample disc of thickness L was kept thermally insulated. After the surface was instantaneously heated up by the laser beam pulse, the temperature response of the back side of the sample was measured with the thermocouple. Figure 2 shows a schematic temperature change of the sample. Dimensionless temperature $T(t)'$ on the back of the sample at time t after the laser irradiation is given by Eq. (1),

$$T(t)' = \left\{ 1 + 2 \sum_{n=1}^{\infty} (-1)^n \exp\left(-\frac{n^2 \pi^2 \alpha t}{L^2} \right) \right\} \times (T'_{max} - T'_0) + T'_0 \quad \text{..............................(1)}$$

where α is the thermal diffusivity, T'_0 is the dimensionless temperature of the sample at time $t=0$, and T'_{max} is the maximum dimensionless temperature on the back of the sample. The values of t, $T(t)'$, and T'_{max} were read on the observed temperature variation curve and the thermal diffusivity α and T'_0 were obtained by the curve fitting method with use of Eq. (1). The Marquardt method[12] was used for the curve fitting. The value of thermal diffusivity was adopted only when the standard deviation of the error of the fitting was within 10%. The value of T'_0 was included in the fitting, because the noise by the laser irradiation caused a shift of the base line on the recording chart.

A simple method,[13] by which thermal diffusivity was obtained by measuring the time when the back of sample attained at half of the maximum temperature, was used sometimes in the measurement with the laser flash method. However, in the method, it was not able to judge whether the experiment had been properly carried out or not. Therefore, this method was not adopted in this work.
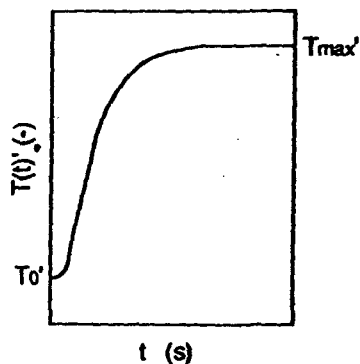
The effective thermal conductivity k was obtained by Eq. (2), i.e., by multiplying the thermal diffusivity α obtained by the curve fitting by the specific heat C_p and the apparent density ρ.

$$k = \alpha \rho C_p \quad \text{..............................(2)}$$

2.2. Sample

Thirteen kinds of coke shown in Table 1 were used for the thermal diffusivity measurement. Nos. 1 and 2 in the table were the charge coke of "A" company. No. 1 was the dry-quenched coke and No. 2 was the water-quenched coke. Nos. 3–12 were the cokes which were sampled by inserting a sampler from the raceway into a blast furnace and are abbreviated hereafter core coke. Nos. 3–8 were core cokes of "A" company and Nos. 9–12 were core cokes of "B" company. No. 13 was the charge coke of "B" company and was dry-quenched coke.

They were prepared to the sample disks of about 10 mm in diameter and about 2 mm in thickness for the thermal diffusivity measurement. Table 1 shows thickness, apparent density, and porosity of each sample. The porosity of the sample was obtained from measured true and apparent densities. The porosity of each sample was in the range of 37–60%.

2.3. Experimental Apparatus

The thermal constants analyzer[13,14] by the laser flash method was used for the measurement of the thermal diffusivity.

2.4. Experimental Method

The experiment was carried out as follows. At first, the sample was set up in the furnace and was heated up to the desired temperature under the vacuum of 1×10^{-3} Pa or less. After the furnace was maintained at a fixed temperature, the laser was irradiated from the upper side on the surface of the sample. The temperature on the back of the sample, which rose by the heat of irradiation of laser, was measured with the Pt–Pt13%Rh thermocouple of 0.1 mm in diameter.

Next, the measurement method of the thermal diffusivity of the porous sample by the laser flash method is explained. Figure 3 shows a schematic diagram for measuring effective thermal conductivity of porous

Fig. 2. Schematic temperature change of the sample.

Table 1. Physical properties of samples.

Sample No.	Thickness (10^{-3} m)	Bulk density (10^3 kg/m^3)	Porosity (—)
1	1.94	0.982	0.496
2	2.00	0.895	0.539
3	2.08	1.11	0.526
4	1.80	1.07	0.543
5	1.41	1.08	0.500
6	2.08	1.02	0.528
7	1.98	1.09	0.528
8	1.98	1.03	0.556
9	1.99	1.05	0.507
10	1.83	1.19	0.422
11	1.78	0.928	0.597
12	1.91	0.952	0.544
13	1.74	1.17	0.378

solid. In a measurement by the conventional laser flash method, the abnormality was found occasionally in the shape of the temperature response curve. It was thought that the laser light might penetrate into the sample because the sample was porous. Therefore, the following method was adopted in the experiment. After the thermocouple was welded on the platinum plate, the platinum plate was bonded on the lower side of the sample with the platinum paste. Moreover, another platinum plate was bonded on the upper side of the sample. The laser light was prevented from entering the sample by bonding the platinum plates on the sample by the method mentioned above. The energy could be instantaneously given on the sample surface. The thickness of the platinum plate, which was 0.05 mm, was thin in comparison with the thickness of the sample. Thermal conductivity of platinum is 70–100 W/mK at 200–1 400 K. It is a number of one to two figures larger than one of coke. The thermal resistance of the platinum part is extremely small. Therefore, the total thickness of coke and platinum was assumed to be the thickness of the sample. The Pt–Pt13%Rh thermocouple was used to measure the temperature response. Therefore, it was imagined that the measured value might be affected by the thermal conduction through the thermocouple. Moreover, there was the possibility in which the measured value might be affected by the thermal leak because of radiation heat transfer in the high temperature region over 1 000°C. However, both influences were supposed to be small, because the diameter of the thermocouple was as small as 0.1 mm. Moreover, the temperature drop on the back of the sample was not observed after attainment of maximum temperature in the temperature response curve (at least twice during the term which it took for the temperature of back side of sample to reach the maximum temperature). This means that both influences were small. Therefore, the correction,[13] by which those influences were considered, was not carried out.

The measurements were carried out at intervals of 100°C from 100 to 1 400°C. The specific heat of coke was estimated by interpolation of the reference values.[15]

Laser beam
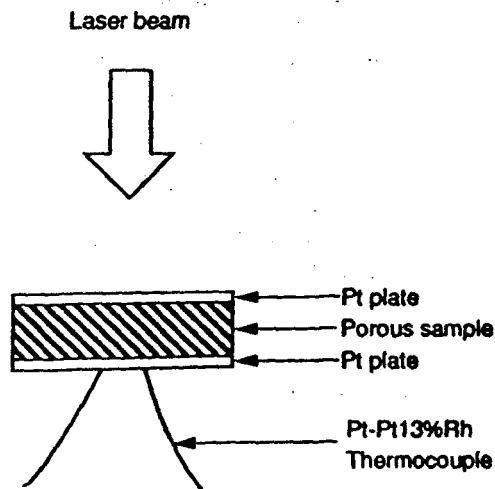
Fig. 3. Schematic diagram for measuring effective thermal conductivity of porous solid.

3. Experimental Results and Discussion

Figure 4 shows an example of the observed data and the fitting results of the temperature response curve. The calculated results agreed well with observed data as shown in Fig. 4.

Next, an example of the temperature dependency of the effective thermal conductivity of the charge coke (No. 1) is shown in Fig. 5. Figure 6 shows an example of the temperature dependency of the effective thermal conductivity of the core coke (No. 7). The values reported
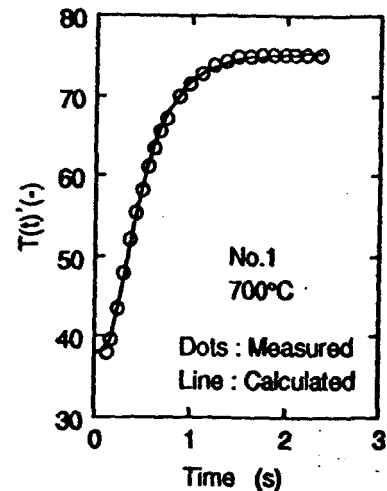

**Fig. 4.** Comparison between observed data and calculated curve.
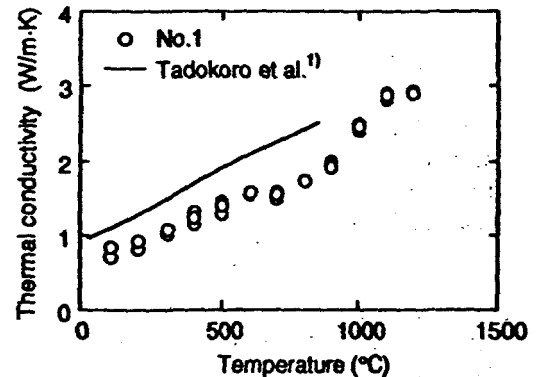
**Fig. 5.** Temperature dependence of thermal conductivity of No. 1 charge coke.
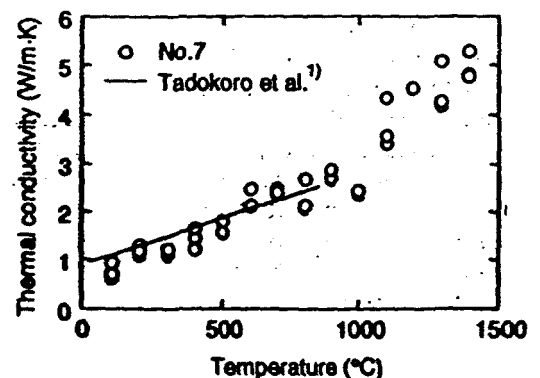
Fig. 6. Temperature dependence of thermal conductivity of No. 7 core coke.

699

by Y. Tadokoro and N. Oda[1] are also shown in Figs. 5 and 6. As shown in these figures, the present data were on a similar level with the values by Y. Tadokoro and N. Oda[1] up to 850°C. The present data over 850°C were on the extrapolated line of the values by Y. Tadokoro and N. Oda. Moreover, the observed effective thermal conductivity increased with a rise of temperature and showed the same tendency as the values by Y. Tadokoro and N. Oda.[1]

The Kunii's equation[16] has been usually used for the estimation of effective thermal conductivity of porous media. The Kunii's equation has some problems that the pore was assumed to have the cylindrical form and that the tortuosity of pore was not considered. However, the following examination was carried out by assuming that the Kunii's equation was able to be applied to the present data.

At first, the influence of the radiation on the effective thermal conductivity was examined by using the Kunii's equation,[16] which is given by Eq. (3),

$$\frac{k}{k_s} = (1-\varepsilon^{2/3}) + \cfrac{\varepsilon^{2/3}}{1-\varepsilon^{1/3}+\cfrac{\varepsilon^{1/3}}{\cfrac{k_F}{k_s}+\left(\cfrac{2}{3}\right)\left(\cfrac{h_r d_p}{k_s}\right)}} \quad ...(3)$$

where k_s is thermal conductivity of solid, k_F is thermal conductivity of fluid, h_r is the radiation heat transfer coefficient, d_p is pore diameter and ε is porosity. The radiation heat transfer coefficient h_r in Eq. (3) is given by Eq. (4) as a function of emissivity E on solid surface and temperature T.

$$h_r = 0.2269 \left(\frac{E}{2-E}\right)\left(\frac{T}{100}\right)^3 \quad ...(4)$$

The right hand side of Eq. (3) is divided into two terms. Then, the first term shows conductive heat transfer in the solid part and the second term shows the rest. Then, k' is defined by Eq. (5).

$$k' = k_s(1-\varepsilon^{2/3}) \quad ...(5)$$

The parameter, which shows the degree of conductive heat transfer in the solid part in Eq. (3), is assumed to be k_1. Then, k_1 is the ratio of k' to effective thermal conductivity k and is given by Eq. (6).

$$k_1 = k'/k \quad ...(6)$$

If k_1 is nearly equal to one, the influence of conductive heat transfer in the solid part is large and the one of the radiation is negligible. The measured values of No. 5, which were shown in Fig. 7, were substituted into effective thermal conductivity k, pore diameter d_p, and the porosity ε in the Kunii's equation, and the influence of the radiation on the effective thermal conductivity was examined. Sample No. 5 was selected because the average pore diameter was the largest among Nos. 1–8. Here, the emissivity E was assumed to be 0.9.[7] Further, the value of thermal conductivity k_F of fluid was assumed to be 0 because the thermal diffusivity was measured in a high vacuum. The influence of the radiation was calculated as follows. At first, the value of k_s was obtained
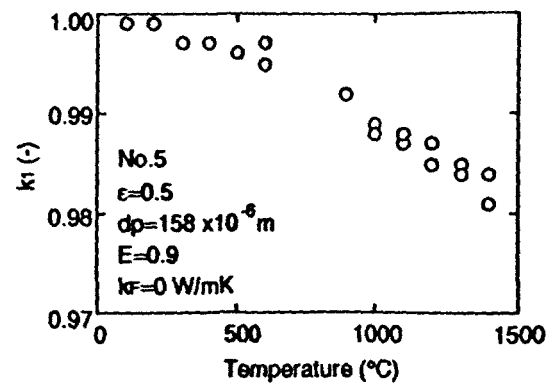

Fig. 7. Temperature dependence of k_1 for No. 5 sample.
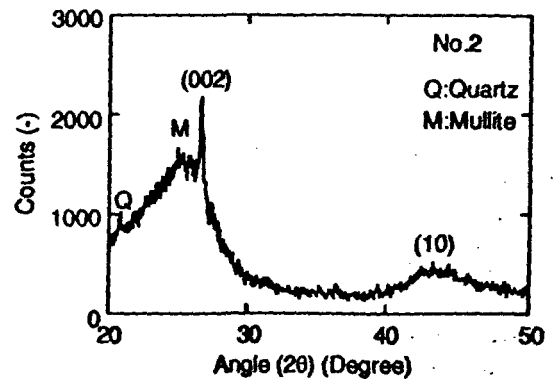
Fig. 8. X-ray diffraction pattern of sample No. 2 using CuKα.

by solving Eq. (3) which is a quadratic equation of k_s. Next, the value of k_1 was obtained from Eqs. (5) and (6) by using the value of k_s.

Figure 7 shows the results. As shown in Fig. 7, the value of k_1 was about 0.98 and approximately 1 even at 1 400°C. Therefore, it was thought that conductive heat transfer in the solid part was mostly predominant in the heat transfer in coke. The influence of the radiation on the effective thermal conductivity of coke was concluded to be negligibly small.

Here, k_s in Eq. (3) is the thermal conductivity of solid coke without porosity. This value is supposed to increase with an increase of the amount of graphite crystal in coke. The amount of graphite crystal increases with an increase of lattice constant L_c defined by Eq. (7). Therefore, the L_c dependency of the effective thermal conductivity was considered as follows. Figure 8 shows an example of powder X-ray diffraction pattern of coke. The peak of the (002) reflection of the graphite shows the size in the direction of C axis, i.e. the piled thickness L_c of carbon reticulation plane. The value of L_c can be estimated by Scherrer's equation[6] that is given by Eq. (7).

$$L_c = A\lambda/(B\cos\theta) \quad ...(7)$$

Here, A is a constant decided by the diffraction plane and is 0.9 in this case. λ is wave length of X-ray and B is the peak width at half peak height and θ is angle at peak position.

Then, the powder X-ray diffraction analysis was carried out and the value of L_c was obtained by using
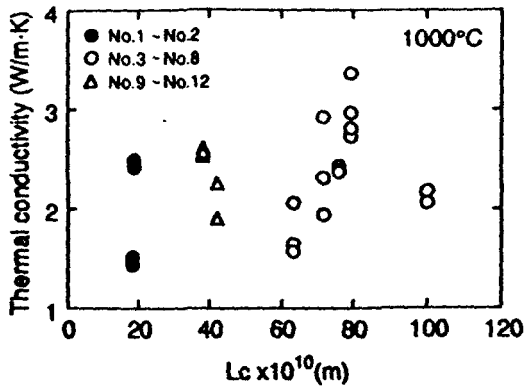
**Fig. 9.** L_c dependence of thermal conductivity.
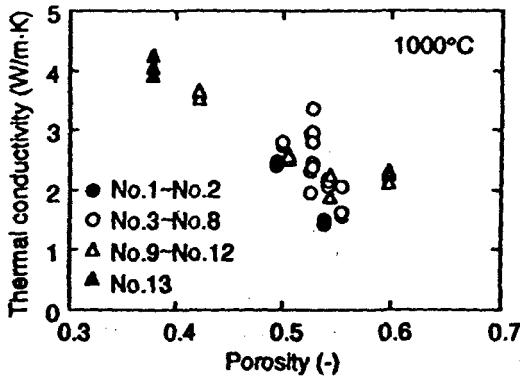
Fig. 10. Porosity dependence of thermal conductivity.

Eq. (7). Figure 9 shows the L_c dependency of the effective thermal conductivity at 1 000°C.

Only the values of thermal conductivity of coke, whose porosity was about 50%, were shown in Fig. 9. As L_c increased in turn of charge coke, (Nos. 1 to 2) core coke (Nos. 9 to 12), and core coke (Nos. 3 to 8), the effective thermal conductivity increased slightly. However, the scattering of data was very large. It was estimated that the scattering was caused by the difference of the porosity and pore structure of each kinds of coke.

Then, the porosity dependency of the effective thermal conductivity was examined at 1 000°C as shown in Fig. 10. Although the data scattered slightly, the effective thermal conductivity decreased with an increase of porosity. Moreover, the effective thermal conductivity of core coke (Nos. 9 to 12) or core coke (Nos. 3 to 8) was slightly larger than the thermal conductivity of the charge coke (Nos. 1 to 2) if those were compared with each other at the same porosity, because L_c of core coke was approximately three to four times larger than L_c of the charge coke and the graphitization of those former cokes proceeded. However, the effect of L_c on the thermal conductivity of coke was small, because the change in L_c was small in this work. The effect of the porosity was large as shown in Fig. 10.

As the effects of the radiation and L_c on the effective thermal conductivity of coke were small in this case, the thermal conductivity of the solid was estimated by using Eq. (5). The thermal conductivity k_s of the coke with zero porosity was estimated as follows. The measured values of effective thermal conductivity and porosity
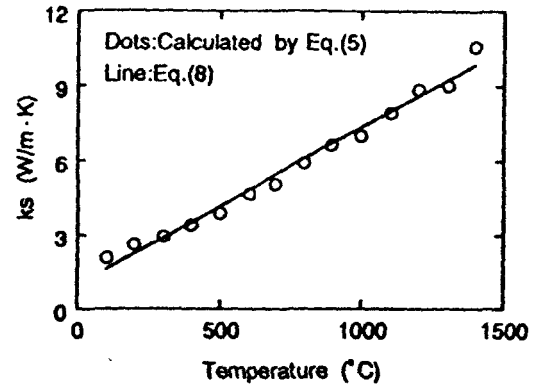

Fig. 11. Temperature dependence of k_s.

were substituted into k' and ε in Eq. (5) and then the values of k_s were obtained. The average values at each temperature were adopted for k_s. Figure 11 shows the results. The thermal conductivity of the solid increased linearly with a rise of the temperature as shown in Fig. 11. The temperature dependence of the thermal conductivity was represented by Eq. (8).

$$k_s = 0.973 + 6.34 \times 10^{-3}(T-273) \quad (373\,K \leqq T \leqq 1\,673\,K)$$
$$............................(8)$$

Further by using Eq. (8), Eq. (9) was obtained for the effective thermal conductivity k of all kinds of coke.

$$k = \{0.973 + 6.34 \times 10^{-3}(T-273)\}(1-\varepsilon^{2/3}) \quad ...(9)$$

4. Conclusion

The effective thermal conductivity of metallurgical coke was measured by using the laser flash method in temperature range from 100 to 1 400°C. The results were summarized as follows.

(1) Effective thermal conductivity k of coke increased with a rise of the temperature and decreased with an increase of porosity of coke.

(2) The effect of radiation on the effective thermal conductivity of coke was very small.

(3) The following empirical equation for the effective thermal conductivity $k(W/m \cdot K)$ of coke was obtained as a function of temperature $T(K)$ and porosity $\varepsilon(-)$.

$$k = \{0.973 + 6.34 \times 10^{-3}(T-273)\}(1-\varepsilon^{2/3})$$

Nomenclature

A : constant (—)

B : peak width at half peak height (rad)

C_p : specific heat (J/kg K)

d_p : pore diameter (m)

E : emissivity (—)

h_r : radiation heat ransfer coefficient (W/m^2 K)

k : effective thermal conductivity (W/m K)

k_F : thermal conductivity of fluid (W/m K)

k_S : thermal conductivity of solid with zero porosity (W/m K)

k_1 : parameter defined by Eq. (6) (—)

k' : effective thermal conductivity defined by Eq. (5) (W/m K)

L : thickness of sample (m)

L_c : lattice constant defined by Eq. (7) (m)

T : temperature (°C)

T'_{max} : maximum dimensionless temperature (—)

$T(t)'$: dimensionless temperature at $t = t$ (—)

T'_0 : dimensionless temperature at $t = 0$ (—)

t : time (s)

Greek

α : thermal diffusivity (m^2/s)

ε : porosity (—)

θ : angle at peak position (degree)

λ : wave length of X-ray (m)

ρ : apparent density (kg/m^3)

REFERENCES

1) Y. Tadokoro and N. Oda: *Seitetsu Kenkyu*, (1944) 168, 79.

2) S. Sato, T. Suzuki, T. Sakai, S. Itagaki and S. Mitani: *Kogakubu-Kenkyu-Shuho, Ibaraki Univ.*, 38 (1990), 175.

3) N. Suzuki, S. Itagaki, S. Mitani, S. Sato and A. Kurumada: *Proc. Sixth Iron Steel Congr.*, 2 (1990), 234.

4) T. Miura, H. Tajima and S. Ohtani: *Kagaku Kougaku Ronbunshu*, 8 (1982), 121

5) T. Miura, J. Fukai and S. Ohtani: *Tetsu-to-Hagané*, 70 (1984), 336.

6) Y. Kasiwaya and K. Ishi: *Tetsu-to-Hagané*, 76 (1990), 52.

7) Thermophysical Properties Research Center, Purdue University: Thermophysical Properties of High Temperature Solid Materials, Vol. 1, Elements, ed. by Y. S. Touloukian, Macmillan Co., (1967), 120, 774.

8) N. Araki: Netsu-Keisoku-Gijutsu, ed. by Mechanical Society of Japan, Asakura Shoten, Tokyo, (1986), 107.

9) H. Shibata, H. Ohta and Y. Waseda: *Bull. Jpn. Inst. Met.*, 30 (1991), 695.

10) K. Matsuzaki: Master's thesis, Kyushu Univ., (1989), 1, 5, 44.

11) N. Hirashima: Graduation thesis, Kyushu Univ., (1984), 5, 12.

12) T. Watanabe, M. Natori and T. Oguni: Fortran77-niyoru-Sutikeisan-Software, Maruzen, Tokyo, (1989), 237.

13) H. Ohta, T. Akiyama, I. Suh, R. Takahashi, J. Yagi and Y. Waseda: *Tetsu-to-Hagané*, 75 (1989), 63.

14) M. Kishimoto, M. Maeda, K. Mori and Y. Kawai: 2nd Int. Symp. on Metallurgical Slags and Fluxes, TMS of AIME, (1984), 891.

15) K. Katsuno: Saishin Nenryo-Binran, ed. by Fuel Institute, Corona, Tokyo, (1984), 162, 163.

16) D. Kunii: Netsuteki-Tani-Sosa, 1st vol., Maruzen, Tokyo, (1976), 123.